NASA/SP—2019-643

Advanced Noise Control Fan: A 20-Year Retrospective of Contributions to Aeroacoustics Research

Daniel L. Sutliff
Glenn Research Center, Cleveland, Ohio

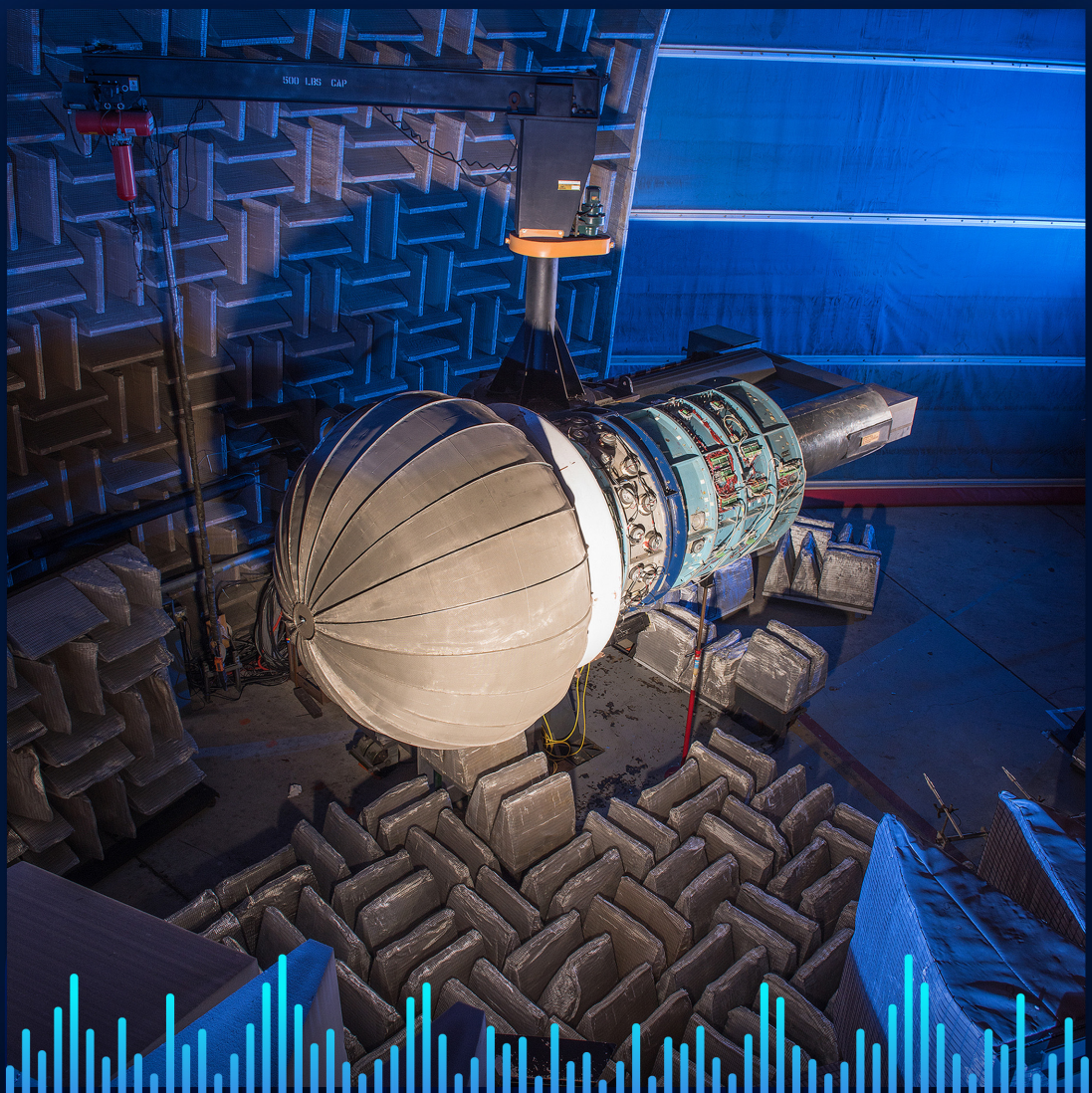

July 2019

NASA STI Program . . . in Profile

Since its founding, NASA has been dedicated to the advancement of aeronautics and space science. The NASA Scientific and Technical Information (STI) Program plays a key part in helping NASA maintain this important role.

The NASA STI Program operates under the auspices of the Agency Chief Information Office . It collects, organizes, provides for archiving, and disseminates NASA's STI. The NASA STI Program provides access to the NASA Technical Report Server—Registered (NTRS Reg) and NASA Technical Report Server—Public (NTRS) thus providing one of the largest collections of aeronautical and space science STI in the world. Results are published in both non-NASA channels and by NASA in the NASA STI Report Series, which includes the following report types:

- TECHNICAL PUBLICATION. Reports of completed research or a major significant phase of research that present the results of NASA programs and include extensive data or theoretical analysis. Includes compilations of significant scientific and technical data and information deemed to be of continuing reference value. NASA counter-part of peer-reviewed formal professional papers, but has less stringent limitations on manuscript length and extent of graphic presentations.

- TECHNICAL MEMORANDUM. Scientific and technical findings that are preliminary or of specialized interest, e.g., "quick-release" reports, working papers, and bibliographies that contain minimal annotation. Does not contain extensive analysis.

- CONTRACTOR REPORT. Scientific and technical findings by NASA-sponsored contractors and grantees.

- CONFERENCE PUBLICATION. Collected papers from scientific and technical conferences, symposia, seminars, or other meetings sponsored or co-sponsored by NASA.

- SPECIAL PUBLICATION. Scientific, technical, or historical information from NASA programs, projects, and missions, often concerned with subjects having substantial public interest.

- TECHNICAL TRANSLATION. English-language translations of foreign scientific and technical material pertinent to NASA's mission.

For more information about the NASA STI program, see the following:

- Access the NASA STI program home page at http://www.sti.nasa.gov

- E-mail your question to help@sti.nasa.gov

- Fax your question to the NASA STI Information Desk at 757-864-6500

- Telephone the NASA STI Information Desk at 757-864-9658

- Write to:
  NASA STI Program
  Mail Stop 148
  NASA Langley Research Center
  Hampton, VA 23681-2199

NASA/SP—2019-643

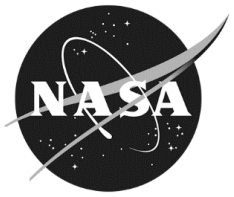

Advanced Noise Control Fan: A 20-Year Retrospective of Contributions to Aeroacoustics Research

Daniel L. Sutliff

Glenn Research Center, Cleveland, Ohio

National Aeronautics and
Space Administration

Glenn Research Center
Cleveland, Ohio 44135

July 2019

Available from

NASA STI Program
Mail Stop 148
NASA Langley Research Center
Hampton, VA 23681-2199

National Technical Information Service
5285 Port Royal Road
Springfield, VA 22161
703-605-6000

This report is available in electronic form at http://www.sti.nasa.gov/ and http://ntrs.nasa.gov/

Acknowledgments

The author wishes to thank Larry Heidelberg, who originally conceived of the Advanced Noise Control Fan (ANCF), and significantly influenced him and others (Figure 1). Tony Shook, Julius Giriunas, and Kevin Konno contributed considerably to the design and installation of the ANCF. Technical support during the crucial early years was expertly provided by David Hauser, Michael Bronczek, Rick Herrlick, and Ben Dastoli. Steve Wnuk provided professional engineering operational support during the early to middle years. TFOME staff (Mark Jacko, Lenny Smith, Bruce Groene, Ed Mysliwiec, Joeseph McAllister, Joel Lauer, Mark Lasky, Devin Podboy, and Brian Rouse (Figure 2) and predecessor organizations continued the tradition of exceptional support. Current high-level managers in the Aeronautics Research Mission Directorate (ARMD) were operations engineers on the ANCF (e.g., Ruben Del Rosario). Michael Jones and Douglas Nark of NASA Langley Research Center exhibited the ideal of intercenter cooperation during numerous collaborations. Dr. Bruce Walker, who was also very influential to the author, was a prolific and significant contributing external researcher. Ray Loew is especially recognized in memory of his dedication and commitment.

(a)

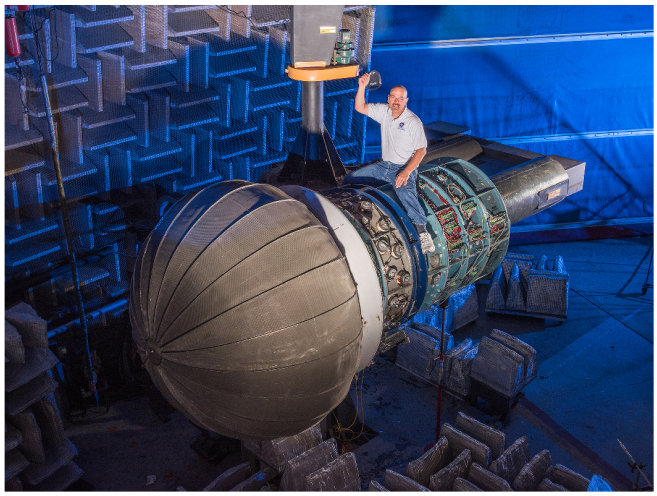

(b)

(c)

Figure 1.—Larry Heidelberg's influence. (a) Heidelberg's imitation of Major T. J. "King" Kong in Dr. Strangelove. (b) Sutliff imitating Heidelberg. (c) Rafael Cuena on the University of São Paulo fan.

Figure 2.—Selected Advanced Noise Control Fan team members.

♦ Contents ♦

♦ Summary ♦

The Advanced Noise Control Fan (ANCF) (formerly the Active Noise Control Fan) was utilized in the design, test, and evaluation for technical risk mitigation of most of the innovative fan noise reduction technologies developed by NASA over the past 20 years (Figure 3). The ANCF is a low-speed ducted-fan testbed for measuring and understanding fan-generated aeroacoustics, duct propagation, and radiation to the far field. It is considered a low technology readiness level (TRL) testbed. The international aeroacoustics research community employed the ANCF to facilitate advancement of multiple noise reduction and measurement technologies and for code validation. From 1994 to 2016, it was located in the NASA Glenn Research Center's Aero-Acoustic Propulsion Laboratory (AAPL). In 2016, the ANCF was transferred to the University of Notre Dame (UND) where it is expected to continue to positively impact ducted-fan aeroacoustic research. This paper summarizes the capabilities and contributions of the ANCF to the field by documenting its history.

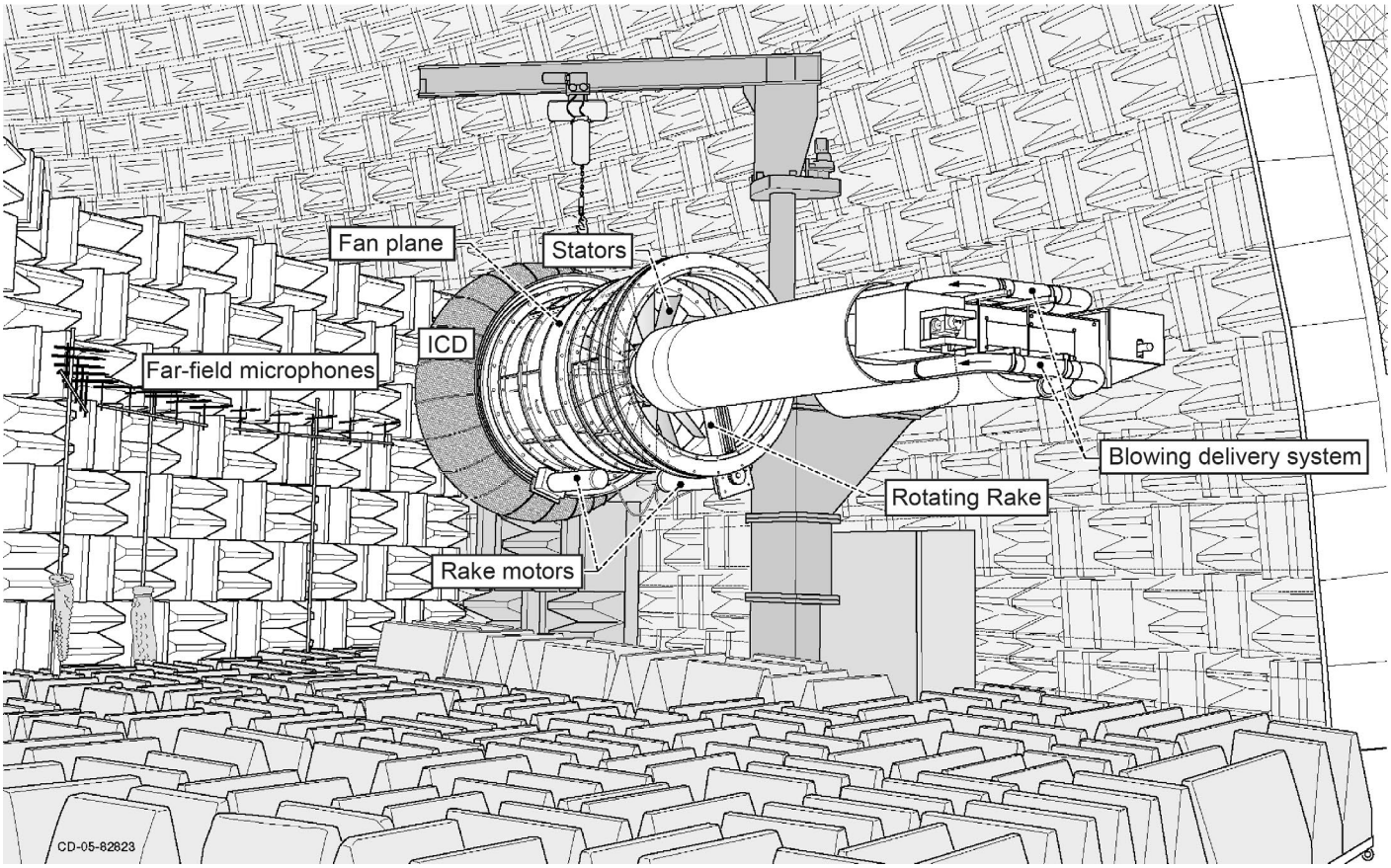

Figure 3.—Advanced Noise Control Fan in Aero-Acoustic Propulsion Laboratory line drawing.

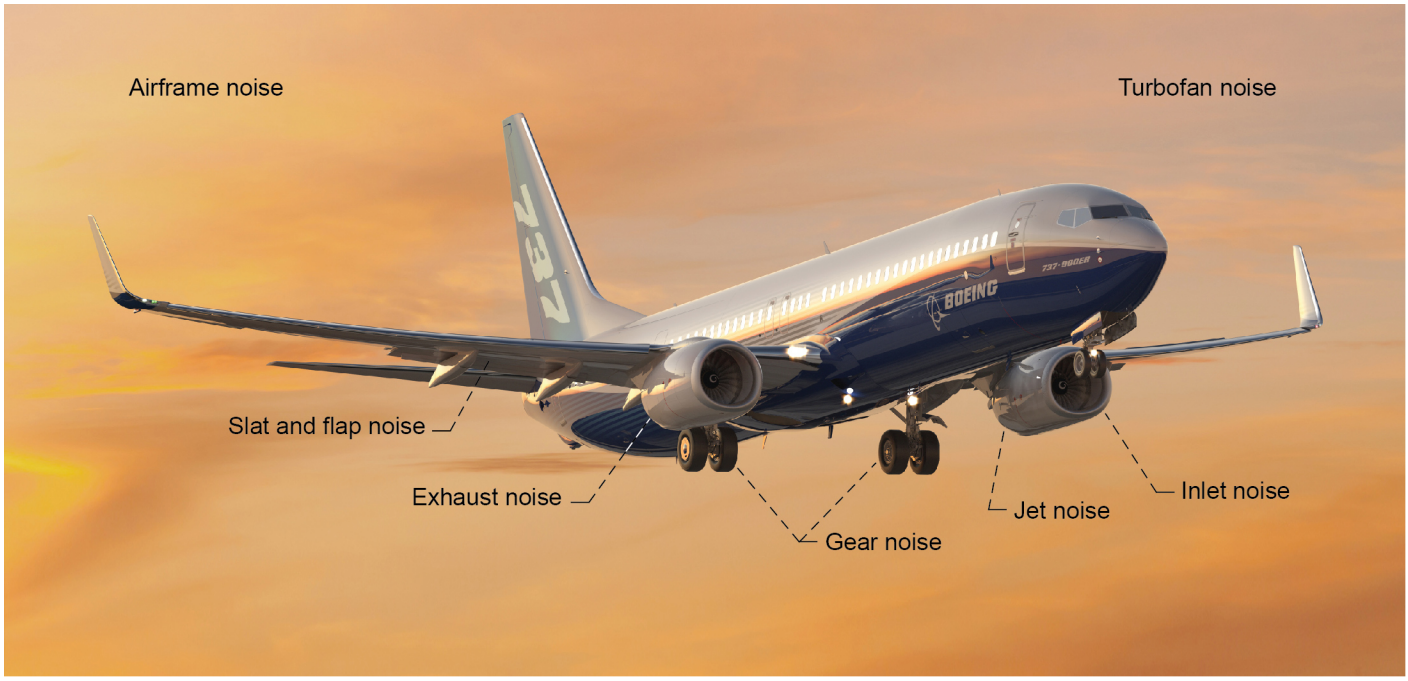

Figure 4.—Sources of in-flight aircraft noise.

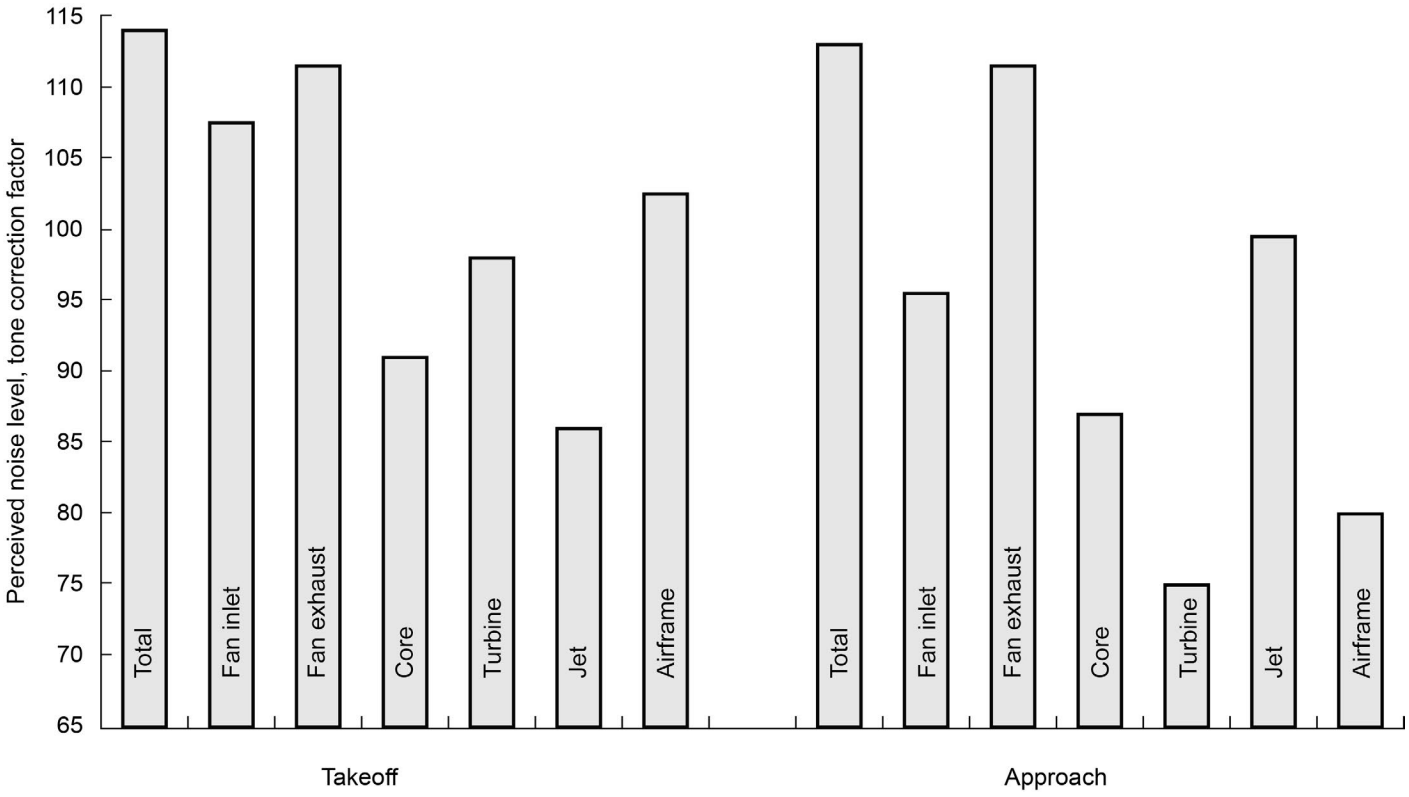

Figure 5.—Representative levels of aircraft noise (from Ref. 3).

♦ 1 ♦

Introduction

1.1 Rationale

The NASA Glenn Research Center has been involved in several aircraft noise research programs[1] (Advanced Subsonic Technology (AST), Quiet Aircraft Technology (QAT), the Fundamental Aeronautics Subsonic Fixed Wing, and currently, Advanced Aircraft Transport Technology) whose goals were the reduction of the adverse impact of aircraft noise on the public.

These programs employed multiple strategies to address this issue—code predictions (system analysis and physics-based), measurement tool development, and component database acquisition—all supporting the development and application of noise reduction concepts. Several focal points, emphasis, and/or success metrics were stressed in individual programs, but the reduction in the transport aircraft noise attributed to the turbofan engine was a continual focus consistent across all these programs.

Novel means of noise reduction were required in order to meet the ever more aggressive noise reduction targets of these programs. In order to implement NASA's philosophy of high-risk, high-benefit technologies (i.e., Fail-Smart[2]), a highly flexible, low-cost testbed was needed to quickly evaluate the noise reduction concepts.

1.2 Aircraft Noise

Aircraft noise[3] can be separated into two general sources: (i) propulsion noise and (ii) airframe noise (Figure 4). Depending on the aircraft and flight conditions, the relative levels of these sources vary; generally, the turbofan engine noise dominates. Figure 5 presents notional relative strengths of these sources.

Turbofan noise results from a variety of sources within the engine (Figure 6). A major component of turbofan noise is caused by the aerodynamic interaction between the fan rotor and stator and other interactions, coupled to duct propagation, which then radiates to the far field. Physically, this source of noise is generated by the impingement of the rotor wakes on the stator vanes. This periodic interaction generates a pressure response from the stator that coalesces into acoustic duct modes.[4] Figure 7 is a flowchart of the generation and measurement of fan noise.

Currently, there are two primary means to reduce propulsion noise: (1) through careful design of the source (though aeroacoustics take a lower priority relative to other concerns, most notably performance, operability, reliability, and maintenance) or (2) attenuation of the noise after it is generated.[5,6] A few examples of source design include stator vane count change, increased blade row spacing, and blade and/or vane shaping.[7] The main method for reducing noise after it is generated is through the inclusion of passively absorptive liners (honeycomb with a resistance sheet) in locations internal to the turbofan that have relatively moderate aerodynamic and thermodynamic conditions (in the bypass area as compared to the core, for example).

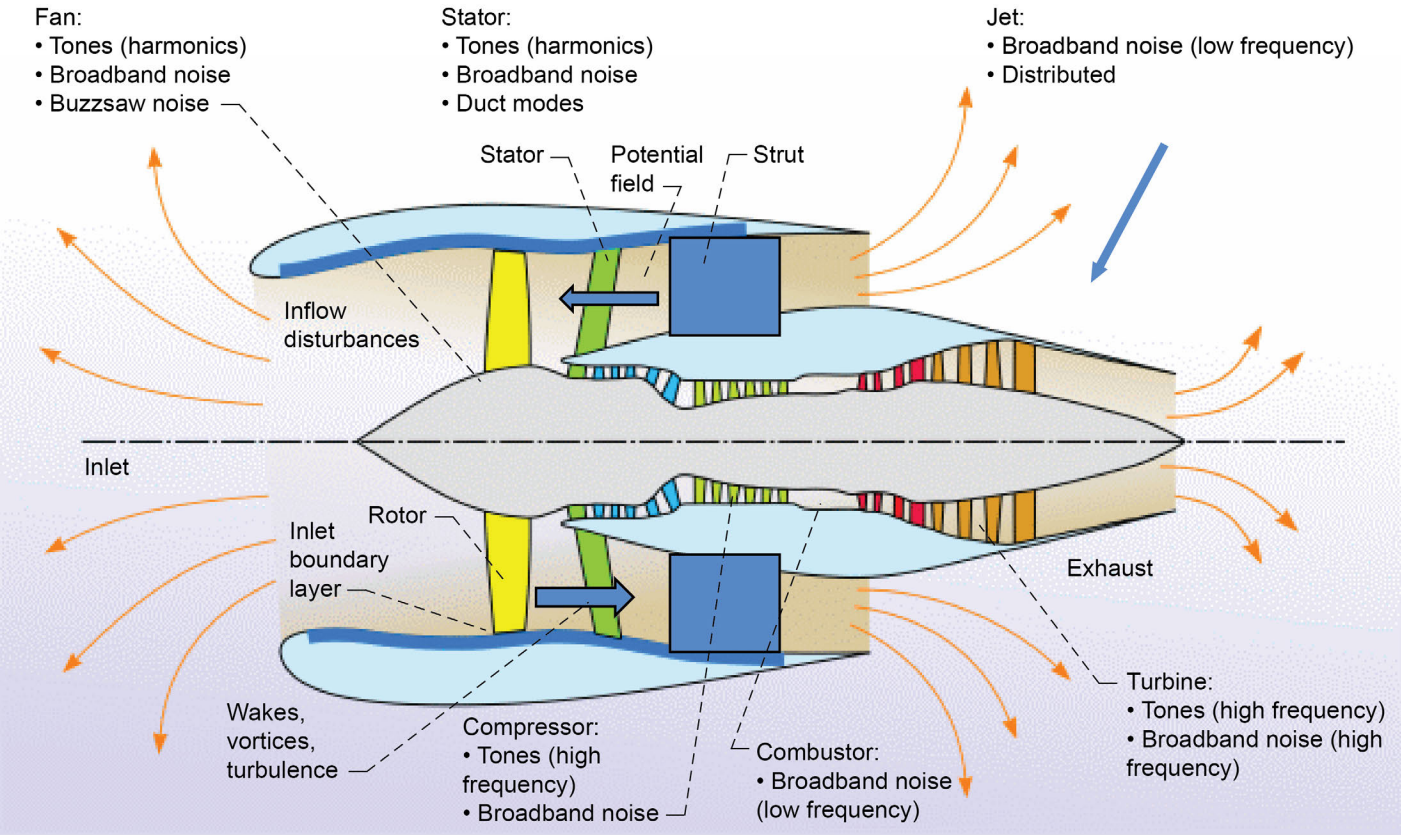

Figure 6.—Sources of turbofan engine noise.

Active Noise Control Fan:

- Can generate the fan noise sources depicted.
- Has the capability to measure the components of aeroacoustic sources.

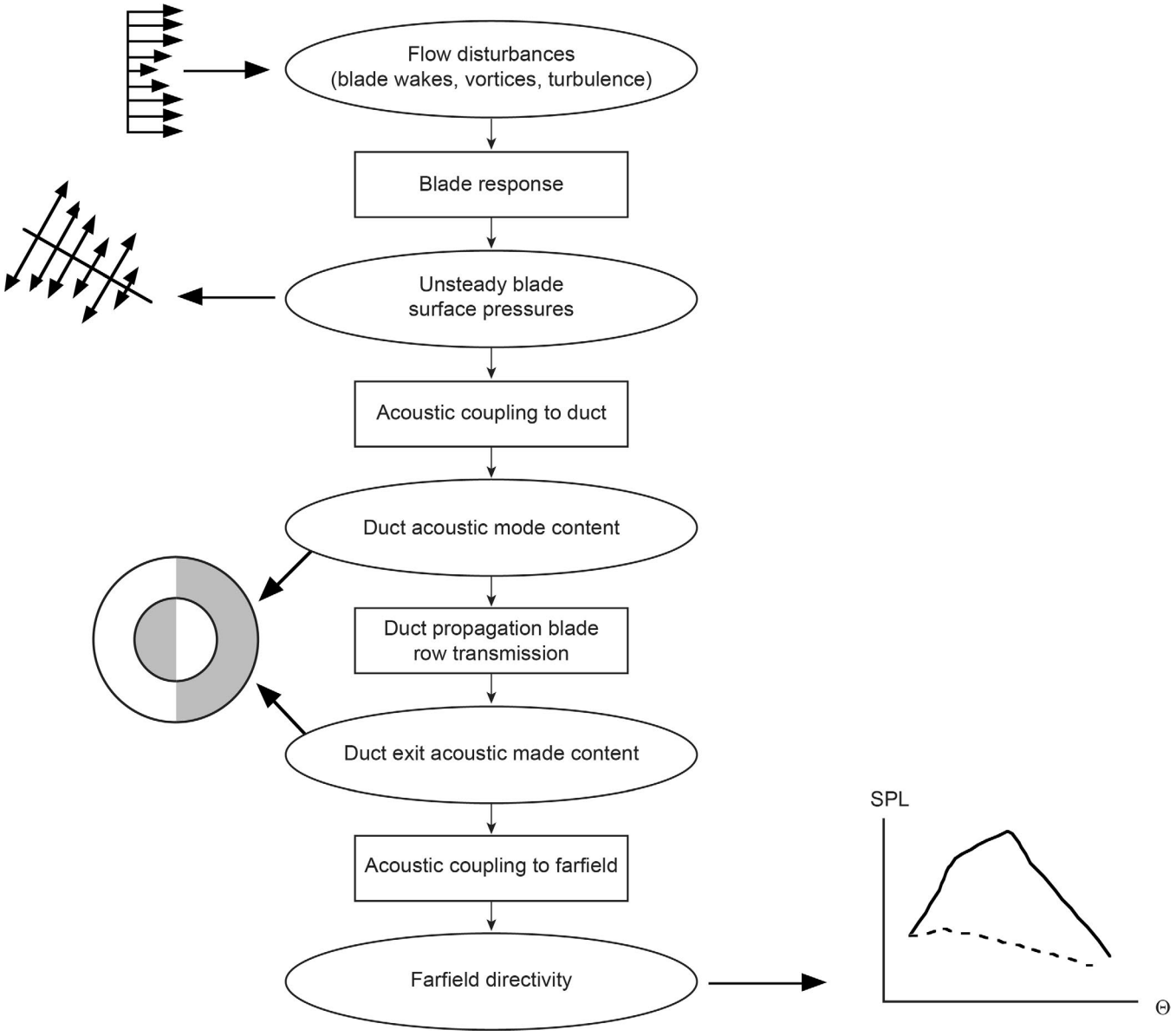

The ovals represent physically measurable quantities.
The rectangles represent transfer functions that can be investigated for noise reduction or code verification.

Figure 7.—Rotor-stator interaction diagram (from Ref. 3).

Figure 8.—Advanced Noise Control Fan located in Aero-Acoustic Propulsion Laboratory.

♦ 2 ♦

Prologue

Laurence J. Heidelberg conceived the Active Noise Control Fan (original name, currently referred to as the Advanced Noise Control Fan) (ANCF) in the early 1990s as a low-cost experimental testbed for developing fan noise reduction technologies. Originally, this was specifically for Active Noise Control (ANC), but he also foresaw its usefulness for acoustic database expansion to increase the understanding of aeroacoustic physics and code validation. Mr. Heidelberg oversaw the design, installation, and early checkouts of the rig. Since then, the ANCF has been upgraded several times over the last 20 years in order to continue making significant contributions in the aeroacoustics field while located at NASA Glenn Research Center.

2.1 Basic Features

The ANCF[8,9,10] is a highly configurable, 4-ft-diameter ducted fan that was located in the Aero-Acoustic Propulsion Laboratory[11] (AAPL) at Glenn for the period covered in this paper. The AAPL is a hemispherical anechoic (above 125 Hz) test facility used for acoustic measurements. An exterior view of the 65-ft-high dome is shown in Figure 8. The ANCF, shown in Figure 9, operated inside an enclosed, compact, anechoic arena designed[12] such that it is in an anechoic environment (Figure 10). This allowed for the continual acquisition of far-field data without moving the rig or impacting the overall productivity of the other AAPL test rigs.

The ANCF fan is composed of a centerbody that is cantilevered from a U-shaped support structure, which is shown from several angles in Figure 11. This structure supports the electric motor, which is coupled to the rotor by a dual-shaft and pulley arrangement. A pedestal column supports the main duct structure so that the centerline is 10 ft from the floor.

The nominal operating condition[13] of the ANCF is 1,886 revolutions per minute, corrected (RPMc), resulting in a tip speed of ~400 ft/s, an inlet duct Mach number of ~0.15, and a fundamental blade passing frequency (BPF) of ~500 Hz. The fan speed can vary from 100 to 2,400 RPM. The frequency range of 250 Hz to 2.5 kHz is representative of the range of concern for community noise impact, based on the effective perceived noise level (EPNL) metric. The maximum rotor tip speed of ~500 ft/s and the duct Mach number of up to 0.16 is low, but does allow for limited studies on the effect of flow on fan noise. The fan pressure ratio[14] is nominally a few inches of H_20, and therefore not relevant to study turbofan performance utilizing the ANCF.

The ANCF can be run in a rotor alone configuration, and the pitch of the 16 fan blades, nominally at 28°, can be adjusted to either 18° or 38°. A variable count stator hub is attached to the centerbody downstream of the rotor to study rotor-stator (RS) interaction noise. Stator vane counts can vary and their stagger angle can also be adjusted. Inlet flow disturbances can be simulated using circumferentially distributed, radially extended rods installed in front of the rotor.

An inflow control device (ICD) is integrated into the ANCF inlet lip. This ICD[15] is used for static engine testing to break up ground vortices and modify the turbulence that would otherwise be ingested by the fan and create spurious noise. The ANCF ICD is an equipotential surface with longitudinal segments. The original ICD had 11-longitudinal segments, which was found to generate cut-on modes based on the 11 segments in the acoustic study region of interest. To avoid this problem, a 22-segment ICD was built. Fine wire mesh on either side of the honeycomb structure of the ICD is used to modify reduce the turbulence.

The unique feature of the ANCF, and its sine qua non is the Rotating Rake[16,17] mode measurement system. The Rotating Rake, which was developed based on the modal theory of Tyler-Sofrin[4] and implemented by Heidelberg,[18] provides a complete map of the acoustic duct modes present in a ducted fan, and hence enabled the research described in the next sections. In addition, multiple aeroacoustic measurement capabilities were integrated into the ANCF rig as shown in the Figure 12 schematic, with closeup photos in Figure 13.

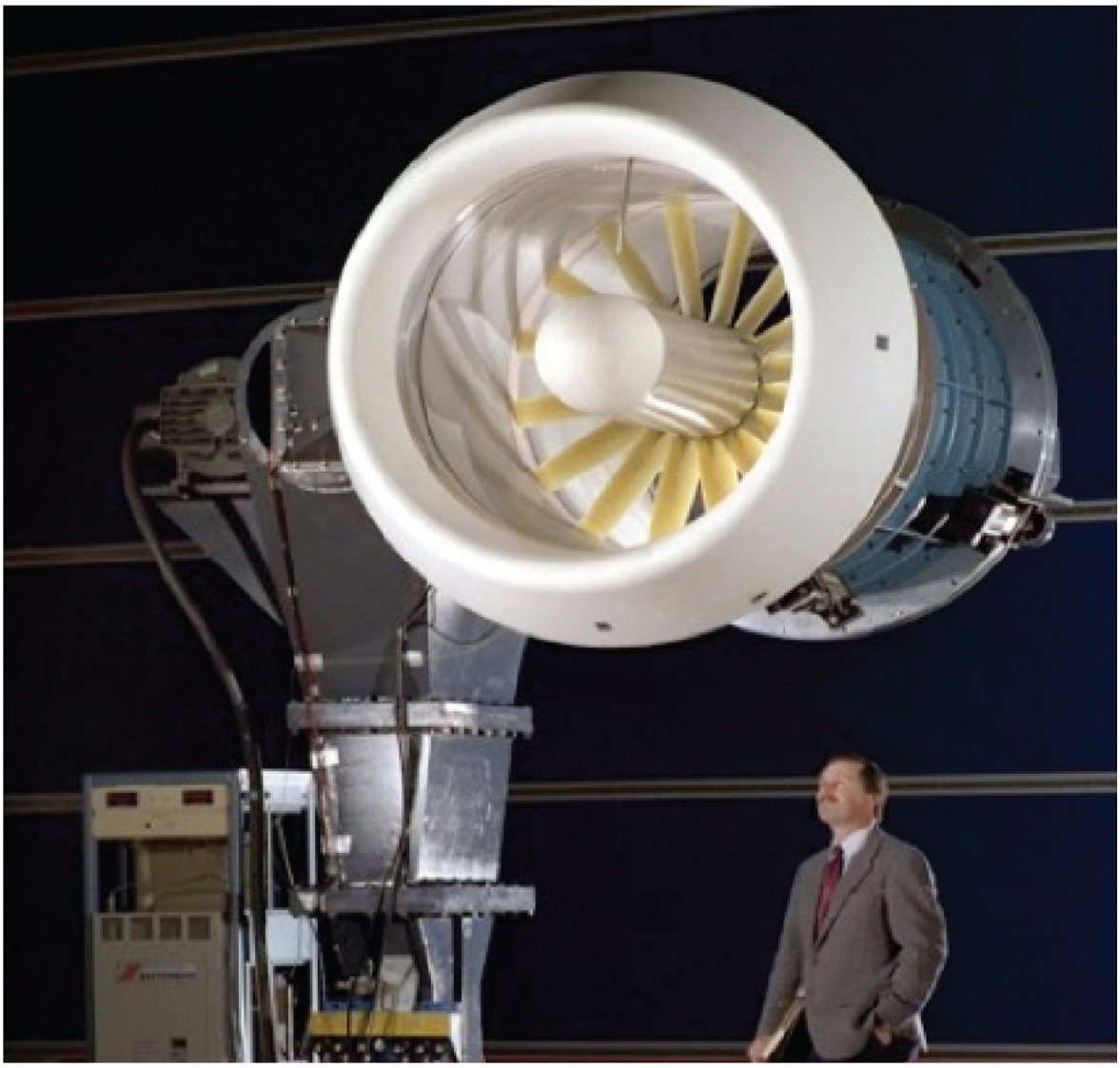

Figure 9.—Active Noise Control Fan was originally built as part of Advanced Subsonic Technology (AST)/Quiet Aircraft Technology (QAT) engine noise reduction program circa 1992. Initial operation began in 1994 to 1995. It was a highly flexible, fundamental testbed capable of testing multiple configurations, including rotor alone. It consists of a 4-ft-diameter ducted fan with a 75-hp electric motor. It is a low-speed fan (variable) Ω = 1,886 RPM and $V_{tip} \approx 400$ ft/s and $M_{duct} \approx 0.14$. Fan was used to evaluate Active Noise Control technologies and develop a duct mode database. In early 2000s, fan was upgraded to a 200-hp motor where Ω = 2,500 RPM and $V_{tip} \approx 525$ ft/s. It was renamed to Advanced Noise Control Fan (ANCF) when research emphasis changed.

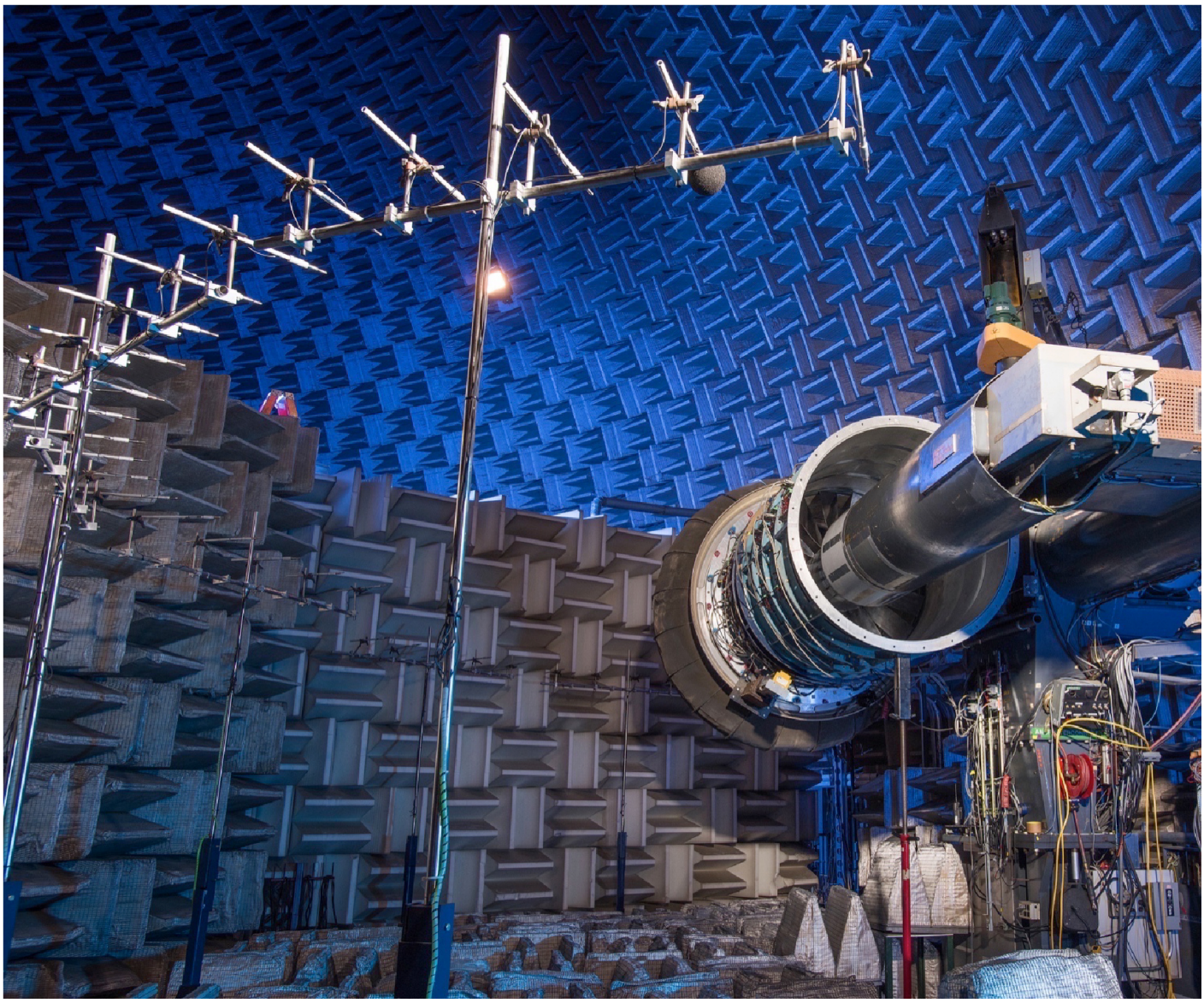

Figure 10.—Advanced Noise Control Fan in enclosed compact far-field arena for continuous usage and final answer. Arena contains an array of 30 far-field microphones with 15 forward and 15 aft arc at a 12 ft radius and 10 ft height separated into six stands of five microphones each. Microphones (Piezotronics 130D20) have a 10-kHz upper limit.

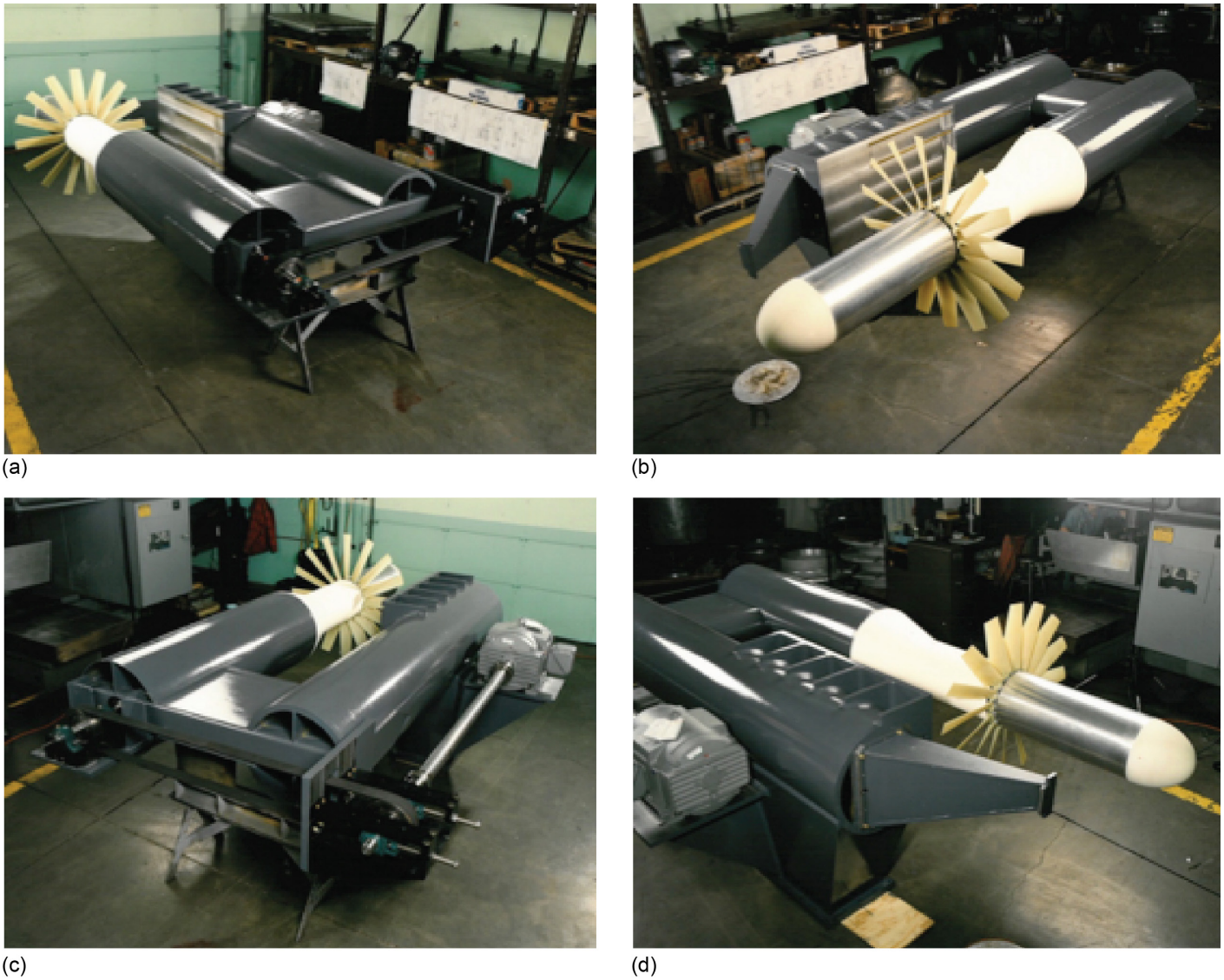

Figure 11.—Advanced Noise Control Fan cantilevered main structure shown with long spinner. (a) Left rear. (b) Left front. (c) Right rear. (d) Right front.

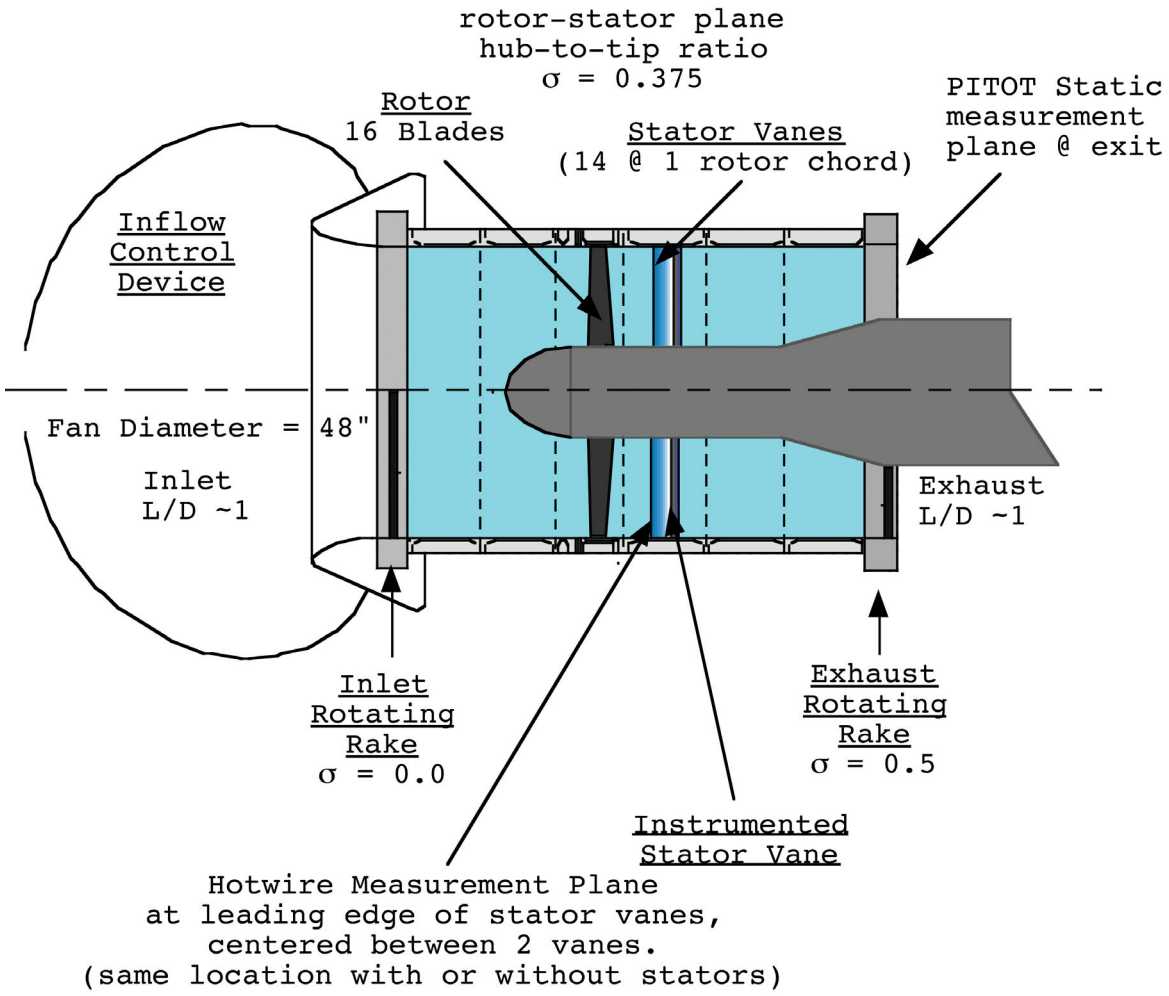

Figure 12.—Advanced Noise Control Fan (ANCF) measurement locations. ANCF contains an inflow control device (ICD) for flow conditioning. Spool pieces can be configured and rearranged (e.g., to install microphones or pressure taps) or replaced with a specialized spool. Centerbody is also configurable and available for instrumentation. Location of traverse mechanism can be varied and hotwire, Kiel, or static pressure probes utilized. Measurement capabilities include in-duct-mode levels (Rotating Rake), rotor wakes, stator vane pressures, duct wall pressures, and far-field directivity. ANCF has 16 rotor blades with a 5.25-in. chord and approximate 15-in. span with variable pitch (18°, 28°, and 38°) mounted on hub. ANCF has 26-, 28-, and 30-count stator vane hubs. Stator vanes have a 4.5-in. chord and approximate 15-inch span with typical variable spacing of 0.5, 1.0, and 2.0 C.

Figure 13.—Advanced Noise Control Fan measurement locations. (a) Rotating Rake. (b) Instrumented vane.

The general technology readiness level (TRL) of the ANCF is considered to be 2 to 3 for representing a turbofan engine.

2.2 Configurable Fan Artificial Noise System (CFANS) Derivative

CFANS[19] was developed and utilized to generate and control circumferential modes (m) and to generate radial modes (n) for the purpose of providing an even wider distribution of acoustic sources to evaluate modal propagation and for the assessment of the efficacy of noise reduction technologies. The system consists of four axially distributed rows, each with 16 circumferentially distributed sets of electromagnetic drivers flush mounted on the inner wall. There are two spool pieces, each having two driver rows (see Figure 14). A LabVIEW™ program (National Instruments) is used to generate the waveforms independently sent to each driver in the proper phase relationship to generate the desired circumferential mode. The signals to each row can be adjusted globally to affect the radial distribution, if desired. The practical limits of the system are $|m\text{-order}| \leq 7$, and frequency ≤1,500 Hz. Figure 15 shows the typical high-quality output from the CFANS for a sample case where mode $m = 2$ was the target mode generated. (For interpretation of these tombstone plots, see Section 3.2.)

2.3 Programmatic Impact

The ANCF was the primary research rig in two NASA Research Agreements, six Small Business Independent Research grants, four Space Act Agreements, two internal Glenn Strategic/Director's Research Funds, and four AeroAcoustic Research Consortium projects. These were integrated into Glenn's noise reduction program milestones. The resulting database of fan noise measurements together with the fan geometry is the only complete aeroacoustic data and/or geometry set publicly available. Approximately 100 papers and reports were published based on ANCF tests, data, and/or geometry (up to ~4 to 6 per American Institute of Aeronautics and Astronautics (AIAA) Aeroacoustics Conference in the last two decades).

Almost all of the fan noise reduction concepts and some of the high-fidelity prediction methods for fan tones were evaluated on or used data from the ANCF. While the general development path for noise-reduction concept development is a sequence of increasing TRL models or tests, a few concepts have gone directly from a proof-of-concept on ANCF to a full-scale turbofan engine test. The most notable of these concepts were the Herschel-Quincke (HQ) tubes, which were on the Honeywell TECH7000,[20] and the highly successful over-the-rotor (OTR) foam-metal liner (FML) installed on the Williams International FJ44 turbofan engine.[21] Manufacturing techniques and the efficacy of an advanced

multidegree of freedom (MDOF) liner were validated on the ANCF to convince Boeing that this type of design could be built in a flightworthy product prior to a recent flight test on a Boeing 737 MAX.[22]

In addition to the direct contributions made through studies on the ANCF, the capabilities, skill set, and experience developed by the team enabled several significant contributions to the greater NASA mission. Perhaps the most notable was the participation in the NASA Engineering and Safety Center (NESC) Return-to-Flight Flow-Liner Cracking root-cause determination.[23] Also, the unique Ultrasonic Configurable Fan Artificial Noise Source (UCFANS) series of tests that contributed to the Environmentally Responsible Aviation (ERA) Hybrid Wing Body shielding studies[24] were based on ANCF and CFANS lessons learned.

The remainder of this paper provides brief summaries of a number of studies conducted using the ANCF. Some of the more pertinent results of these studies are noted herein, but the reader is directed to the supporting references for more thorough discussions of the individual tests or topics.

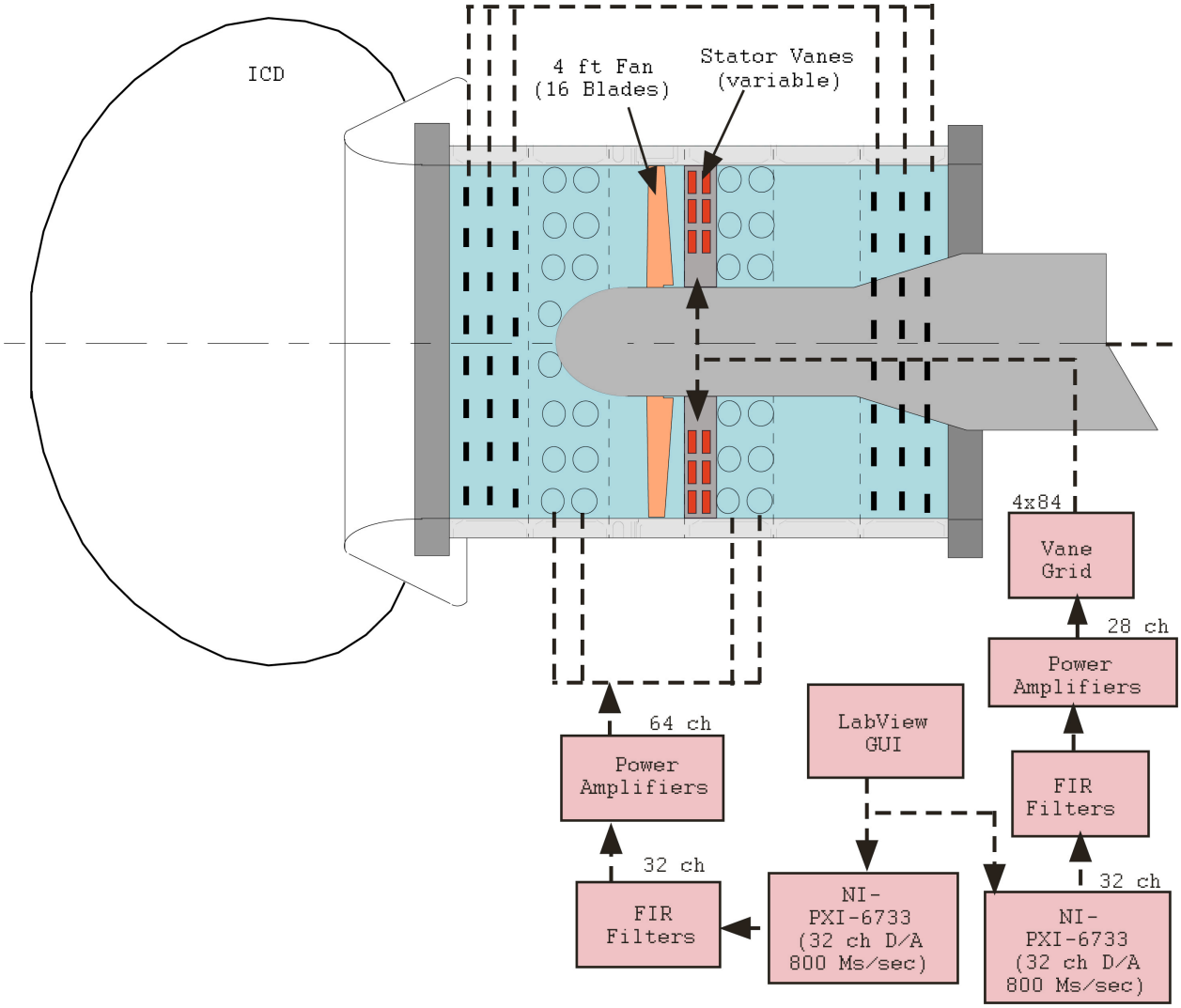

Figure 14.—Configurable Fan Artificial Noise Source (CFANS). CFANS initially had 32 channels, which were upgraded to 64. There are four rows of 16 drivers each. Noise source is generated in software (S/W) and each channel is independent. LabVIEW™ virtual instruments or 2 by 32 channels of finite impulse response (FIR) filters shape output. Phase delays are used to simulate modal versus random sources and time delays simulate rotating versus stationary sources. Operational bandwidth is 250 Hz < frequency < 1,500 Hz $|m| < 6$; $n < 4$. Where D/A is digital to analog, GUI is graphical user interface, and ICD is inflow control device.

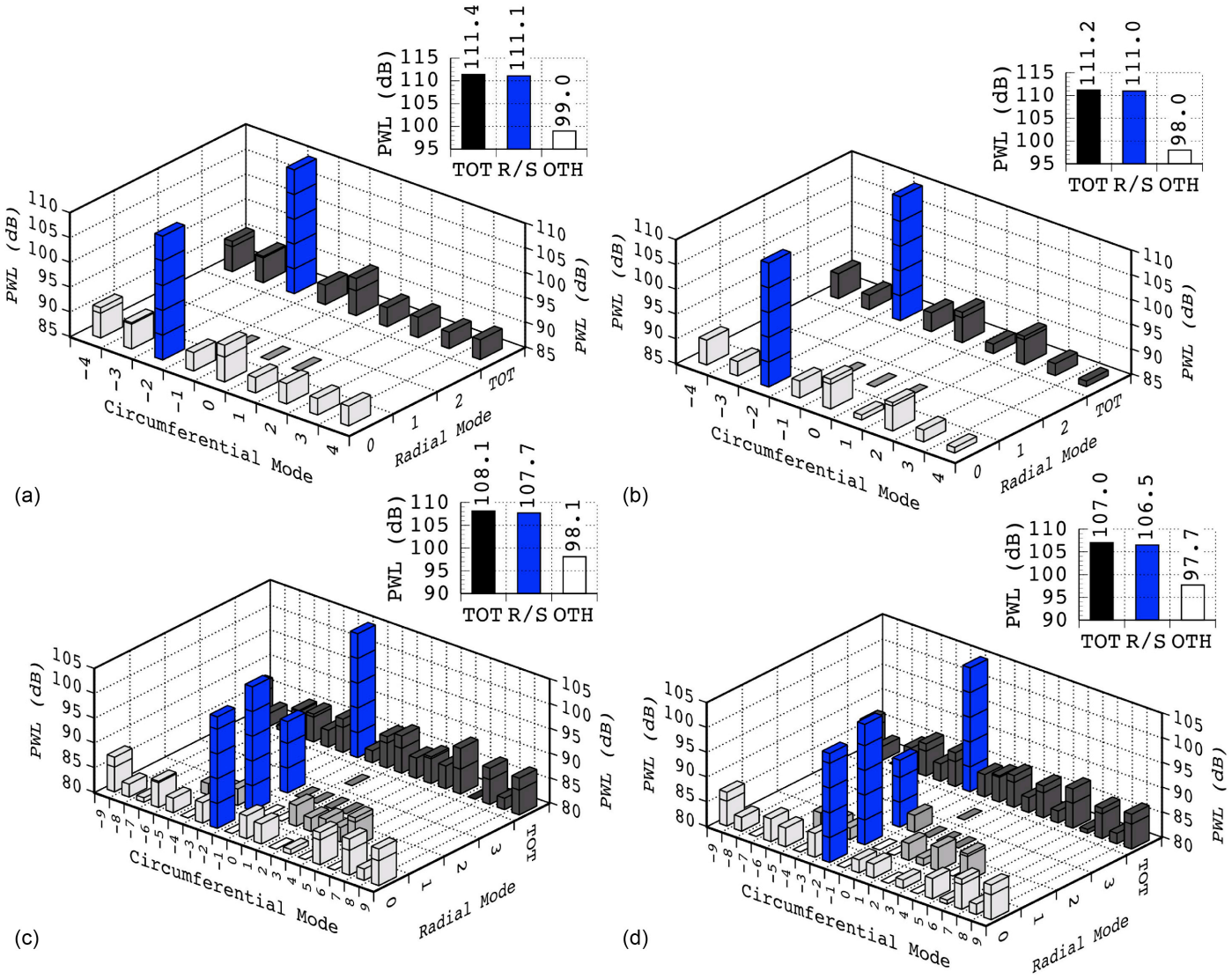

Figure 15.—Sample output of Configurable Fan Artificial Noise Source. (a) Build 1: 480 Hz, mode 2. (b) Build 2: 480 Hz, mode 1. (c) Build 1: 960 Hz, mode 2. (d) Build 2: 960 Hz, mode 2. Where OTH is other, RS is rotor-stator, and TOT is total.

♦ 3 ♦

History

The Advanced Noise Control Fan's (ANCF's) initial focus was to initiate and support the NASA effort in ANC research in the 1990s. As the NASA Aeronautics Research Mission Directorate (ARMD) research focus changed, the first letter in ANCF was changed from Active to Advanced and significant research into other noise reduction concepts and aeroacoustic investigations were accomplished. Along the way, many interesting changes and events occurred. Figure 16 presents a timeline of the research emphasis over the last two decades. This section is divided roughly between these topics, preceded by a general history.

3.1 General

The initial checkouts of the ANCF occurred in May 1994. The checkout runs were performed with rods installed upstream of the fan rotor. (During the period of study, inlet-guide vanes were not a feature in contemporary aircraft turbofan engine design.) The main reason for utilizing rods in the inlet for the checkout was to generate strong tones and duct modes relative to the broadband (BB) noise level to ensure a clear and convincing duct modal structure and strong fan tone harmonics in the far field. The database of the stator vanes acoustic characteristics was first acquired in February 1995. Initially, a long spinner (from rotor to inlet plane) was installed for evaluation of the acoustic character, but dynamic issues resulted in a short spinner being used for the remainder of the history.

While the rig was located in the Aero-Acoustic Propulsion Laboratory (AAPL) facility, early control was from the second floor of the 10- by 10-Foot (Abe Silverstein) Supersonic Wind Tunnel control room (Building 90). Rotating Rake and other in-duct measurements were acquired with the ANCF near the wall just inside the main door opening of the AAPL. Far-field data were acquired with the ANCF located in the center of the AAPL arena. This necessitated moving the ANCF, which required disconnection and reconnection of the control and power cables. Far-field data were then acquired using the AAPL sideline array. (This array comprised 30 microphones mounted on 10-ft-high poles at a 40-ft-radius arc centered on the Nozzle Acoustic Test Rig (NATR). Initially, the ANCF was on an air bearing so the entire 20,000-lb rig could float across the concrete floor, in theory. The roughness of the floor and the less than full directional control made the movement to the Center a rather interesting event, more so for the spectators than the operator who worked the flow control while standing on the ANCF's platform base. That, coupled with the required umbilical reconnection and connection and loss of test time for the primary AAPL test rig (the NATR) necessitated the design and installation of a compact far-field arena for acquiring far-field data. Two walls with anechoic wedges were placed and angled about the ANCF as it was situated in the in-duct data location. The wall in front of the ANCF was fixed; the wall on the left side, where a microphone array was situated, could pivot to allow access to beneath the AAPL mezzanine. These walls, combined with the sidewall of the AAPL, provided three anechoic surfaces for this location. The fourth anechoic surface was the open main door, and of course, the hemispherical ceiling; the floor would be covered with movable wedges to complete the anechoic environment. The microphone array arcs were at 10 to 15 ft horizontally from the centerline of the duct (eventually sited at 12 ft) and level with the duct centerline in the vertical direction. Far-field data comparisons[12] between these arcs and the 40-ft arc showed the data was essentially similar (some increase in the low-frequency BB levels below 0.5BPF were noted, probably due to increased turbulence from the proximity of the wedge wall to the inlet of the ANCF for which the ICD could not fully dissipate).

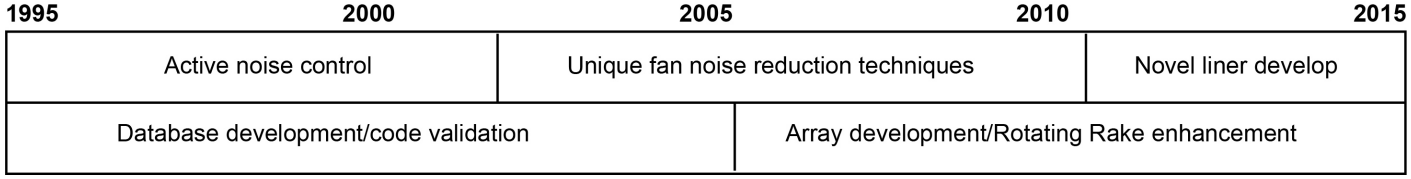

Figure 16.—Advanced Noise Control Fan research emphasis timeline.

A 75-hp motor originally powered the ANCF. However, as research requirements continued to increase, it was replaced with a 125-hp motor in 1999 to accommodate the higher fan speeds (up to 2,500 RPM) required to achieve greater modal density. The revolutions per minute increase was accomplished by reducing the rotor pitch angle to keep the torque below the design limit. This had the unforeseen consequence of generating flutter. The lower pitch resulted in the blade intersecting the wake of the preceding blade, causing unloading and depitching of the blade, followed by an elastic return past the nominal blade angle, causing a cyclic aeroelastic response. The noise generated by the flutter was so loud, even in the control room, that it was assumed to be a propeller aircraft flying low and overhead. Toolboxes were shaken off of nearby benches due to the vibrations. Several modifications to the blades were attempted to prevent the flutter. Weights were added to the tips to dampen the elastic response, holes were drilled to reduce the tip vortex, and several different clippings of the blade leading edge tip were tried. Ultimately, a 5- by 1.5-in. trim from the blade tip prevented the flutter.

A failure occurred in July of 1997. The shaft on the fan side failed. The failed shaft was replaced, and on the checkout run for the new shaft, the motor-side shaft failed. Remarkably, the failure was within 10 percent of the predicted life. The shaft failures were contained since standard rotating machinery safety features were incorporated into the design. A lesson was learned though, when one part fails, peremptorily replace the second identical part with the same life cycle history.

An exciting failure occurred in August 1997,[25] when one of the blades dug into the hard rub strip made of hardened body filler, was drawn forward, and snapped off (see Figure 17). All of the blade fragments spiraled out along the exhaust duct wall and were ejected onto the aft exclusion zone. (Again, demonstrating the wisdom of standard safety practices.) The ANCF rub strip was then replaced with a more abradable and flexible material to prevent this type of failure from occurring. An interesting postscript to this event was that the new rub strip material was installed over the high-speed fan on the 9- by 15-ft Low-Speed Wind Tunnel (9×15 LSWT) drive rig where, due to the significantly higher cyclic forces on the material, it caught fire internally. (While low-TRL environments are critical in developing technology, care must be taken in determining the differing physical and environmental conditions when applying to higher TRLs.)

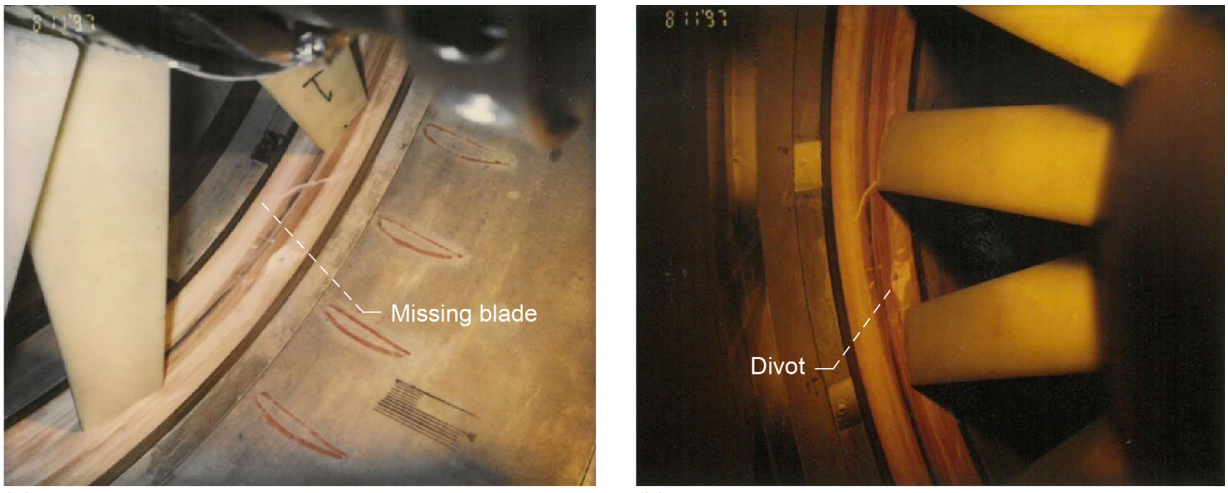

Figure 17.—Advanced Noise Control Fan blade loss. (a) Missing blade shown. (b) Divot on casing shown.

Both of these failures illustrated the robust design of the ANCF, resulting from implementing standard rotating machinery best practices. In neither case was anyone injured nor additional damage to equipment incurred. Indeed, it was difficult to immediately determine anything was amiss except for a change in the sound of the fan monitored by the facility microphone (indicating that the human ear is often an excellent tool for health and safety monitoring).

The original set of fan blades was an industrial set from Crowley. These plastic blades were designed and manufactured for ventilating fans and as such were intended for flexibility of application (one blade design for a variety of diameters and pitches) rather than aerodynamic efficiency. They were attached to a fan hub and installed in a 14.75-in. (hub-to-tip ratio, $\sigma = 0.307$) centerbody. In 2000, a redesign of the rotor blades to create a more realistic loading and efficiency profile in preparation for the trailing-edge rotor blowing (TERB) study (see Section 3.5.1) was performed using rotor design codes. At this time, the center-body diameter was increased to 18 in. ($\sigma = 0.375$). The increased loading from a more efficient design of the fan required a new 200-hp motor installation.

The Massachusetts Computer Corporation (MASSCOMP) data acquisition system was originally used to acquire all dynamic time history data for ANCF research. This system was part of the AAPL facility data system at the time. When an independent data system was required, the Nicolet Odyssey data system was used from 1999, which in turn was replaced by the HBM Genesis data system in 2013. These data systems all featured external sampling (to the shaft encoder) that is an essential requirement for Rotating Rake measurements and a very expedient feature for all other fan-related dynamic data acquisition, a technique that was transferred to the 9×15 LSWT acquisition. The far-field microphone arrays used Knowles (inexpensive ~$5 per unit with in-lab built preamps), which had problematic reliability until in 2003 when the microphones were upgraded to PCB 130D21 ICP microphone and integral preamp.

As mentioned in the beginning of this section, control of the ANCF was from the outside the AAPL dome and ultimately from a purpose-built building (B145). Auxiliary control of specialized equipment, especially the ANC controllers, was inside the AAPL near the ANCF. This proximity control was first accomplished by having the guest researchers and their equipment situated next to the ANCF, in the open. A memorable event was a test that occurred during a typical Cleveland winter. The guest researchers from a warm weather climate huddled under a plastic tarp vainly trying to keep the snow off of them and their equipment while the wind and recirculation from the flow blew the snow from all directions. Regrettably, a photograph could not be found to document their devotion to duty. Their discomfort did not go unnoticed by the author, who promptly procured a heated, soundproof enclosure for when it was necessary for him to acquire auxiliary data.

A very rewarding benefit of being associated with the ANCF was the privilege of meeting the highest caliber individuals in the aeroacoustic community (Figure 18). NASA Administrator Daniel Goldin toured the ANCF very early in the rig's life (who, along with the ANCF developer, Larry Heidelberg, also shown in the picture, attended the City College of New York). Dr. Ed Rice, awarded the prestigious AIAA Aeroacoustic Award in 2014, was an early contributor to the ANC effort. The Honorable Kim Beazley, the Ambassador of Australia to the United States, was treated to an observation of the ANCF running.

(a)

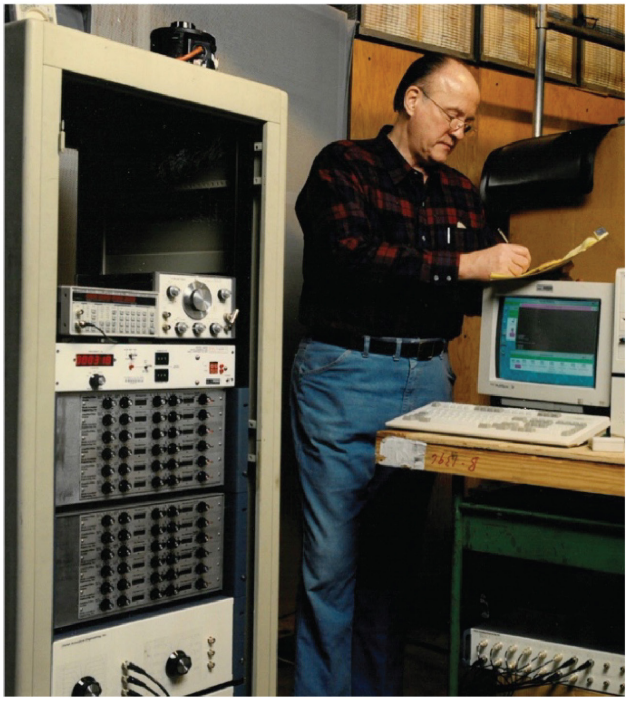

(b)

(c)

Figure 18.—Advanced Noise Control Fan (ANCF) VIPs. (a) NASA Administrator Daniel Goldin views ANCF. (b) Dr. Ed Rice, early contributor to ANCF effort. (c) Honorable Kim Beazley, Ambassador of Australia to United States, observes ANCF in operation.

3.2 Database Development

The primary aeroacoustic database acquired using the ANCF was the variation of stator vane count and spacing. The nominal counts were (13, 14, 15, 26, 28, and 30) at spacing of 0.5, 1.0, and 2.0 stator chords. The lower vane counts generate a cut-on BPF, while the higher counts result in a cutoff BPF, a design condition that is common in modern turbofans. Rotating Rake modal data and far-field spectral data were acquired for most of the combinations of these physical parameters[9,10].

The Rotating Rake modal data is typically presented in the literature by means of tombstone plots. Much information is presented on a tombstone plot, as shown in Figure 19. The circumferential and radial mode orders are indicated on the *x-y* plane with the *z*-axis providing the mode acoustic power level (PWL) in that specific (*m,n*) mode. The lowest level on the *z*-axis is generally the measurement noise floor for modes at that condition. Strong modes will rise significantly above the noise floor. Modes that could propagate, but are below the noise floor will have an indication in the cell; modes that are expected to be cut off due to duct physics will have a clean cell on the *x-y* axis plane. Thus, the well-known mode cut-on triangle is clearly illustrated. The summation of the radial modes within a given circumferential mode is presented along the back wall of the graph. Typically, the total PWL in the tone and the PWL in the expected RS interaction modes will be tabulated, plotted in a small bar graph, and connected to the tombstone plot. This allows for easy data analysis and cross plotting, as shown in Figure 20, where the PWL for individual modes are plotted versus fan RPMc.

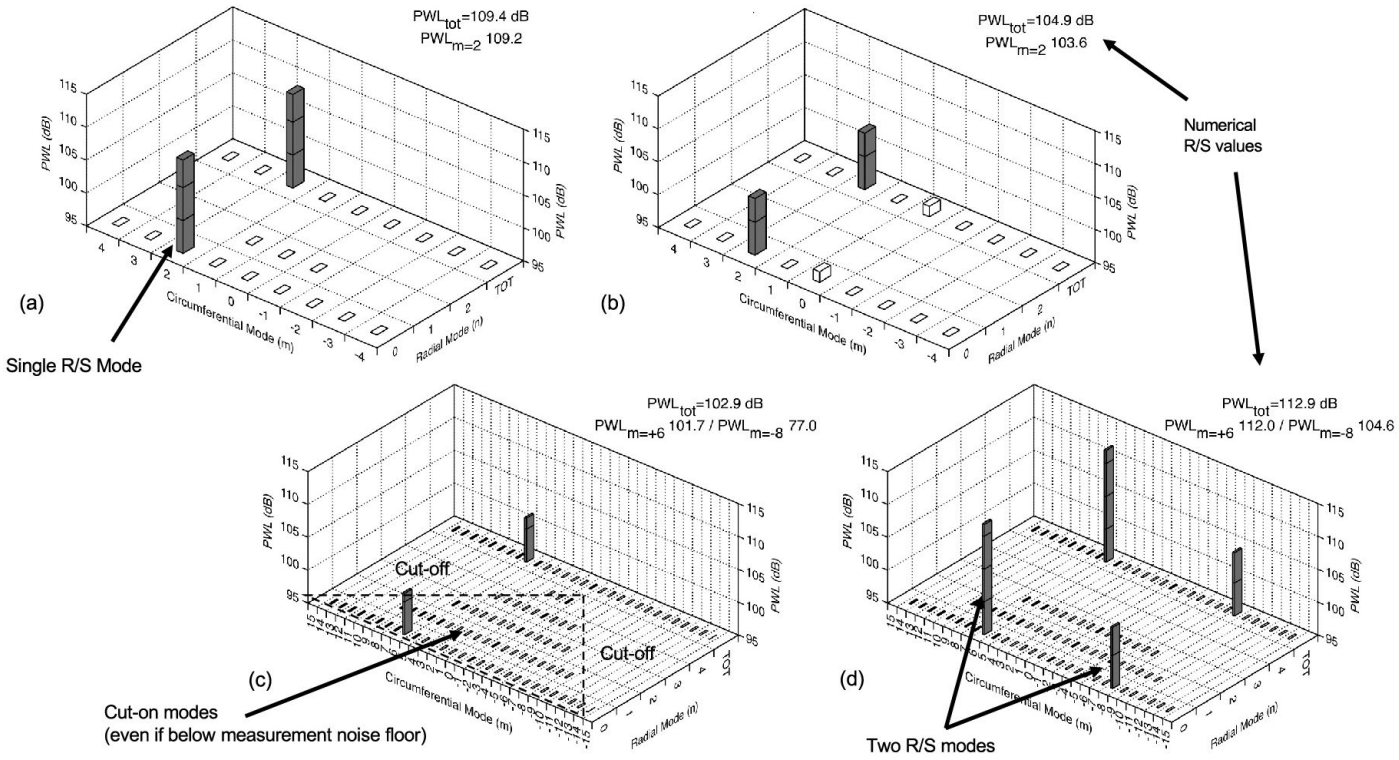

Figure 19.—Tombstone plots for presenting Advanced Noise Control Fan modal content as measured by Rotating Rake. Modal plots are with 14 stator vanes at 1 chord, 1,800 revolution-per-minute, corrected. (a) Blade passing frequency (BPF) inlet. (b) BPF exhaust. (c) 3BPF inlet. (d) 3BPF exhaust.

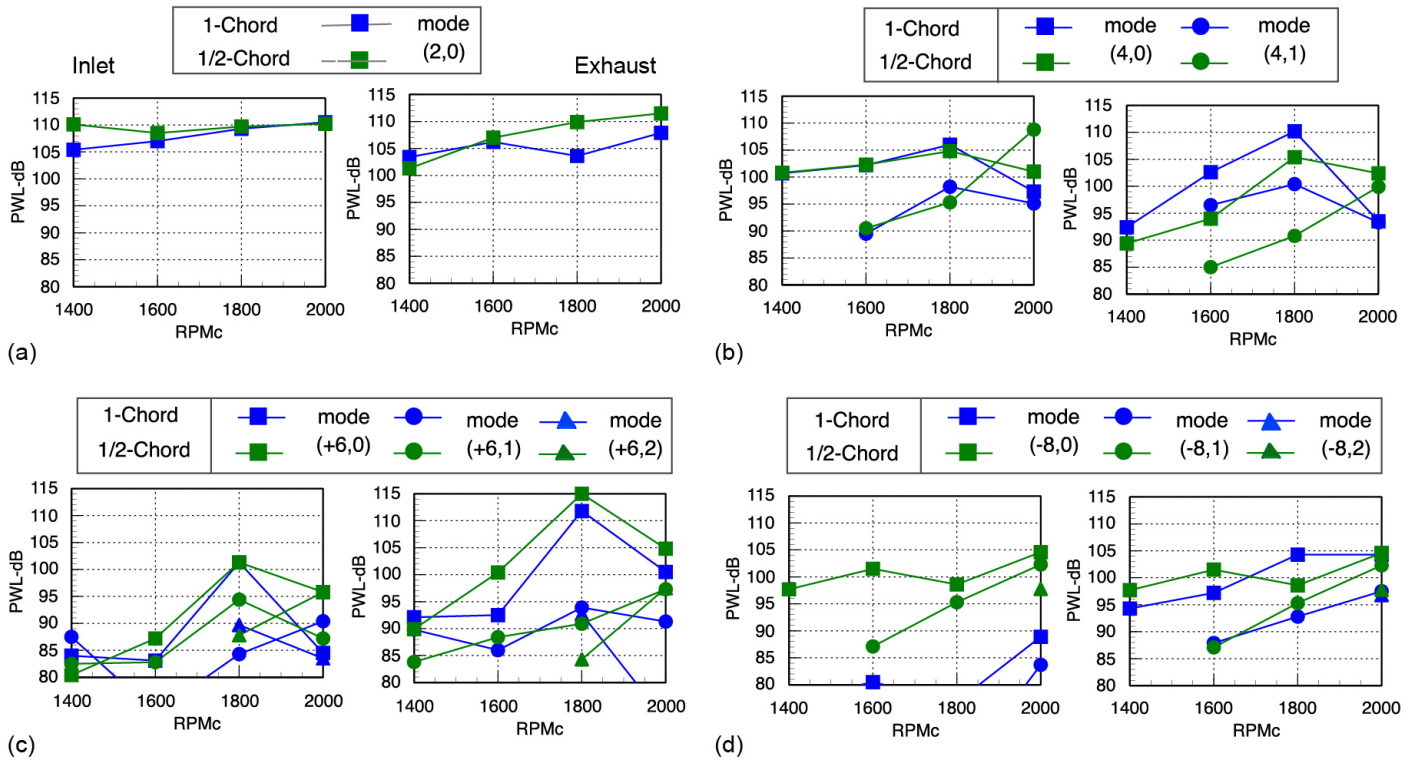

Figure 20.—Representative rotor-stator (RS) interaction modes versus revolutions per minute, corrected (RPMc), for 14 stator vanes as measured by Rotating Rake. (a) 1 blade passing frequency (1BPF) single RS. (b) 2BPF multiple RS radial mode. (c) 3BPF multiple RS circumferential mode. (d) 3BPF multiple RS radial mode.

The time histories used to compute the far-field spectra were also acquired synchronous to the fan shaft rotation. This allows for extremely accurate and easy separation of the fan tones and the BB from the original spectra. Each of these individual spectral components can then be composed into specific bandwidths for detailed analysis. The bandwidth chosen is based on the fan harmonics. They are centered on a fan harmonic (1BPF, 2BPF, …, nBPF) and extending ±0.5BPF around a fan harmonic. This enables presentation of the far-field directivity in a manner suitable for spectra containing harmonics (as opposed to octave analysis). This is illustrated in Figure 21, where the tonal and BB spectral components for 1BPF and 2BPF are plotted separately. Illustrating the educational potential of ANCF, the lobed nature of the far-field directivity and the significant decrease in tone levels due to cutoff (0-vanes)—classic effects of fan aeroacoustics—are presented in Figure 22.

Stator vane surface unsteady pressures are a significant component in the chain of physical processes that result in the generation of fan noise. The distribution of the microphones along the chord and span shown in Figure 23 was used as a prototype for the high-speed fan Source Diagnostic Test[26] in the 9×15 LSWT. A database of pressure and suction side pressures were acquired and a representative sample plotted in Figure 24. These data were reduced using the same separation and harmonic bandwidth analysis as for the far-field spectra. Phasing is very important in the coupling of the surface pressures to duct modes as analytically described by Green's function radiation, and therefore retained in the processing of this data.

The viscous wake is the next step in the flowchart in Figure 7. The upwash on the stator vane from the cyclic changes in the magnitude and direction of flow is the physical cause of the stator vane surface pressure fluctuations. To create this database, two-component hot-film data were acquired. Figure 25 shows the mean flow, turbulence, velocity, and angle of a representative condition averaged over one-blade passage acquired from a two-component hot-film. Again, illustrating the tutorial nature of the ANCF, the tip vortex and hub-distorted low regimes are clearly seen.

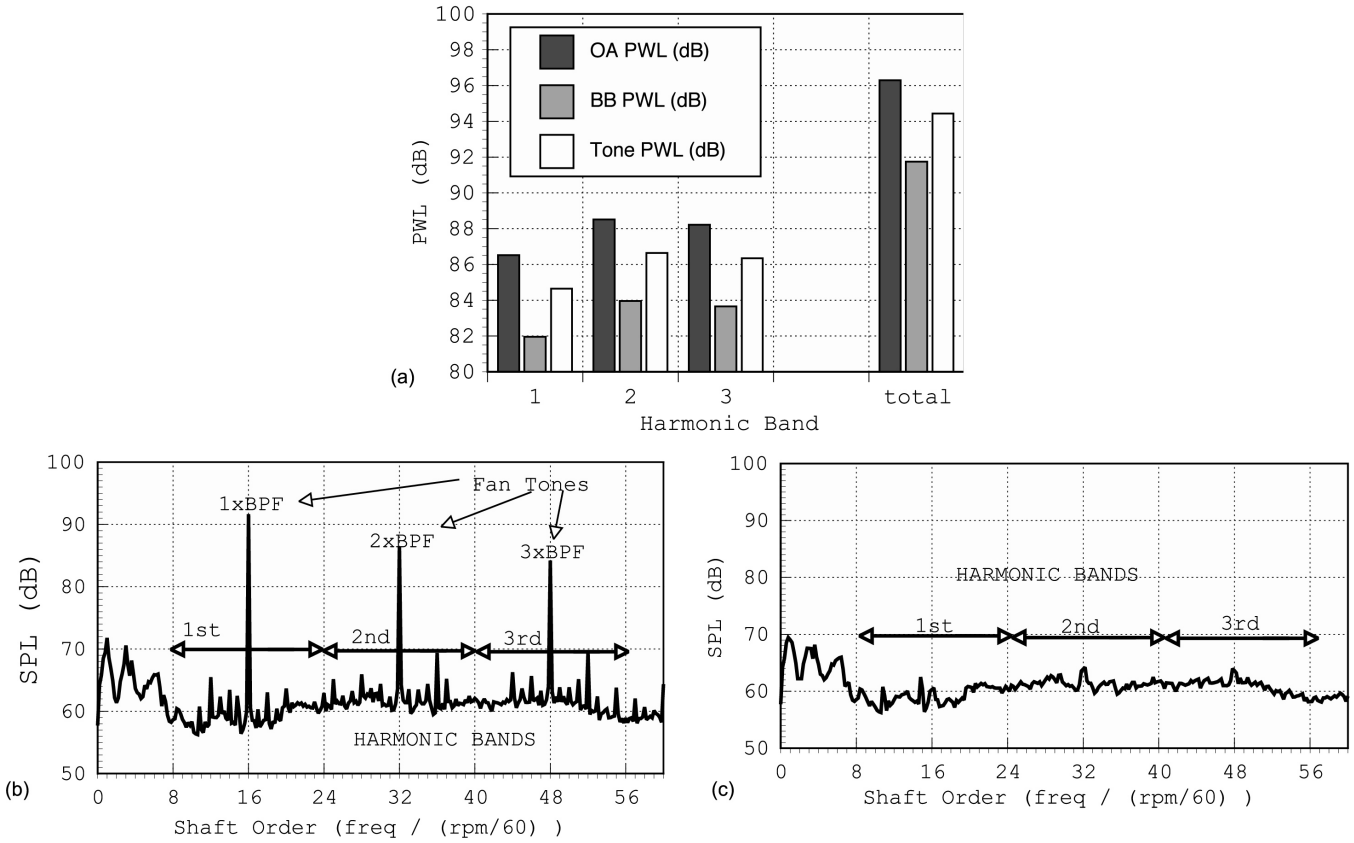

Figure 21.—Tone and broadband (BB) separation technique for dynamic data. Data acquired synchronously sampled to fan shaft at 128/rev. Frequency and time domain were averaged with spectra for each microphone integrated over harmonic bands (i.e., 0.5 to 1.5 harmonics or 8 to 24 shaft orders, etc.) multiplied by area to obtain acoustic power level (PWL). (a) Overall (OA), BB, and tone PWL in dB. (b) Harmonic bands with fan tones. (c) Harmonic bands with tones removed. Where BPF is blade passing frequency and SPL is sound power level.

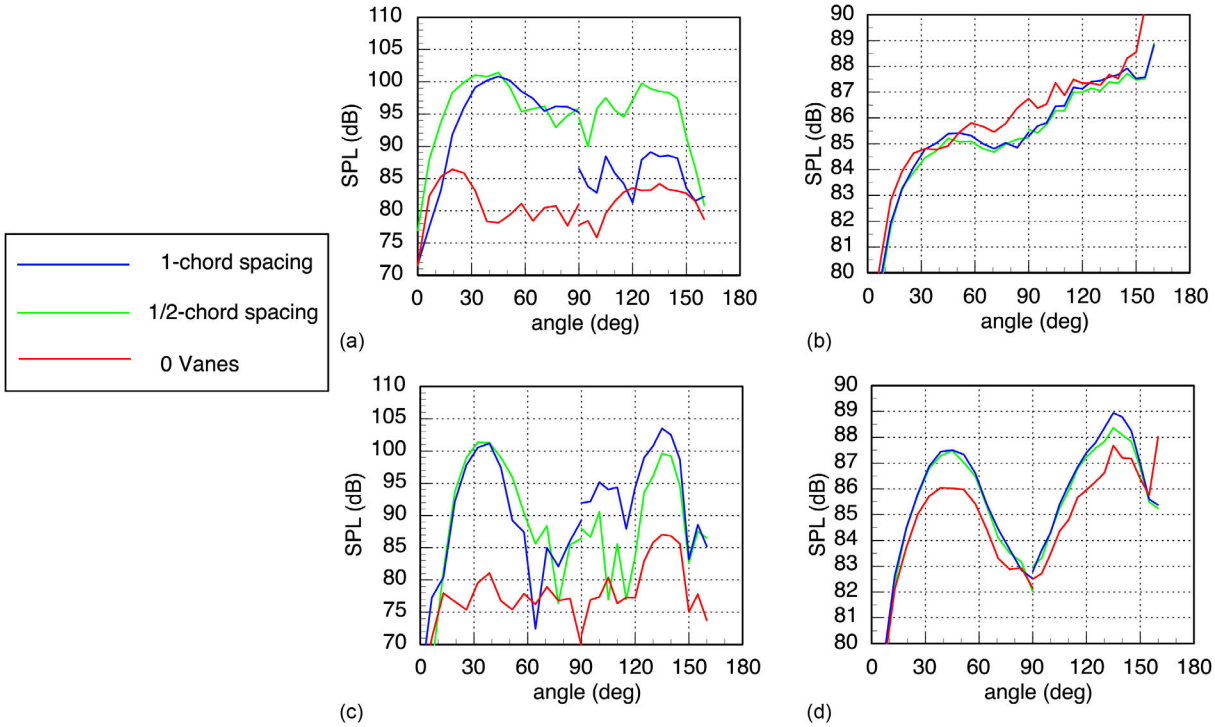

Figure 22.—Representative far-field directivity using tone and broadband (BB) separation methodology. 1 blade passing frequency (1BPF) had large 20-dB tonal penetration due to stators. 2BPF had a 1 to 2 dB increase in BB due to stators. (a) 1BPF tones. (b) 1BPF BB. (c) 2BPF tones. (d) 2BPF BB.

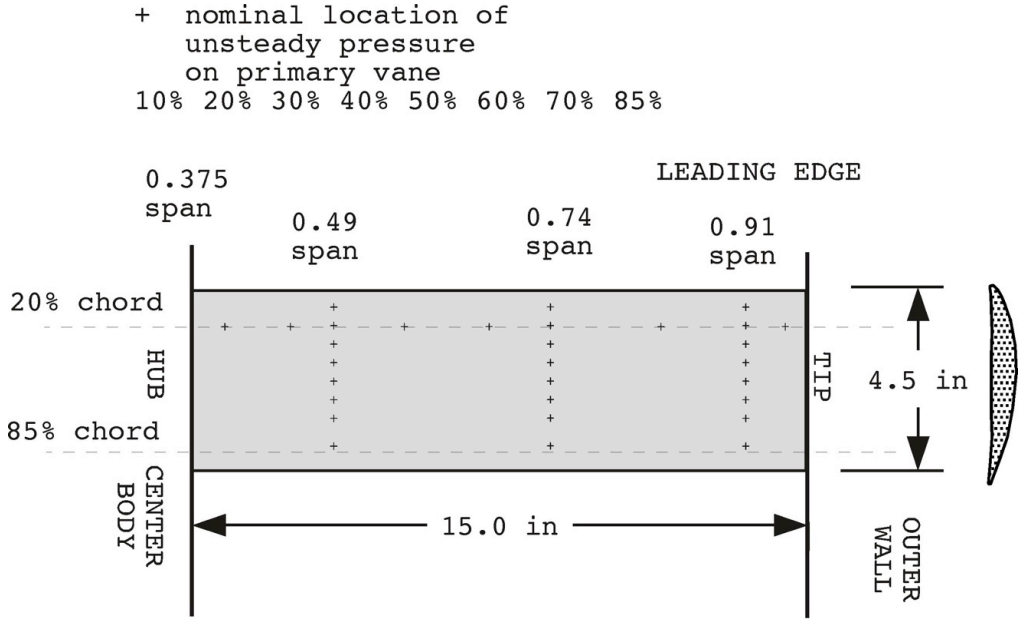

Figure 23.—Stator vane surface pressure locations.

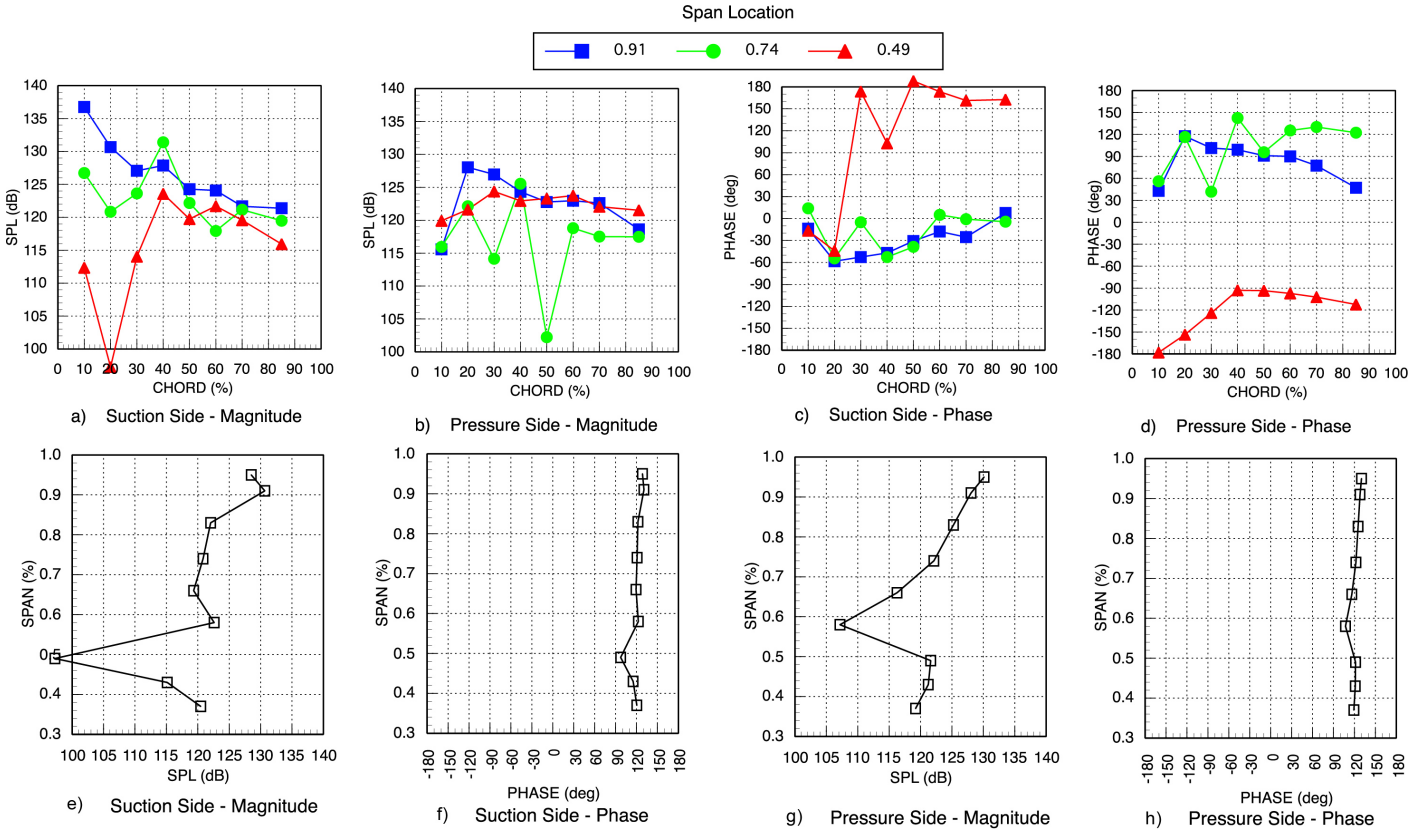

Figure 24.—Chord-wise stator vane surface pressure at blade passing frequency. (a) Suction side sound power level (SPL) magnitude along chord. (b) Suction side phase along chord. (c) Pressure side SPL magnitude along chord. (d) Pressure side phase along chord. (e) Suction side SPL magnitude along span. (f) Suction side phase along span. (g) Pressure side SPL along span. (h) Pressure side phase along span.

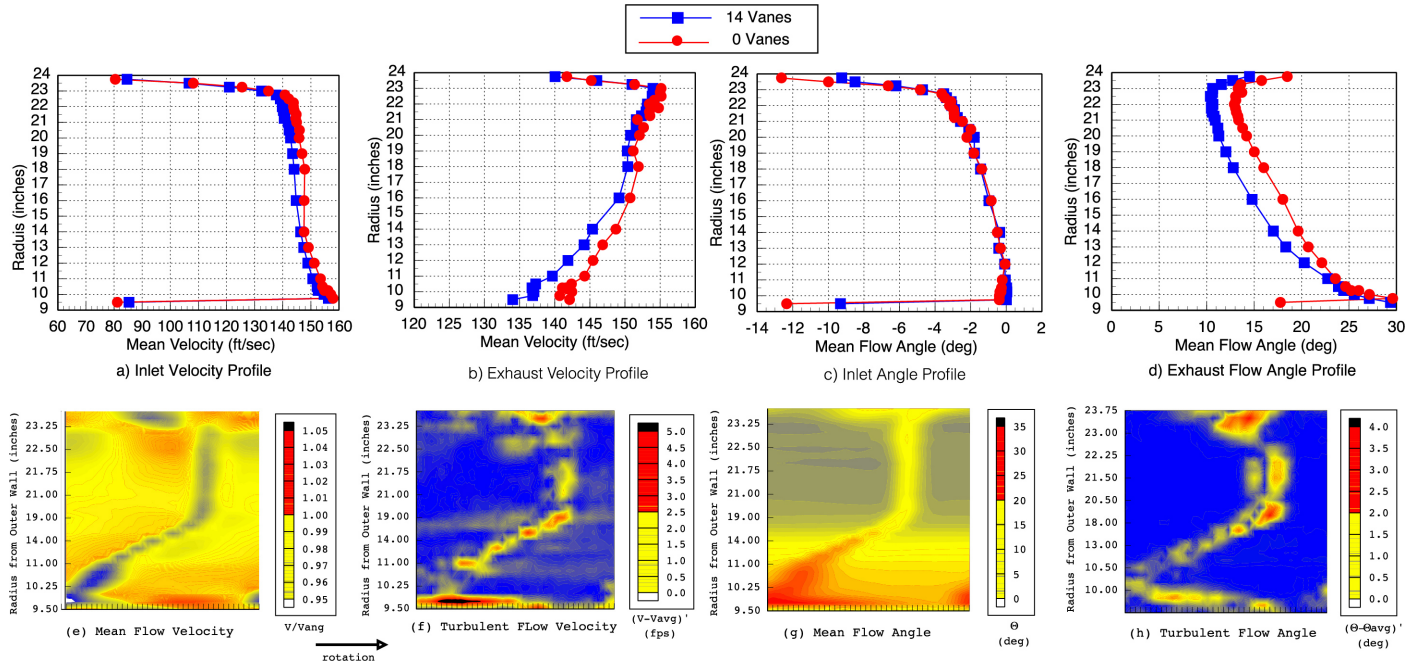

Figure 25.—Two-component hot-film contour plots measured behind rotor. (a) Inlet velocity profile. (b). Exhaust velocity profile. (c). Inlet angle profile. (d). Exhaust flow angle profile. (e) Mean flow velocity. (f) Turbulent flow velocity. (g) Mean flow angle. (h) Turbulent flow angle. Where V is velocity, V_{ang} is angular velocity, V_{avg} is average velocity, θ is flow angle, and θ_{avg} is average flow angle.

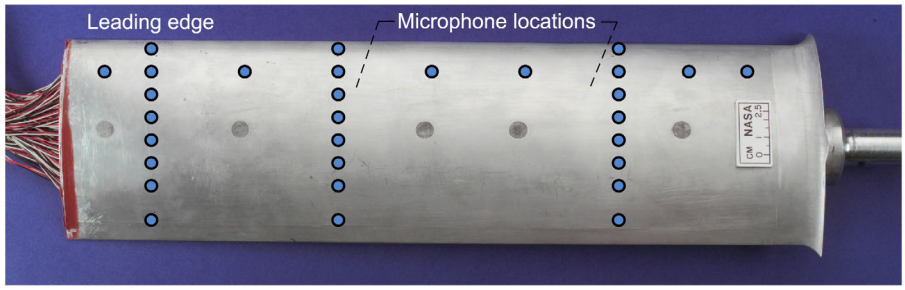

(a)

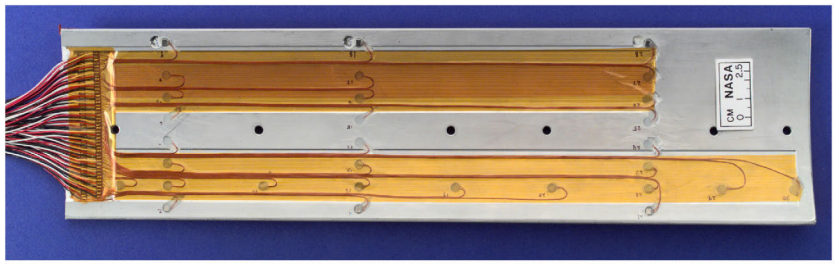

(b)

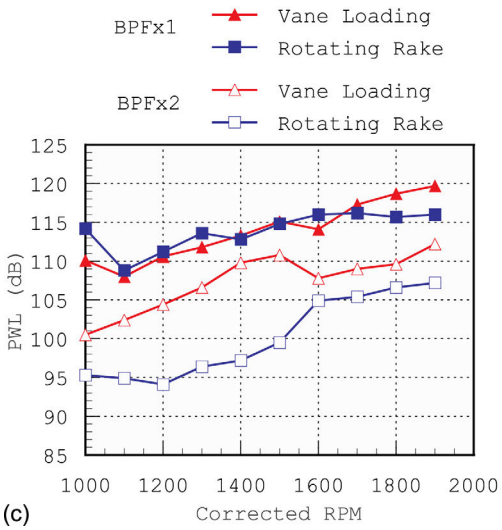

(c)

$$p_l = \frac{S_v}{10^{-12}\rho_0 a_0}\left\{\frac{1}{3}\left[\sum^{41\%,74\%,94\%}\left(\Delta\overline{P}_{rms}\right)\right]^2\right\}$$

(d)

Figure 26.—Instrumented stator vane surface and projected modal coalescence. Stator vane surface pressures are an excellent predictor of noise. (a) Stator vane microphone locations. (b) Stator vane cutaway internal view. (c) Revolutions per minute, corrected, versus acoustic power level. (d) Power equation.

3.3 Code Validation

As a result of the ANCF's geometric flexibility and its ability to acquire multiple aeroacoustic measurements, it is well suited for providing a range of conditions for code validation.

3.3.1 V072 Rotor Wake/Stator Interaction Code

The V072 Rotor/Wake Interaction Noise Prediction Code[27,28] is an analytical model widely used as a simple prediction code for RS interaction tonal prediction. It has been used in a number of cases as a preliminary design tool. An ANCF experiment[29,30] validated the code by comparing experimentally measured mode levels to those predicted by V072. V072 was used to predict the duct mode levels based on the actual wake profiles of the ANCF rotor as measured by a two-component hotwire. V072 calculates the amplitudes of the duct modes via Green's function integrals of fluctuating surface pressure distribution on stator vanes (Figure 26). The pressure distribution, in turn, is related to the upwash on the vanes shown on Figure 27. The upwash is determined from a description of rotor wake velocity profiles. In the V072 code, these profiles are developed from a set of wake correlations or they can also be specified from velocity measurements acquired downstream of the fan. The mode levels were also predicted from the V072 wake models. The experiment indicated that V072 reasonably predicts the mode level trends within the design limits of the code as shown in Figure 28.

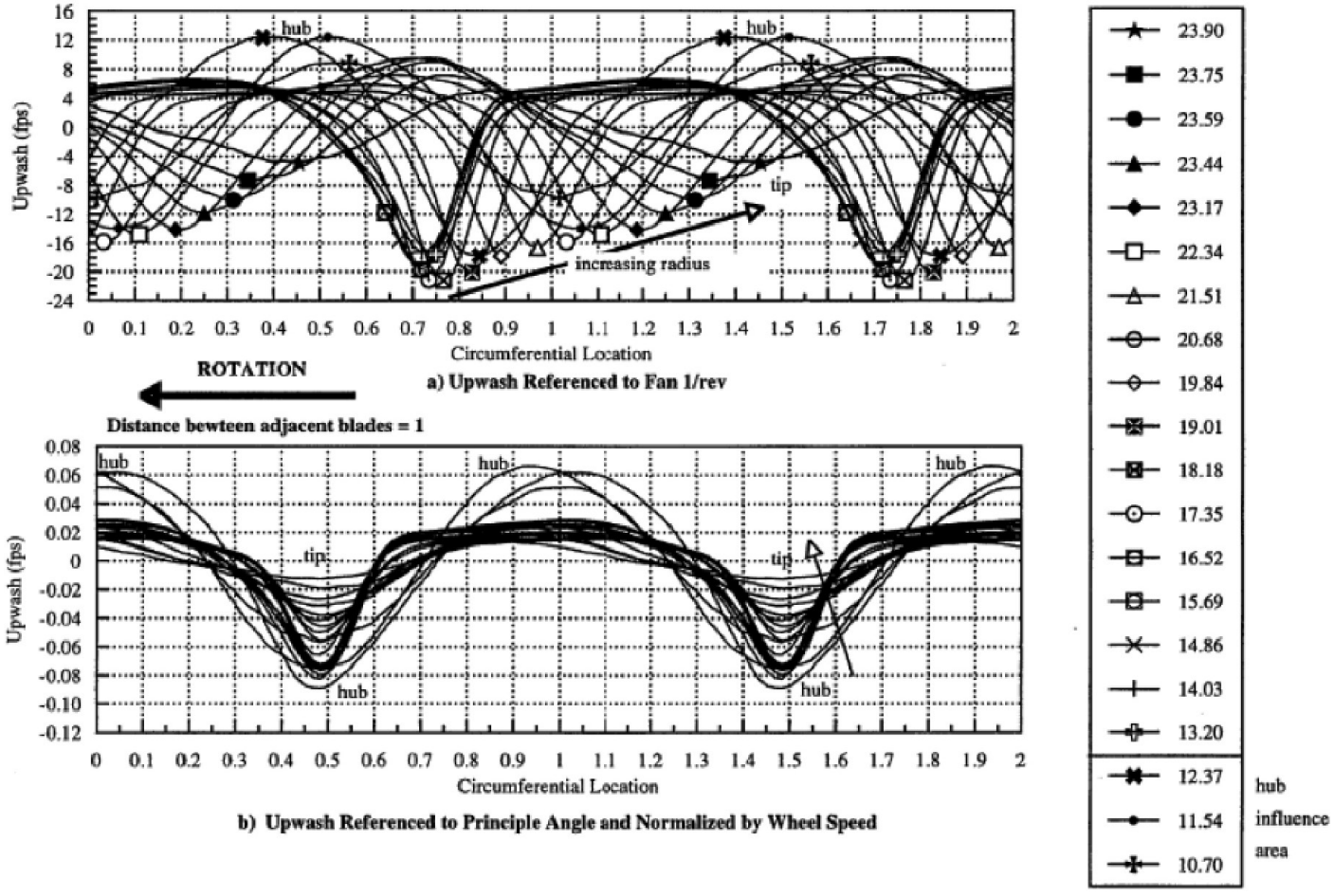

Figure 27.—Upwash from Advanced Noise Control Fan blades. (a) Upwash referenced to fan 1/rev. (b) Upwash referenced to principal angle and normalized by wheel speed.

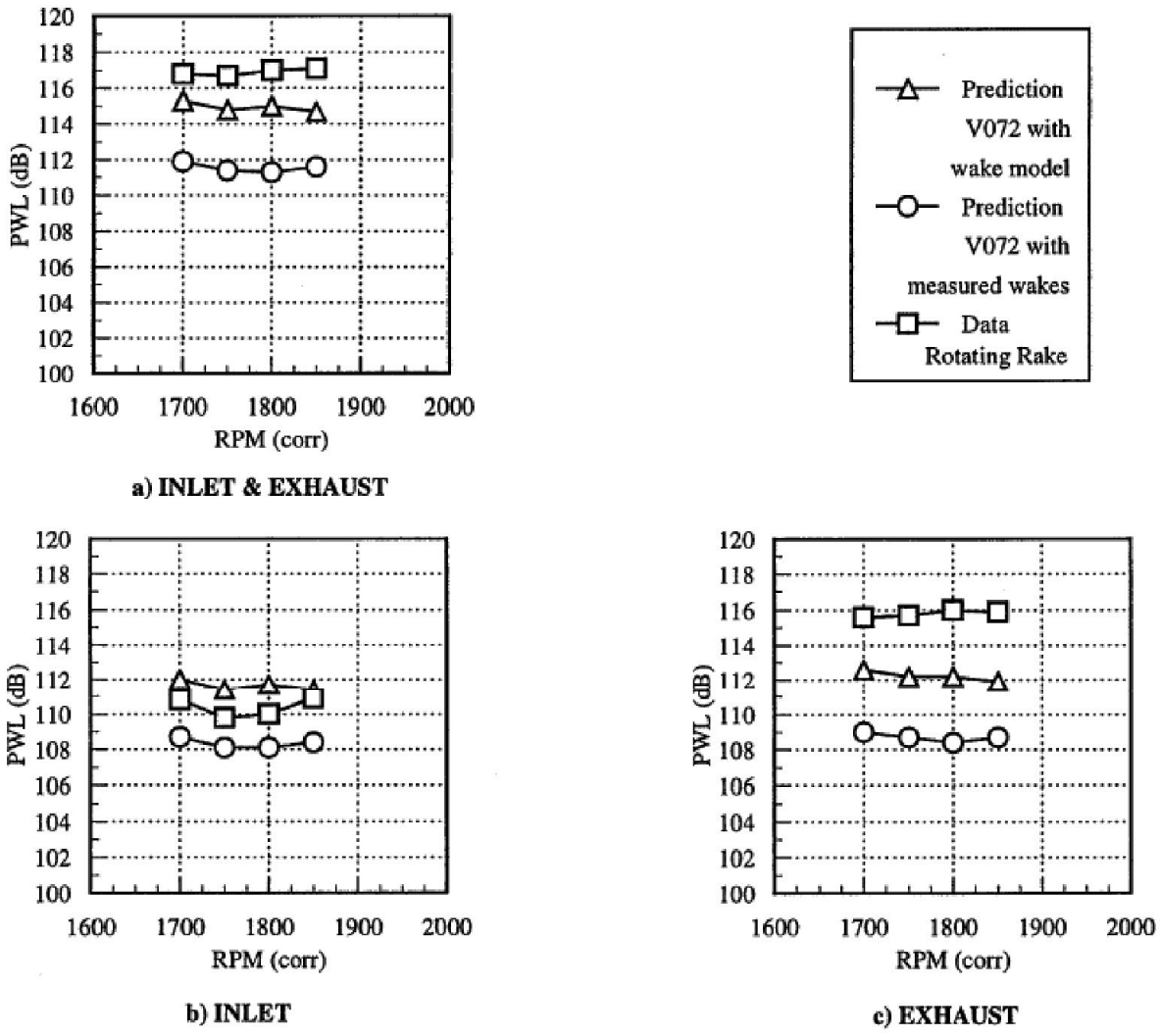

Figure 28.—Comparisons of V072 modal predictions to Rotating Rake measurements. (a) Inlet and exhaust combined. (b) Inlet. (c) Exhaust.

3.3.2 Eversman Radiation Code

The Eversman radiation code[31] is a finite-element-based propagation code to predict the duct propagation and far-field radiated sound field from in-duct modal sources.

3.3.2.1 Azimuthal Variation

The directivity of fan tone noise is generally measured and plotted in the sideline or flyover plane and it is assumed that this curve is the same for all azimuthal angles. When two or more circumferential (*m*-order) modes of the same tone are present in the fan duct, an interference pattern develops in the azimuthal direction both in the duct and far field. In this investigation,[32] two circumferential modes of similar power were generated using the ANCF. Far-field measurements (Figure 29 and Figure 30) showed substantial variations in the azimuthal direction. In-duct mode measurements were made and used as input to the Eversman code, which produced predictions in good agreement with the measured far-field directivity. Although these tests may have represented a worst-case scenario, the investigation implied that the validity of the current practice of assuming asymmetry should be questioned.

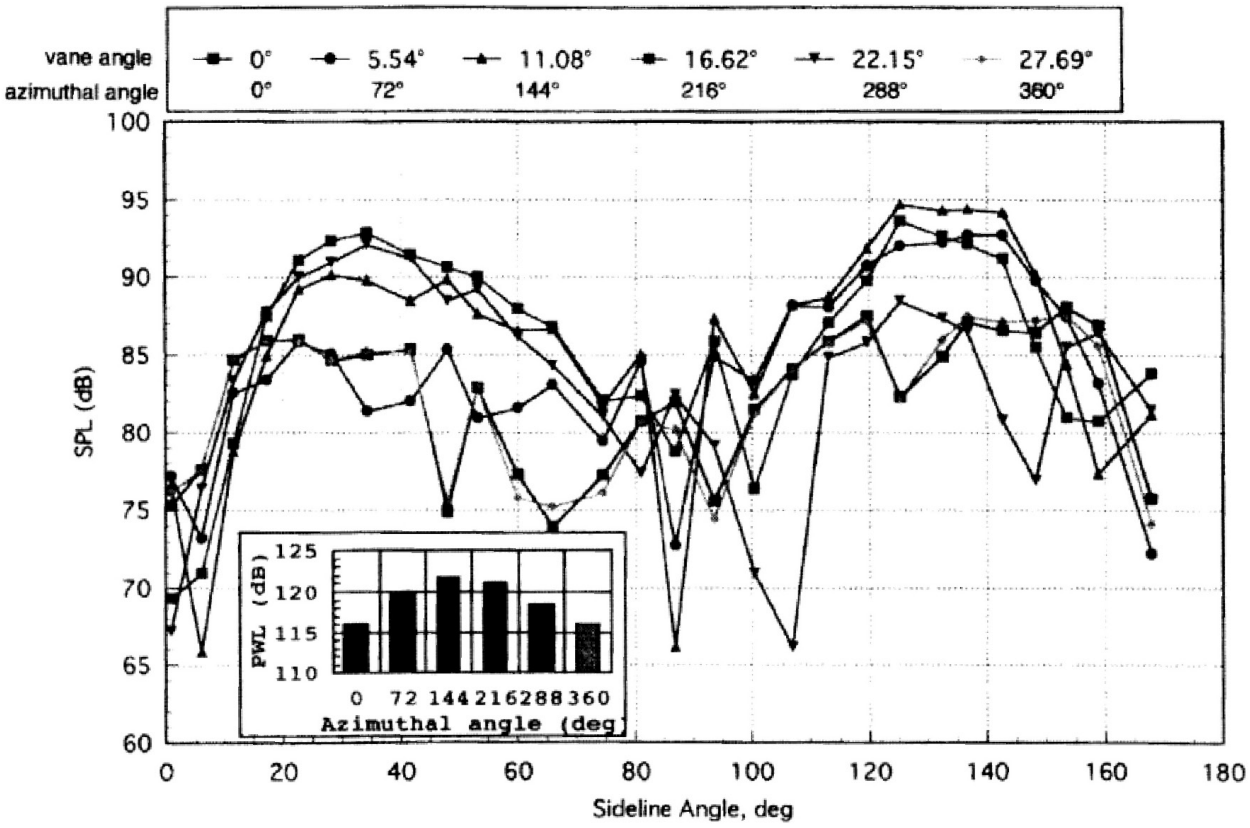

Figure 29.—Azimuthal variation of Advanced Noise Control Fan far-field directivity.

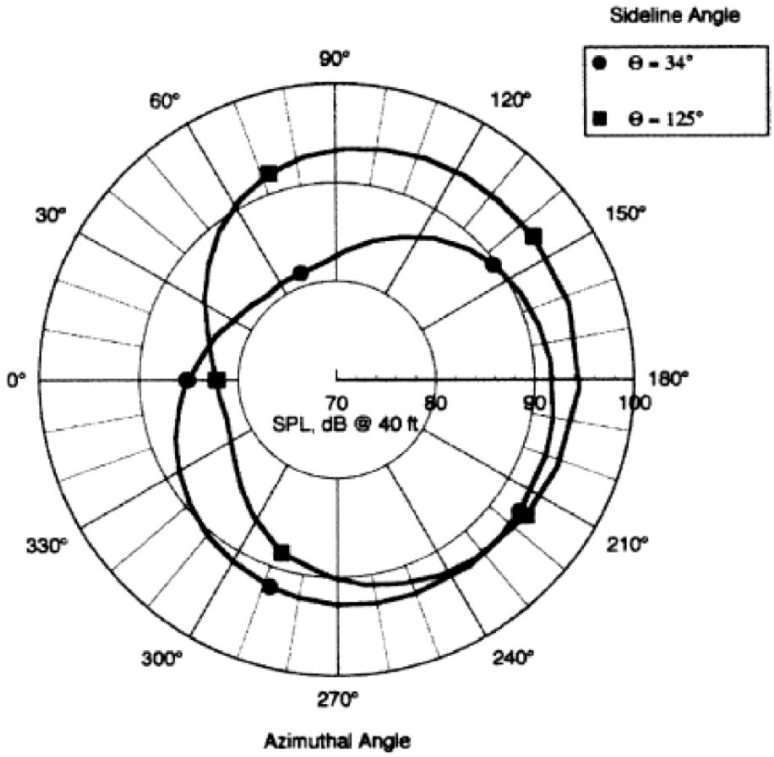

Figure 30.—Far-field azimuthal variation polar plot.

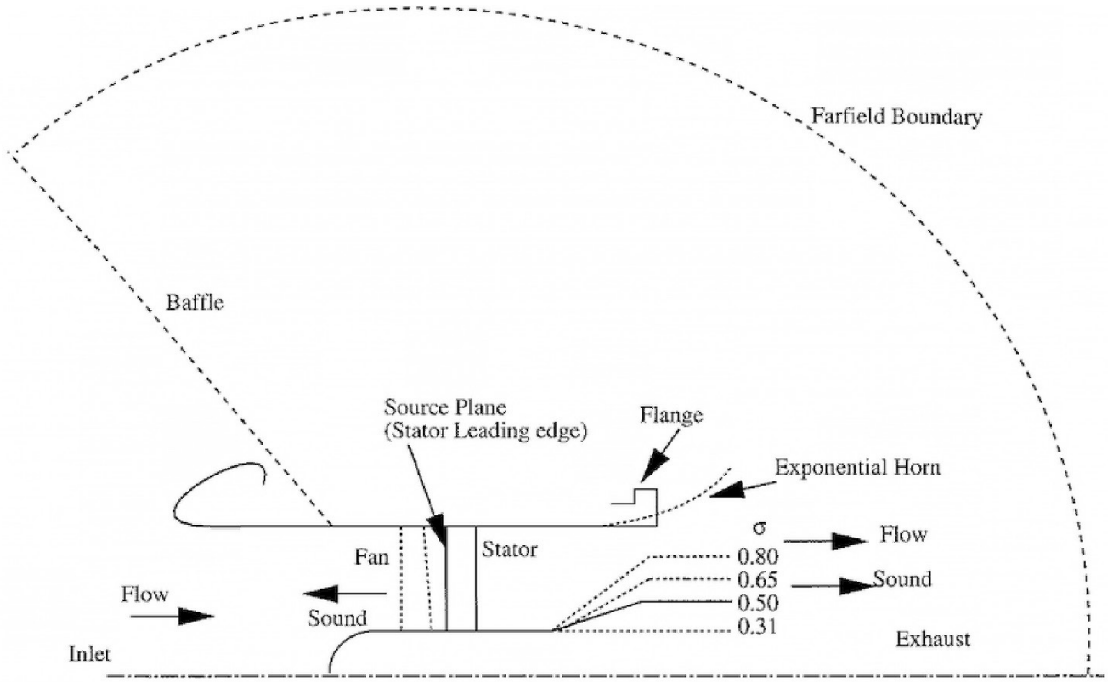

Figure 31.—Hub-to-tip, σ, ratio geometric variation (Eversman radiation code validation).

3.3.2.2 Hub-to-Tip Variation

Acoustic propagation in exhaust ducts of varying cross section was examined[33] in another specific test. The Eversman propagation code and the Rotating Rake modal measurements were employed to measure the effect of variation in the hub-to-tip ratio of the exhaust duct. Modifications to the ANCF exhaust duct inner flow path were made to increase the hub-to-tip ratio of the exhaust duct from its nominal 0.5 up to 0.80 (Figure 31). Even with very large area changes, it was shown that there is no transfer of circumferential modal power from one mode to another. An increase in exhaust hub-to-tip ratio produces a mode-dependent variation in pressure reflection coefficient and far-field shape. The principal lobe peak angle moves away from the exhaust duct axis with an increase in flow Mach number at all cutoff ratios, consistent with earlier findings. The computed axial variations of acoustic power and phase angle of acoustic pressure from the finite element solution showed good agreement with the experimental data (Figure 32).

3.3.3 Inlet Distortion

Fan inflow distortion tone noise was studied experimentally and analytically. The tone noise generated when a fan ingests circumferentially distorted flow was studied by experiments[34,35,36,37] conducted on the ANCF. The inflow was distorted by inserting cylindrical rods radially into the duct, upstream of the rotor. The rods were arranged in circumferentially irregular patterns as indicated in Figure 33. They were installed one rotor chord length upstream of the fan. Acoustic mode levels were measured in the inlet and exhaust duct of the fan using the Rotating Rake. Sound power levels (SPLs), calculated from the measured data, were plotted as a function of circumferential mode using several different methodologies described in each of the references. The predictions from the combined quadrupole-dipole method are shown in Figure 34.

Far-field and in-duct acoustic pressure measurements were recorded. An analytic description of acoustic pressure resulting from the interaction of a rotor and an asymmetric stator was presented to represent the highly asymmetric configurations tested. Trends in circumferential mode power levels were predicted and shown to be in good agreement with the measurements. This predictive capability is a beginning step in developing tools to estimate the mode power levels produced by fans ingesting distorted inflow, an area of concern for those developing aircraft with embedded engines.

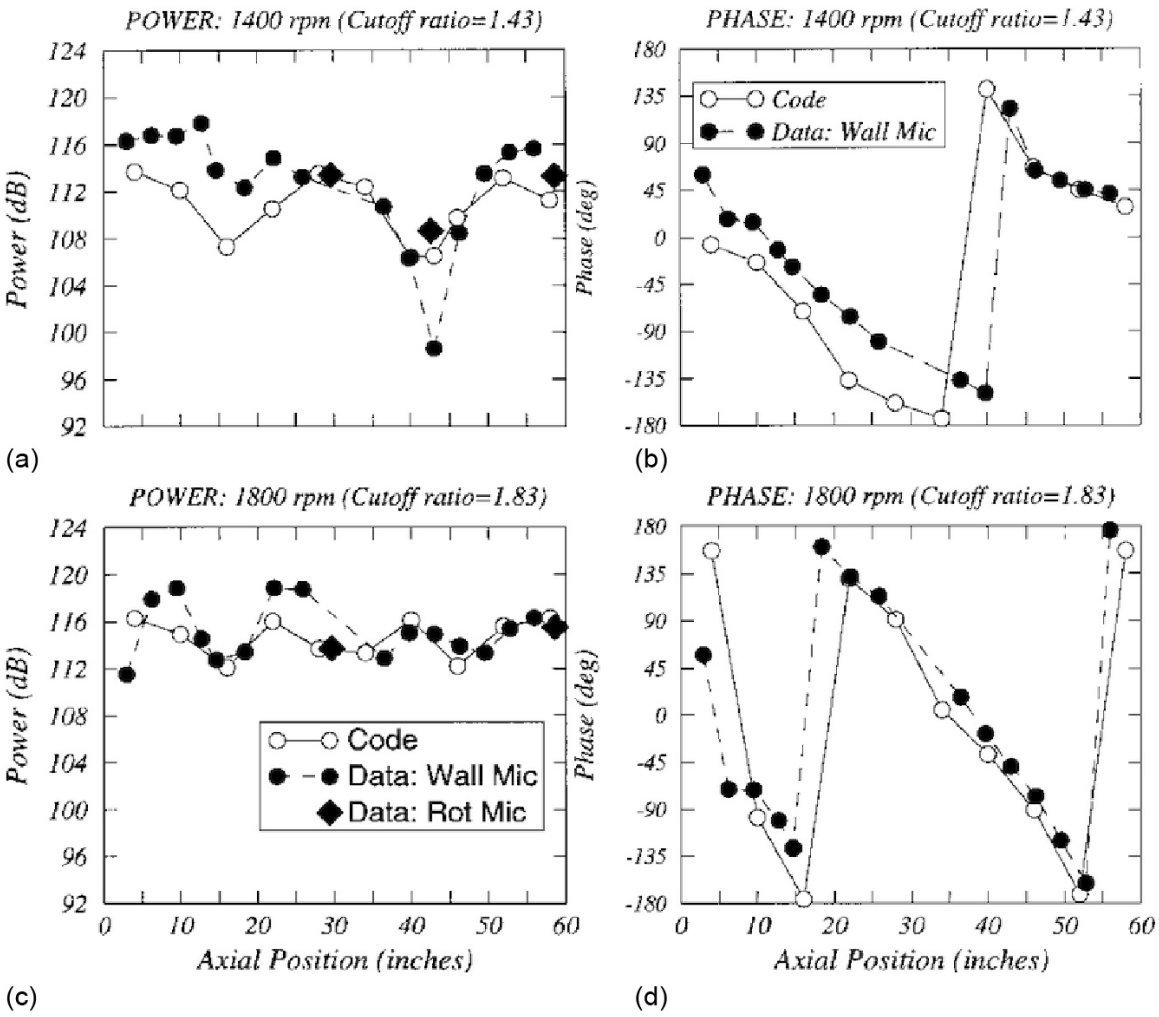

Figure 32.—Aft duct propagation (Eversman radiation code variation). (a) Power at 1,400 RPM, cutoff ratio = 1.43. (b) Phase at 1,400 RPM, cutoff ratio = 1.43. (c) Power at 1,800 RPM, cutoff ratio = 1.83. (d) Phase at 1,800 RPM, cutoff ratio = 1.83. Where Mic is microphone and Rot is rotating.

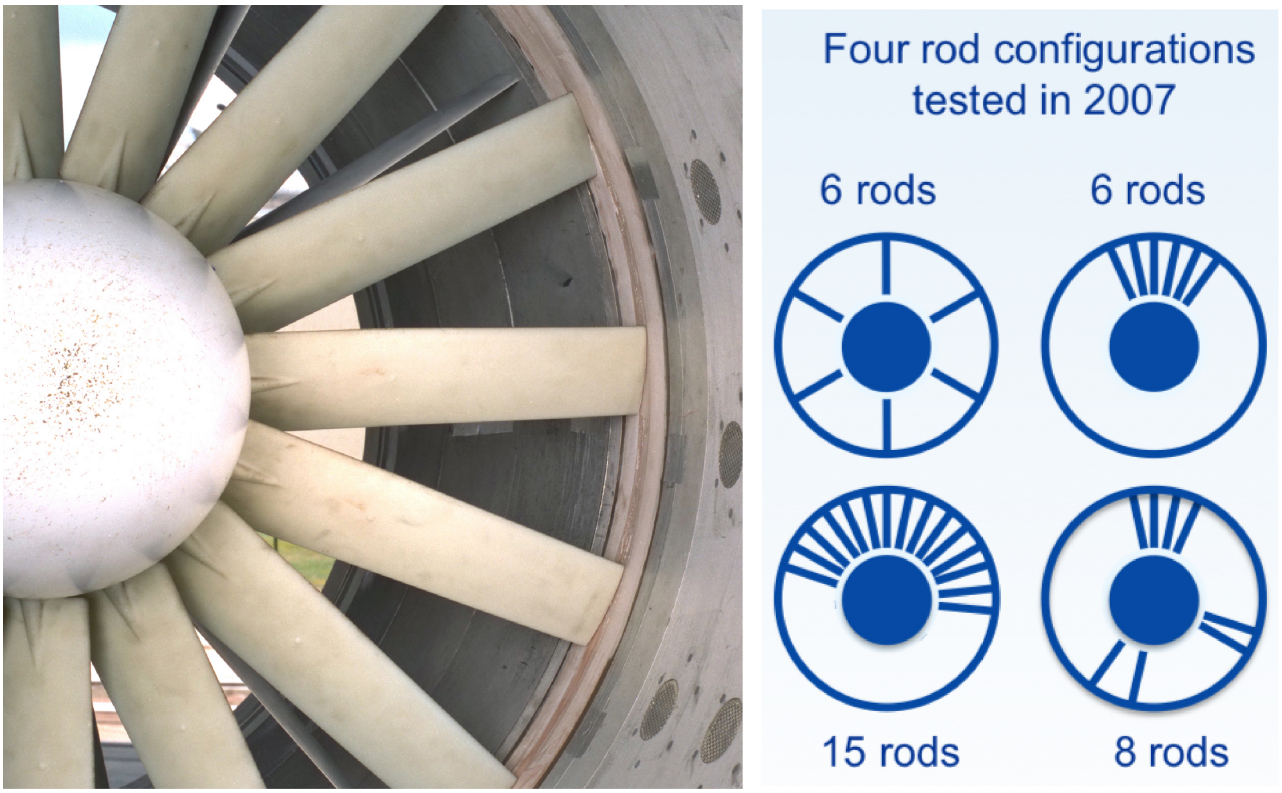

Figure 33.—Inlet distortion experiment configurations.

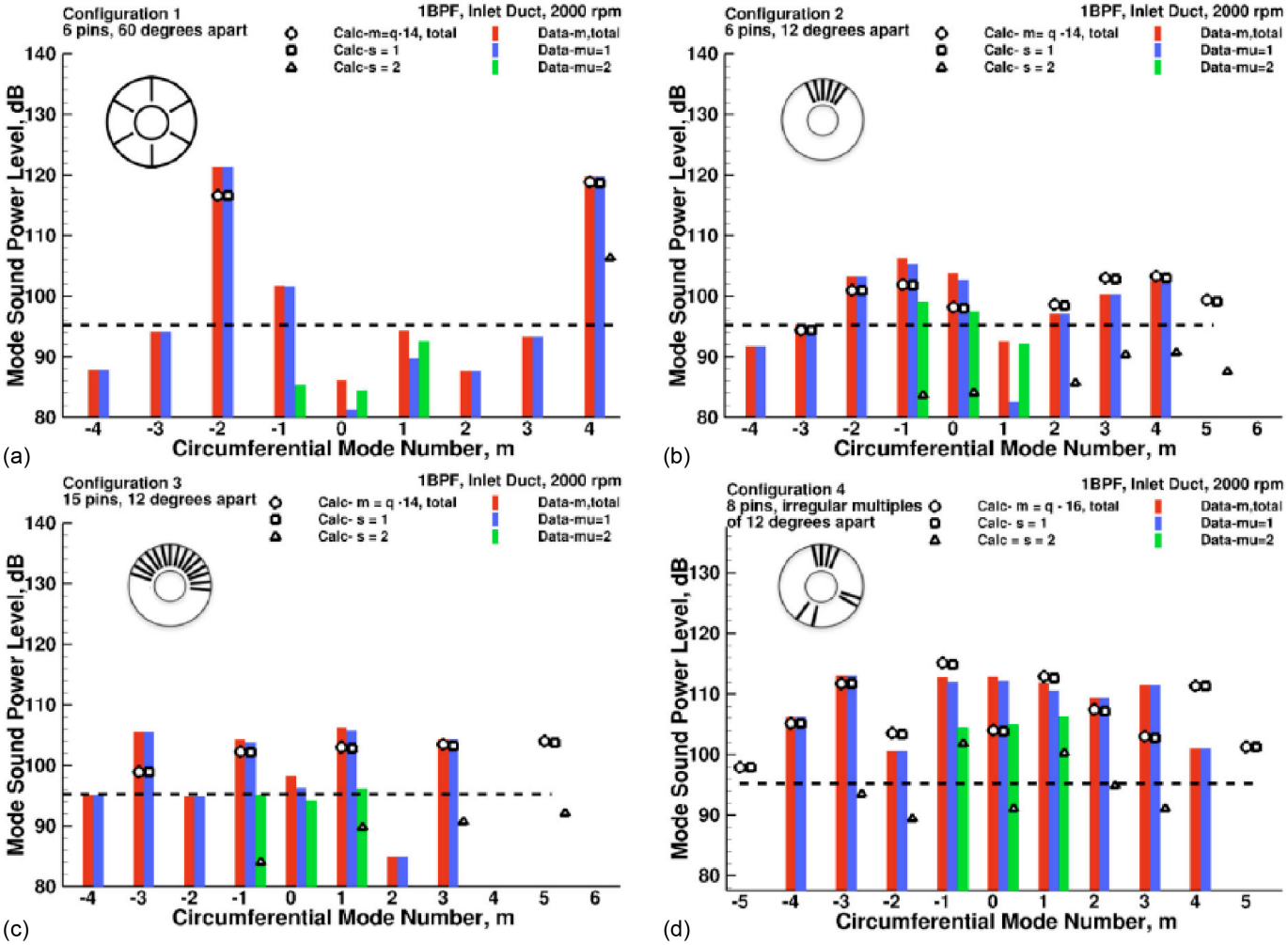

Figure 34.—Inlet distortion database sample (Ref. 33). (a) Configuration 1, 1 blade passing frequency (1BPF) with inlet duct at 2,000 RPM, 6 pins, 50° apart. (b) Configuration 2, 1BPF with inlet duct at 2,000 RPM, 6 pins, 12° apart. (c) Configuration 3, 1BPF with inlet duct at 2,000 RPM, 15 pins, 12° apart. (d) Configuration 4, 1BPF with inlet duct at 2,000 RPM, 8 pins, irregular multiples of 12° apart.

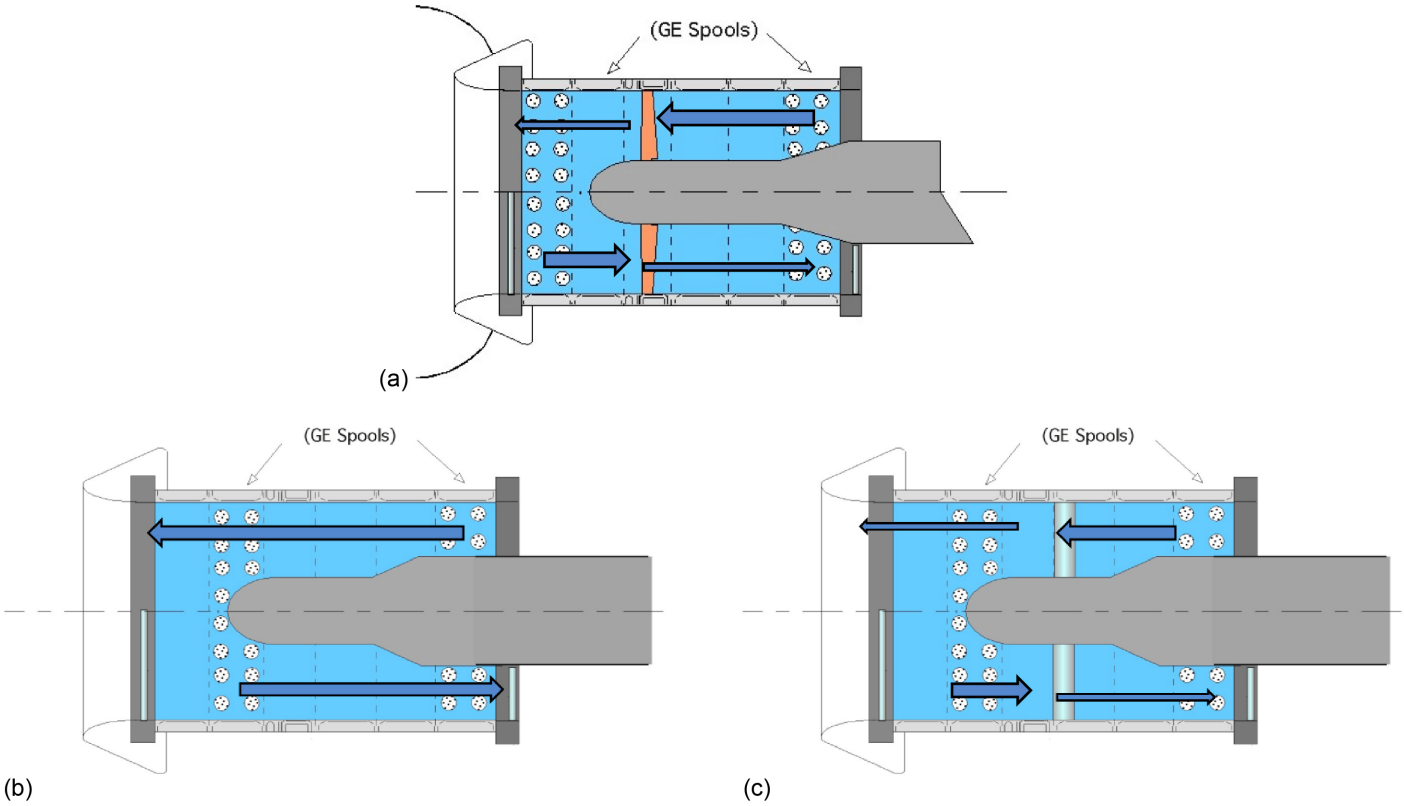

Figure 35.—Transmission loss and blockage experimental configurations. (a) Rotor alone blockage configuration at several different pitches and revolutions per minute (18°, 28°, and 38°). (b) Unblocked configuration. (c) Stator blockage configuration at several different pitches and counts (14 and 28 V at 20° and 45°). Rake and fan were desynched by approximately 1 percent to measure transmitted mode. Assume modes generated by Configurable Fan Artificial Noise Source (CFANS) in clean configuration remain consistent for all configurations and that mode source does not change with Mach number ≈0.15. Where GE is General Electric.

3.3.4 Acoustic Transmission Loss

The objective of this test was to obtain the effect of geometrical obstructions on mode propagation,[38] that is, blockage (or transmission loss). Blockage effects were measured separately for stationary geometry (stator vanes) or for rotating geometry (fan blades). In order to provide a larger database, and to take advantage of the flexibility inherent in a no-flow condition, the CFANS was used to generate modes for the study. The centerbody was retained, creating a transition from $\sigma = 0$ at the inlet to $\sigma = 0.5$ at the exhaust exit plane. The existing ANCF stator vanes were pitched at a range of angles. The Rotating Rake and data acquisition system were synchronized to the CFANS rather than the fan, so the modes measured were those generated by the CFANS and the fan modes were filtered out by the process.

The baseline case was a clean duct, with no stator vanes or fan blades. A parametric set of modes was generated at either the forward or aft driver set, and measured by the opposite Rotating Rake as illustrated in Figure 35. That is, modes generated by the forward driver set were measured by the exhaust rake; modes generated by the aft driver set were measured by the inlet rake. The Rotating Rake mode measurements were repeated with 14 or 28 stator vanes installed at various pitch angles. Separately, the rotor blades were installed at three different pitch angles. The nominal pitch angle for ANCF is 28° and that configuration was run at three different fan speeds. The fan pitch angle was changed by ±10° and run at a single fan speed for those two angles.

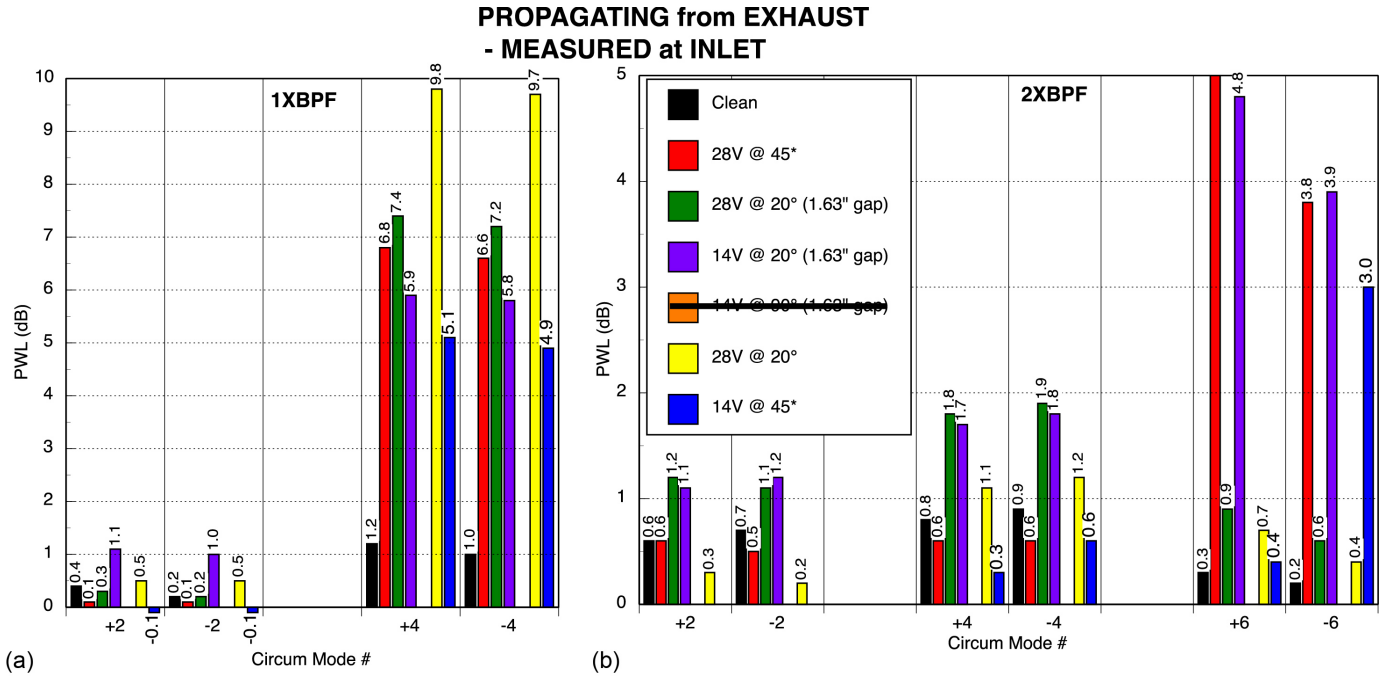

Figure 36.—Transmission loss and blockage sample results, propagating from exhaust and measured at inlet. (a) 1 blade passing frequency (1BPF). (b) 2BPF.

The assumption is made that the source does not change under these conditions so that the blockage can be computed by subtracting the mode PWL measured with stators installed from the mode PWL measured in the clean configuration (either with flow or without flow). The blockage is defined as the mode amplitude measured by the Rotating Rake with the duct in the clean configuration minus the mode amplitude measured with the desired blockage installed between the source and the rake. Thus, a positive number indicates the mode amplitude has been reduced due to blockage. Figure 36 shows the results for mode blockage at various stator vane configurations for modes at 480 and 960 Hz. Blockage levels obtained with the rotor (alone) at various rotor revolutions per minute and pitch angles are also shown in that figure.

The case labeled “clean” is actually the difference between two clean cases several weeks apart. As such, it can provide an estimate of the significance for a measured blockage value. This number is about ±1 dB. Anything less than that cannot be assumed to be a result relevant to blockage.

Little blockage is seen at low *m*-orders in either direction. These modes’ circumferential propagation angles are relatively low as a result of their higher cutoff ratios. The higher order circumferential modes (m = 4 at 480 Hz, m = 6 at 960 Hz) are significantly blocked as a result of their higher circumferential propagation angles. The stator vane count is seen to increase the mode blockage levels. Thus, it appears as if projected area is the biggest influence on blockage levels under these conditions.

3.3.5 Short Duct Effects

Duct mode propagation theory assumes a long duct as defined by the length to diameter ratio (L/D >> 1) in order for the classic mode structure to develop into the conventional analytical forms. In reality, even a cutoff mode can be said to propagate from the source, albeit at a significant decay rate. Modes that are well below cut-on may decay at a rate of 80 to 100 dB per duct diameter, while a mode just below cut-on may decay at a rate of only 2 to 3 dB per duct diameter.[4] To investigate this effect, the ANCF (in the CFANS configuration) was tested with two duct lengths, with the actuated driver row one diameter from the duct exit, or one-quarter diameter from the duct exit (Figure 37).

The modes were measured at the inlet entrance plane. The aft end of the duct was filled with absorptive material to prevent reflections as well as far-field contamination from aft duct radiation. Corresponding far-field directivity data were acquired. The far-field array was kept at a constant distance from the duct inlet entrance plane. Typical in-duct

mode results for the two duct lengths are shown in Figure 37. The generated mode was $m = +2$ or -2. For the long duct, all of the extraneous modes have decayed to the measurement floor ~75 to 80 dB. The modes in the short duct configuration have not decayed and are nearly equal in strength to the target mode. The total PWL in all modes, PWL in the generated mode, and the sum of the nontarget mode is compared. For the long duct, the majority of the power is in the target mode, but for the short duct, the extraneous modes carry measurable energy.

The effect in the far field indicates that the modes measured at the inlet plane do in fact propagate to the far field. The long duct directivity shows the characteristic flat lobe associated with a well cut-on mode. Note the symmetry between the positive and negative modes. The pattern radiated from the short duct shows significant departure from the classical directivity. It also shows an asymmetry between the positive and negative generated modes. These effects are due to the superposition of the far-field radiation from multiple modes resulting axisymmetric variation.[32]

3.4 Active Noise Control (ANC)

As mentioned in the prior sections, the ANCF was built to support the NASA ANC research efforts. ANC is the use of sound equal in magnitude, frequency, and spatial characteristics but 180° out of phase to the original, resulting in destructive interference of the original acoustic field. An ANC system[39] requires three main components: detection microphones to measure the signal to be canceled (or its residual), a control algorithm to determine the necessary signal, and actuators to generate the canceling acoustic signal. The NASA effort addressed the fan harmonics and utilized a modal approach. It implemented an increasing complexity approach by continuously introducing higher source content, actuator concepts, and more efficient control algorithms. The order of discussion that follows is not necessarily chronological, rather grouped by concept.

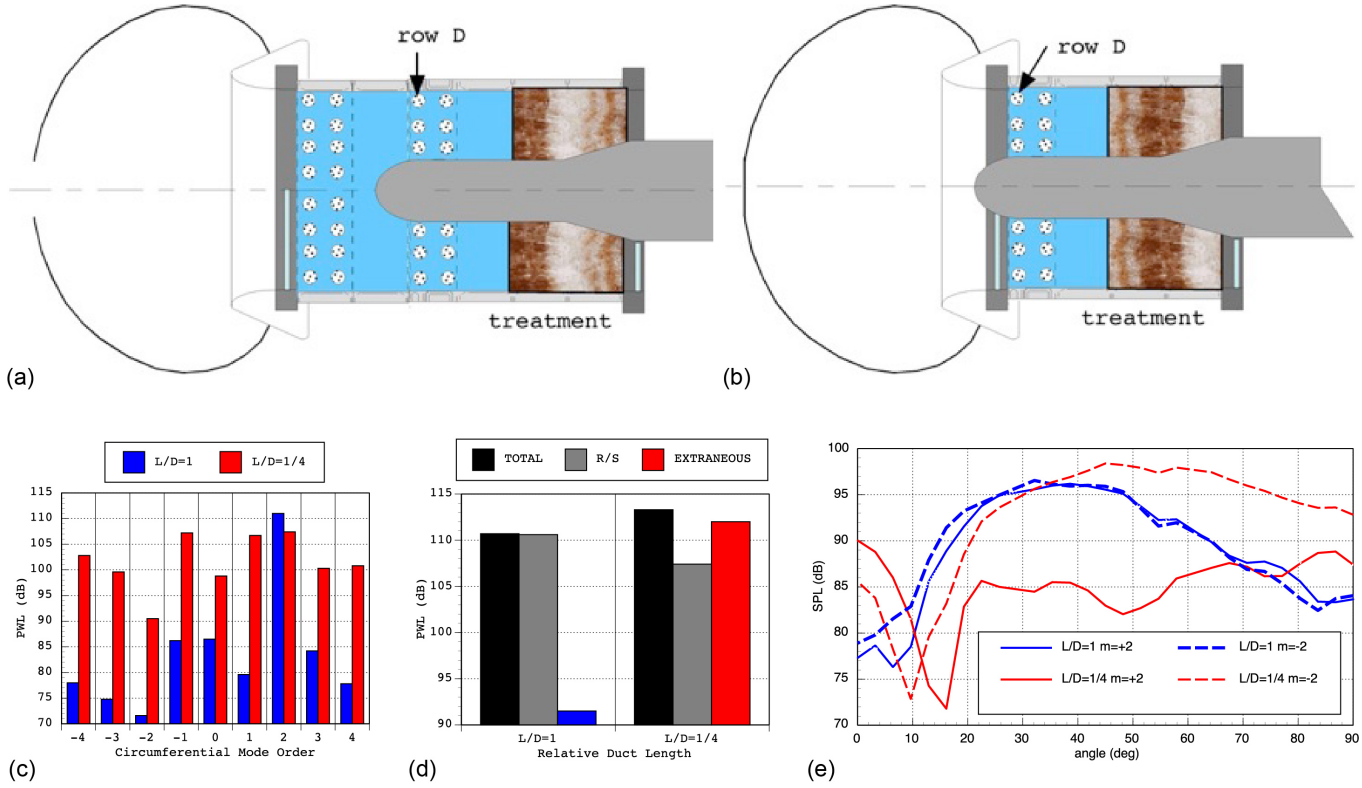

Figure 37.—Effect of short duct on modal content and far-field directivity. Trend in turbofan engines is toward shorter ducts so that infinite duct theory for mode propagation and radiation to far field may not be valid. Need to obtain database for code validation. Compares acoustic power levels (PWLs) with length to diameter ratio (L/D) of 1 to one-quarter. (a) Longer duct turbofan engine. (b) Shorter duct turbofan engine. (c) Circumferential mode order versus PWL at 1 blade passing frequency (1BPF). (d) Relative duct length versus PWL at 1BPF. (e) Far-field angle versus SPL.

3.4.1 Single Mode Using Plate Actuators

The maiden ANC test was the General Electric (GE) ANC Flat Plate Actuator study[40] (Figure 38). The goal of this study was to assess the feasibility of using wall-mounted secondary acoustic sources and sensors within the duct of a high bypass ratio turbofan engine for active noise cancellation of fan tones. The modal control system was based on a single-input, single-output (SISO) controller revolutions-per-minute feed-forward controller modal control approach. Controller inputs were signals from a shaft encoder and a microphone array that senses the residual acoustic mode in the duct. The modal controller generates the canceling modal signal. The key results were that the (6,0) mode was completely eliminated at 2BPF (960 Hz) and substantially reduced elsewhere. Global attenuation of PWL was obtained using an actuator and sensor system totally contained within the duct. This was the first successful ANC test of a complex nature.

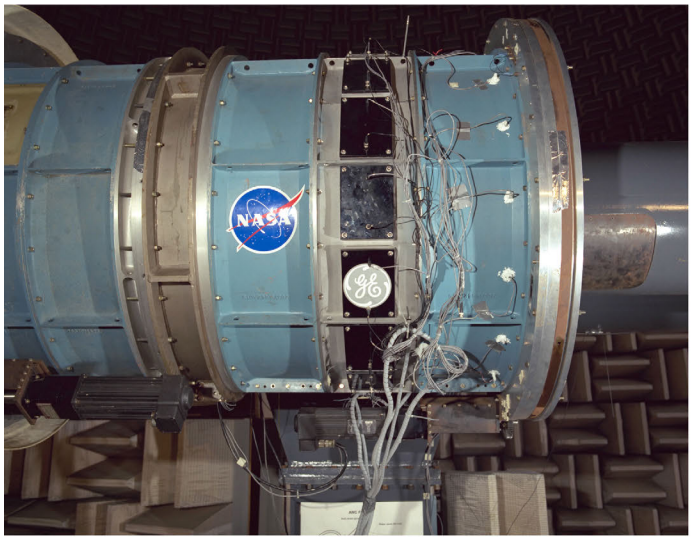

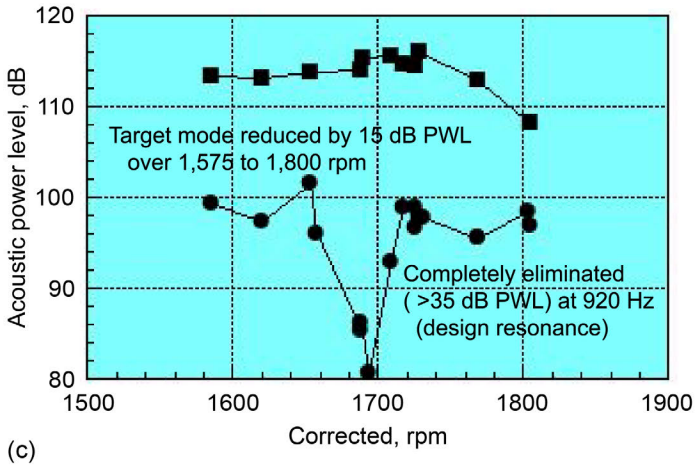

Figure 38.—General Electric Advanced Noise Control Fan using lead zirconate titanate (PZT) flat plate actuators to reduce single mode 16B, 26 V at 2BPF, mode (6,0). Documented modal control as feasible and established in-duct and far-field correlation. (a) PZT flat plate actuators system outer view. (b) PZT flat plate actuators mounted in ring source on inner duct view. (c) Acoustic power level reductions achieved versus revolutions per minute, corrected.

3.4.2 Multiple-Harmonic Control With Active Resonators

The next level in complexity was to effect control of the first two fan harmonics, with two radial modes at 2BPF in the inlet, and to provide unidirectional control (that is no increase in noise in the exhaust direction). In addition, the active resonator concept was applied. Hersh Walker Acoustical Engineering, Inc. (HWAE) developed an active-passive resonator concept,[41] whereby an active element in the actuator base extends the range of a Helmholtz resonator and the slight BB character of a resonator is maintained. The concept was successful as the three radial modes were attenuated (which actually required six control multiple input, multiple output (MIMO) control channels to prevent an increase in the exhaust). Figure 39 shows the results. The resonators were tuned at BPF and substantial attenuation is noted; the active portion has no effect. At 2BPF, the passive control has no effect and the active control reduces the far-field level.

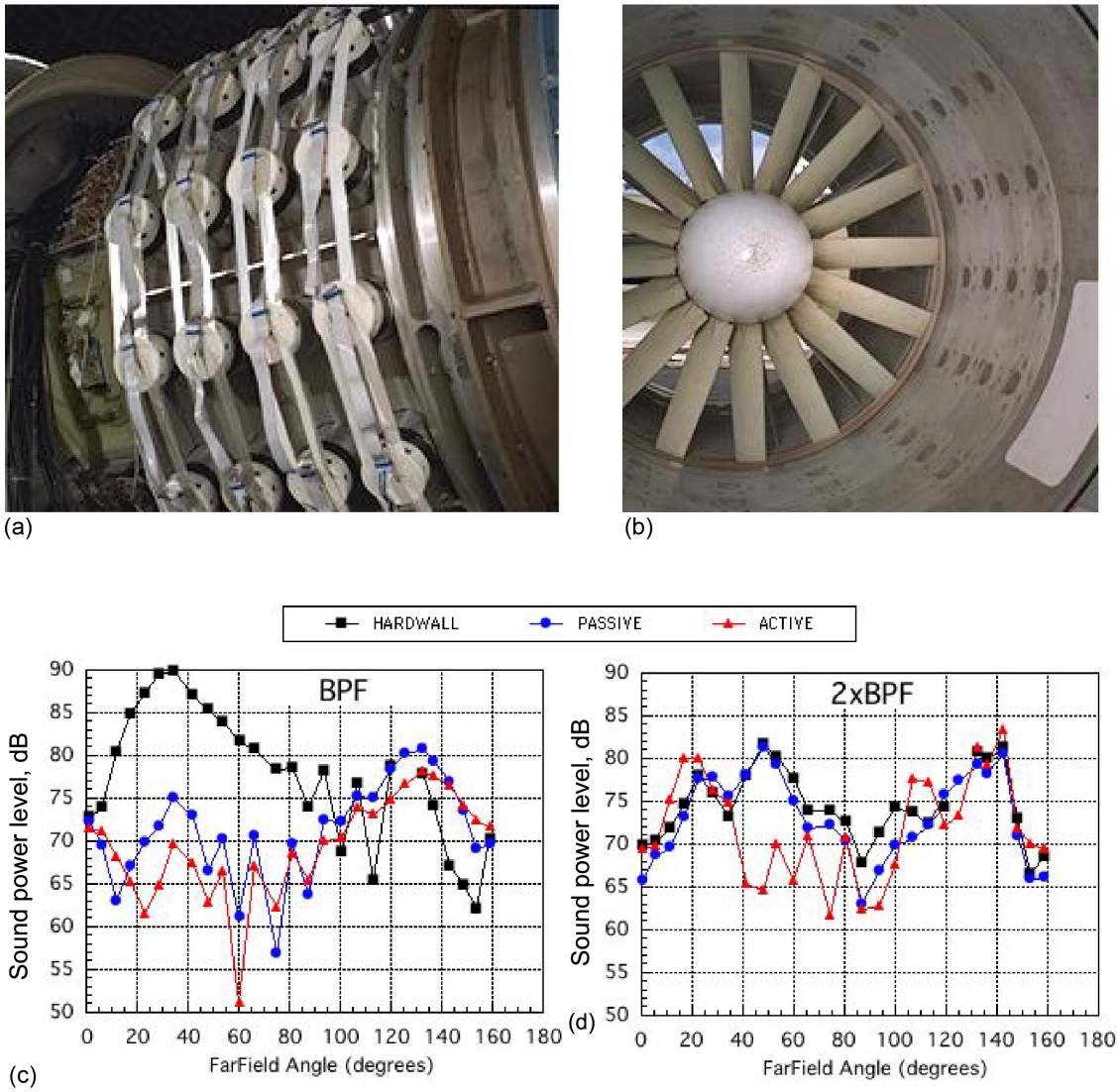

Figure 39.—Hersh Walker Acoustical Engineering active resonators. Active element in base extends range of Helmholtz resonator and broadband character maintained. Unidirectional control with no change in exhaust. (a) Active and passive resonators external mounting locations. (b) Resonator locations inside of duct. (c) Far-field angle versus sound power level (SPL) for blade passing frequency (BPF) mode (2,0).(d) Far-field angle versus SPL for 2BPF, modes (4,0)(4,1).

3.4.3 Combined Global Control of Multimodes and Harmonics Using Wall-Mounted Actuators

The number of modes targeted for cancellation continued to increase. The number of targeted radial modes was increased to four at $m = 2$, 2BPF, in a task performed by GE using four rows of wall-mounted electromagnetic speakers. This radial mode density approaches that of a cut-on BPF turbofan or 2BPF at approach. Radial modes can be more difficult to cancel since their axial wavelength can vary significantly. Indeed, this test ran into a radial distribution problem. The (2,1) mode was relatively low compared to others and was difficult to couple into and actually increased, thereby limiting the net reduction. Figure 40 shows this result. Later numerical simulations showed that this can be overcome by over specifying the ANC control system by increasing the MIMO channels or increasing the duct length for the error sensor distribution (not really a potential option).

The emphasis on simultaneously developing actuator technology was continued as HWAE integrated piezoelectric drivers surrounding the stator vanes: two rows on the duct wall near the tip and two rows on the hub near the base of the stator. The additional utilization of the inner wall provided a more efficient ability to couple to the radial modes since there were now two boundary conditions specified in the radial direction. Multidirectional control in a more compact arrangement was successfully demonstrated. Figure 41 shows the reduction in both the forward and aft far-field levels for total PWL attenuation.

Figure 42 summarizes an attempt to simultaneously control multiple modes and harmonics in both the inlet and aft ducts. This was accomplished by combining the GE and HWAE systems from the earlier tests. Simultaneous multimode control of the inlet and exhaust, with seven radials at $m = 2$ and 2BPF (four in the inlet, three in the exhaust) approaches the modal density of turbofans at 2BPF under most conditions. This combined control successfully. The exhaust reduction was nearly the same as earlier separate control results. The inlet reduction was still limited by (2,1) radial increase but performed slightly better than separate control.

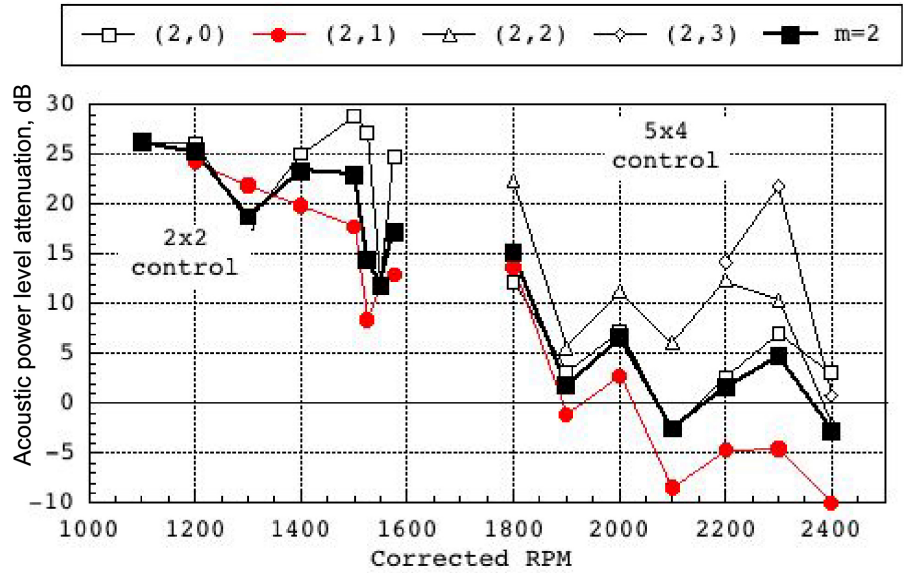

(a)

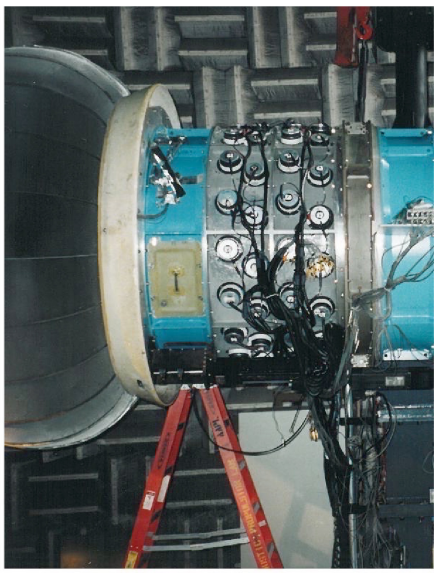

(b)

Figure 40.—General Electric multiple mode Active Noise Control (ANC). Four radials approximate modal density of blade passing frequency (BPF) cut-on or 2BPF approach. Fan (2,1) mode was relatively low compared to others; difficult to couple into and actually increased so net reduction was limited. Later simulations showed solution is to increase ANC multiple input, multiple output channels (overspecify), and increase duct length for error sensors. (a) Acoustic power level attenuation versus revolutions per minute, corrected. (b) Photograph showing multiple mode test configuration installed in inlet of ANCF.

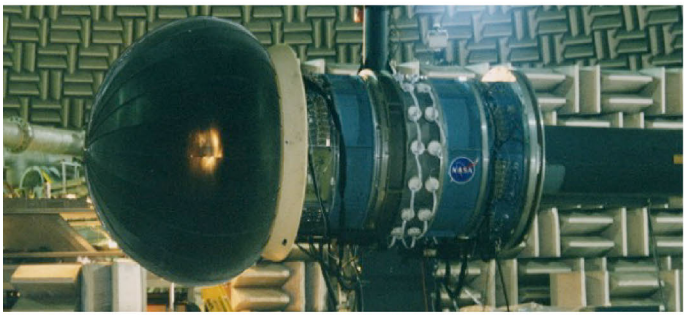

(a)

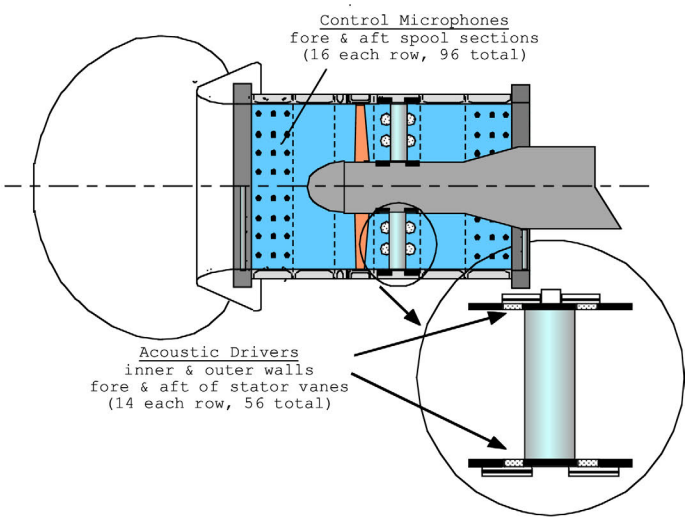

(b)

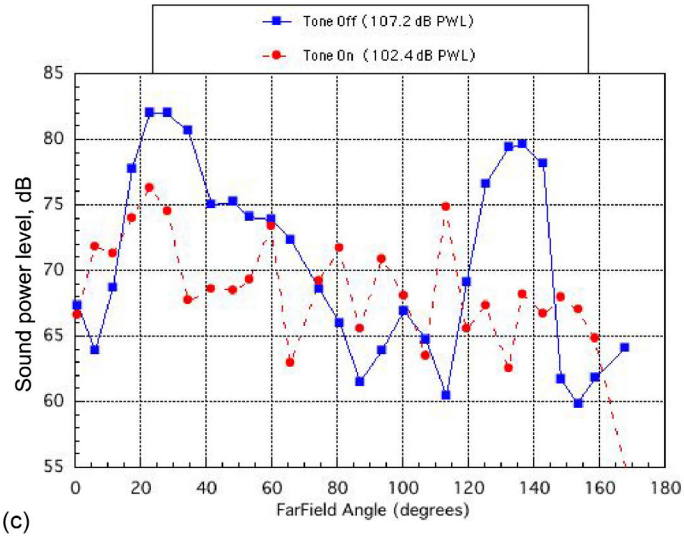

(c)

Figure 41.—Hersh Walker Acoustical Engineering, Inc., control near source. Two radials in both duct directions (equivalent to four radials) with four rows of piezo-ceramic actuators and inner wall suitable for mode coupling, multidirectional control was demonstrated. (a) Advanced Noise Control Fan positioned in Aero-Acoustic Propulsion Laboratory. (b) Test configuration diagram. (c) Far-field angle versus sound power level. Where PWL is acoustic power level.

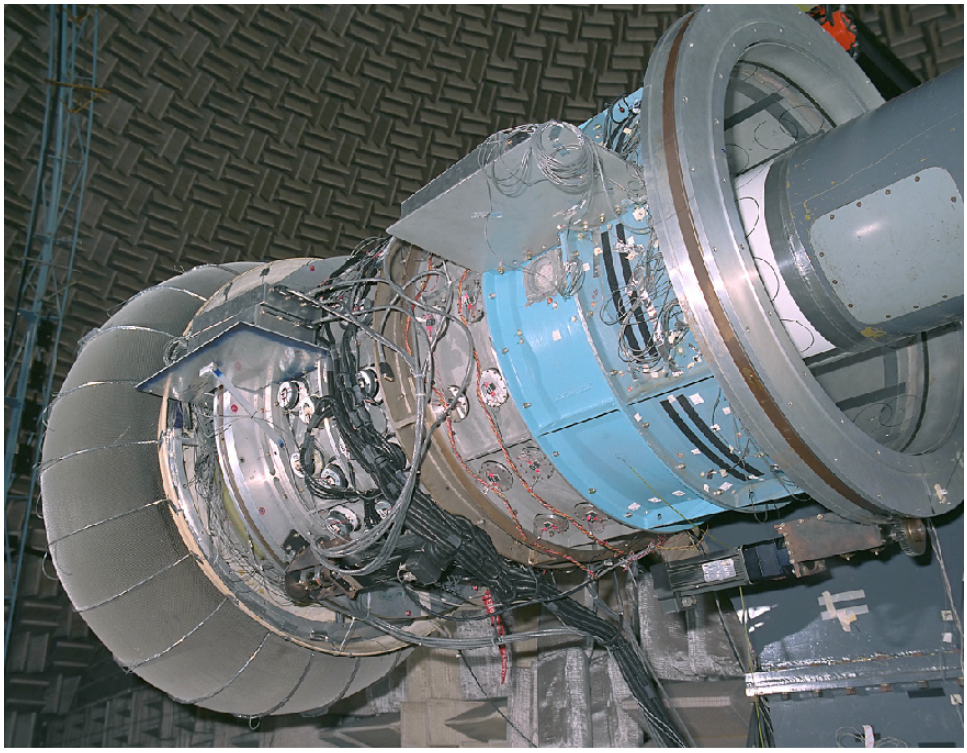

Figure 42.—General Electric and Hersh Walker Acoustical Engineering, Inc., combined Active Noise Control. Simultaneous demonstrating multimode control of inlet and exhaust: Seven radials at m = 2, 2 blade passing frequency (2BPF) (four inlet, three exhaust), which approaches modal density of turbofans at 2BPF under most conditions. Inlet: four rings of 16 electromagnetic actuators per ring. Exhaust: annular arrays of 15 equally spaced piezo/aluminum laminate actuators with two arrays on each, outer and inner duct wall. Combined control was successful; exhaust reduction nearly same as separate control, up to 15-dB-mode acoustic power level reduction; inlet reduction limited by (2,1) radial increase, slightly better performance than separate control.

The preceding tests used the adaptive-quadrature (A–Q) control algorithm in single and multitone suppression systems, based on bandwidth capability, rapid convergence, and processing simplicity. The A–Q algorithm performs the following functions in sequence:

- Measures the fan signal from all error sensor channels
- Injects the BPF harmonic signal into each controlled actuator channel and measures the fan plus actuator signal from all error sensor channels
- Subtracts the fan signal from each fan plus actuator to error sensor transfer function
- Computes and applies the minimum-norm actuator channel drive vector (complex) that will combine with the fan noise to produce a minimum in the sum of the squares of the error signals
- Following the initial adaptation, the system sequentially perturbs the real and imaginary parts of the actuator drive signals and determines online corrections to maintain the minimization of the error signals

Unlike the Filtered-X or similar algorithms, which process an externally synthesized reference signal for application to the actuators, the A–Q algorithm generates the real and imaginary parts of control signals using lookup tables and uses a fan tachometer only for system timing. The results of the solver in the algorithm are multipliers for the reference signals, so that the actual control calculations can be carried out at a slower rate than the signal input/output (I/O). Control updates must, however, occur more rapidly than fluctuations in fan parameters.

The phase retarding network was implemented using all analog components to minimize digital I/O and signal processing burden. The disadvantage of this approach is that microphones must be well matched in each annulus and that a separate network is required for each mode to be resolved. Generalized ANC system design guidelines indicate that minimums of *N* independent control channels are required to control *N* radial modes. In summary, it consists of

- Eleven circumferential arrays of 10 error sensors: 5 in the inlet, 3 each on the inner and outer exhaust duct walls
- Microphone preamplifiers and spatial filter networks to produce a mode $m = 2$ output signal from each microphone array
- Nine-input, eight-output A–Q controller, including 2BPF sine and cosine signal synthesizer timed by the fan tachometer and processing means to seek the least mean square (LMS) sum 2BPF error signal
- Eight signal distribution systems: 4 to drive 16 actuators each with a 45° per actuator phase advance; 4 to drive 15 actuators each with a 48° per actuator phase advance
- Power amplifiers and electromagnetic actuators arranged in four circumferential arrays of 16 each in the inlet duct
- Power amplifiers and piezo-aluminum actuators arranged in two inner wall and two outer wall annuli of 15 each flanking the stator vanes

Controller algorithms were implemented on a PC-based digital signal processor board, with the following I/O assignments:

- Nine error signal inputs
- 128× fan shaft pulses timing signal input
- Eight control channel outputs
- Sine and cosine reference signals output
- Direct current output proportional to mean-square error

All signal outputs were conditioned for anti-aliasing or signal reconstruction using eight-pole low-pass filters with a pass-band limit of 1,250 Hz. Following installation of microphone and actuator arrays on ANCF, a final calibration was conducted for each transducer.

3.4.4 Multiple Radial Modes Using Vane Actuators

Taking advantage of the radial coupling of the vane mounted actuators, attenuation of higher order radials was attempted in two separate entries[42,43] as depicted in Figure 43. Two RS configurations were evaluated. These generated (4,0:1) or (2,0:3) modes at 2xBPF. The development of the vane actuators was based on THUNDER (Thin UNimorph DrivEr and sensor) actuator technology implemented by BBN. These are highly resonant to enable higher amplitudes to be generated, potentially at the level of full-scale turbofans, at least at approach.

The core control system implemented a synchronous multichannel Filtered-X LMS algorithm. The control and source filters were three-tap digital finite impulse response (FIR) filters. The source was identified in the presence of the disturbance in a two-step process. The first step designs a set of parallel digital filters that internally cancel the disturbance tone. These filters are then used to detect the increment in residual microphone signals when the controller in turn activates each of the four-actuator arrays. The controller then designs a set of 24 filters that model the transfer function from each controller output through each actuator array to each microphone array and controller input. The source identification can also be run with the fan disturbance noise at a different frequency to the actuator drive signals when a function generator is then used to clock the controller. The core control is then implemented. This is a synchronous adaptive feed-forward scheme based on the Filtered-X LMS.

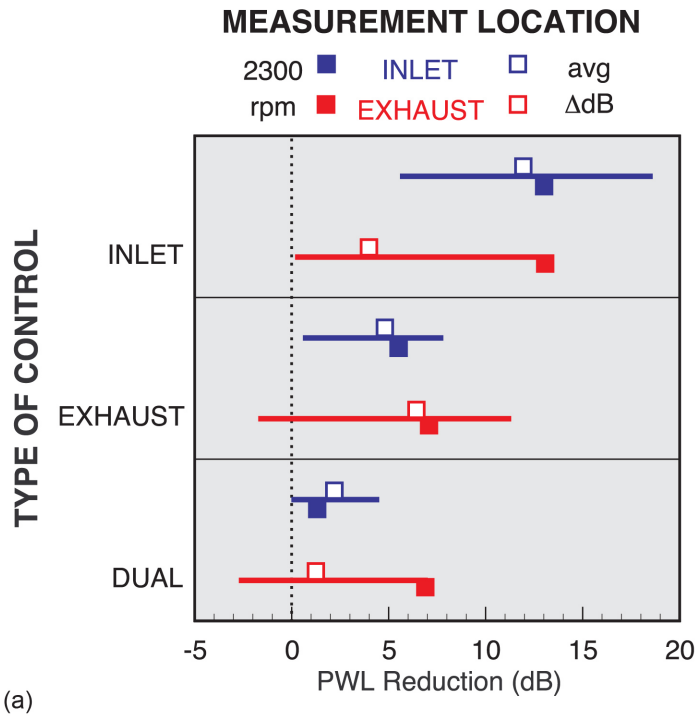

(a)

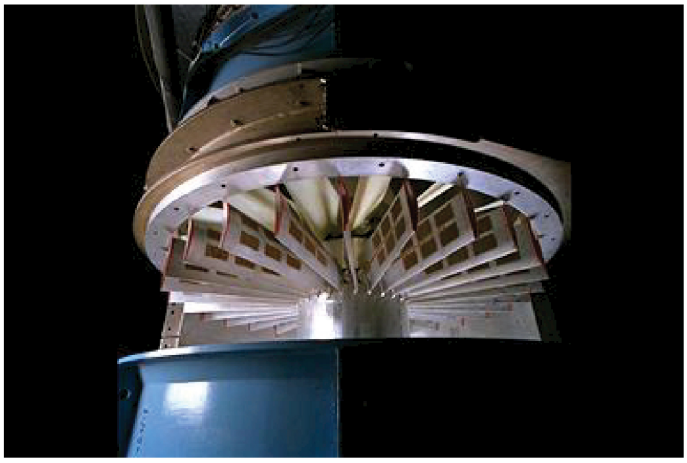

(b)

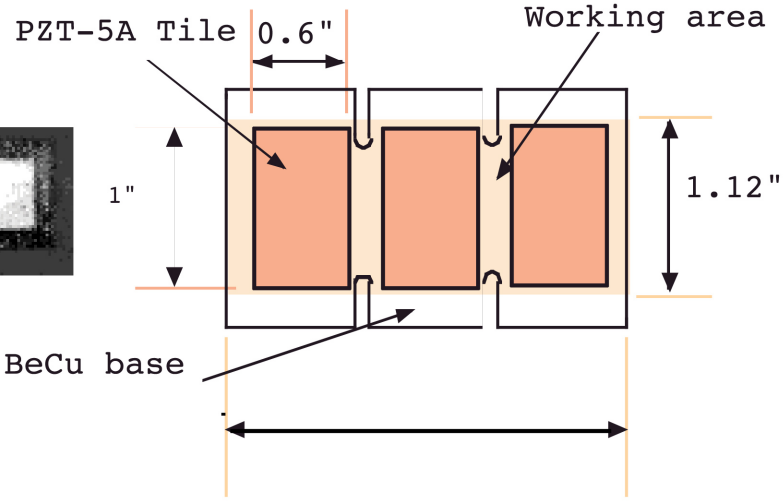

(c)

Figure 43.—BBN Technologies vane actuators Active Noise Control. Lead zirconate titanate (PZT) actuators embedded in stator vane requires less duct length and couple better to radial modes. Using unidirectional control array results in both inlet and exhaust reductions due to close-coupling of source and antisource. (a) Sound power level reduction versus type of control. (b) Photograph showing vanes with actuators installed in ANCF. (c) PZT actuator diagram.

The results were the vane actuator ANC system reduced total power levels in the target modes in the inlet while at the same time exhaust power levels were reduced. The reduction in the 2BPF-tone PWL was achieved in the inlet and in the exhaust. A simplified control system with just two actuator arrays at different radial locations was demonstrated to simultaneously reduce tonal power in both inlet and exhaust. A benefit of vane actuators is that they act at the source of the disturbance. If both fan interaction and control sources are at the same location and are both dipole sources, then they should couple with the duct aeroacoustics in the same way. The baseline control strategy was successful, resulting in control of the seven radials in $m = 2$ (four in the inlet, three in the exhaust). An important result from the baseline configuration was the simultaneous reduction in the inlet and exhaust when control was attempted in the inlet only. To say this is essentially an underspecified control system is a substantial simplification. The reason for this dual control may be due to the close physical proximity of the antisource (actuators) and the source (stator vanes). Other configurations in this test tended to confirm this result.

3.4.5 Active-Passive Hybrid Control

After the successful demonstration of ANC, it was recognized, and studies showed, that any loss of treatment required to install an ANC system would result in penalties due to the loss of treatment that could be greater than that obtained from the ANC.

Hersh Acoustical Engineering, Inc. (HAE)/Rice developed an ANC system[44] that was coupled to a Grumman passive liner. The ANC portion of the combined system was to set up the two-targeted radial modes ((4,0) and (4,1)) so that the passive liner was more effective at cancellation. Figure 44 shows the optimized active-passive liner achieved a greater reduction than either alone. Keeping the passive liner in the configuration maintained the BB attenuation. Indeed, the combined system yielded greater attenuation than the sum of the active and passive acting separately with the hybrid generating a synergistic effect as intended.

While the aforementioned hybrid configuration demonstrated the efficacy of a combined and/or active system, the passive liner extent was reduced to incorporate sensors into the hard wall (HW). A passively treated duct section was used to investigate fully incorporating passive treatment into an ANC system that embedded the sensors. A duct section with bulk passive treatment of 1.4 to 0.5i design specific impedance and an L/D of 0.375 was installed in the inlet. Two inlet control error arrays were used: a standard set with all four circumferential error-sensing arrays upstream of the treatment and the other with two of the four arrays embedded in the treatment. Comparisons were made of the ANC performance with baseline HW (treated section taped over) to ANC performance with the treated section exposed. A comparison was made between the typical method of using the error-sensing microphones upstream of the exposed treatment and embedding the microphones in the treatment. Embedding the error microphones in the treatment can simplify the system by shortening the inlet length.

Figure 45 shows the ANC reduction obtained in the target mode PWL with the liner section exposed. The reduced levels achieved with sensors embedded in the liner are similar to those obtained with the sensors embedded in the upstream HW section, demonstrating that control can be successfully achieved with standard LMS convergence algorithms with sensors embedded in a liner. The demonstrated result that the embedded sensors are similar to or better than those obtained with the sensors in the upstream untreated duct section is important, since it indicates that there is no noticeable noise reduction performance penalty associated with embedding error sensors in wall treatments. The ability to embed the sensors in the treatment increases the flexibility for the locating error sensors in ANC systems and avoids any noise reduction performance penalties associated with eliminating a very small portion of the passive treatment.

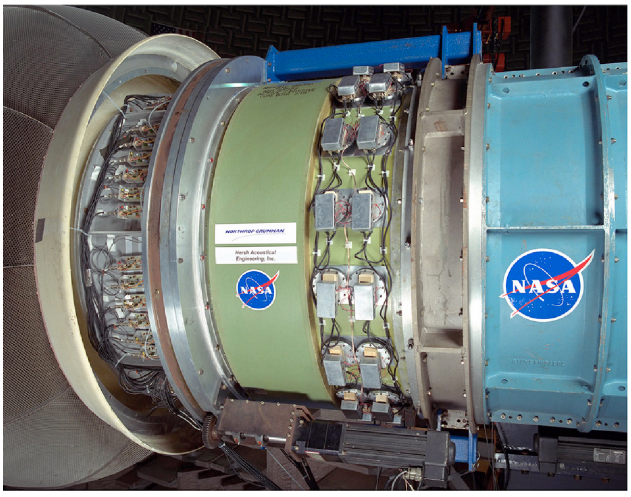

(a)

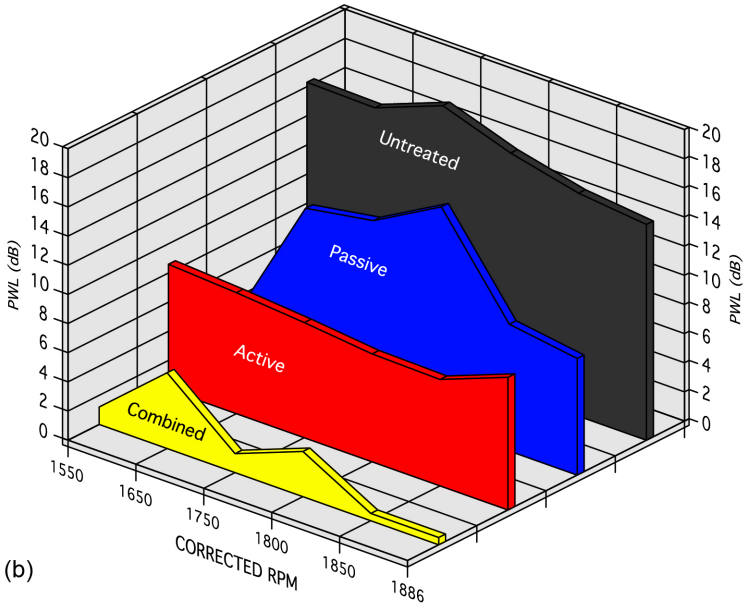

(b)

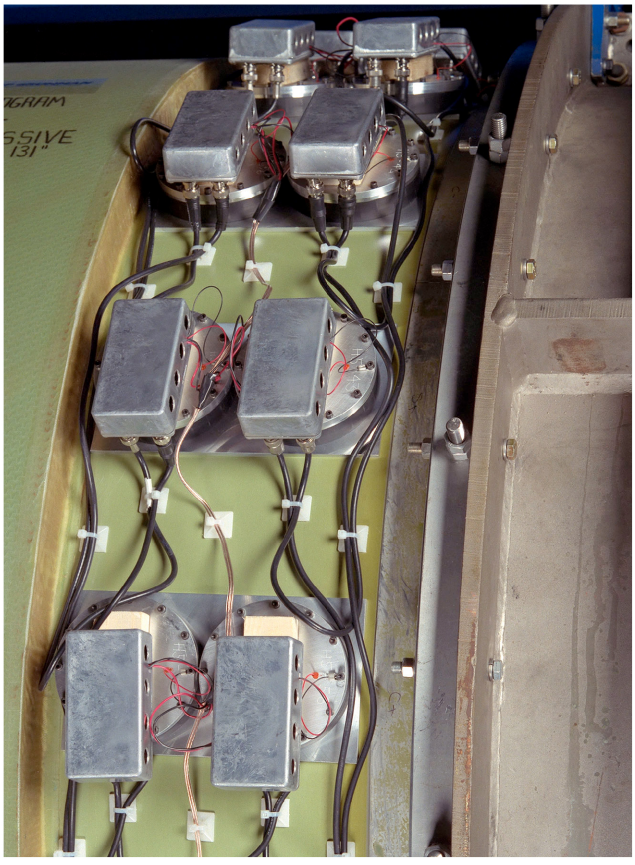

(c)

Figure 44.—Grumman-Hersh Acoustical Engineering, Inc./Rice hybrid Active Noise Control with multiple radial modes (4,0) and (4,1) and integration of active with passive treatment optimized as a system (active-passive hybrid). Elimination of multiple radial modes demonstrated, and integrated passive treatment to maintain broadband reduction. Carefully designed active-passive hybrid yields synergy. (a) Advanced Noise Control Fan (ANCF) positioned in Aero-Acoustic Propulsion Laboratory. (b) Sound power level versus revolutions per minute, corrected. (c) Photograph showing microphone preamps mounted on ANCF.

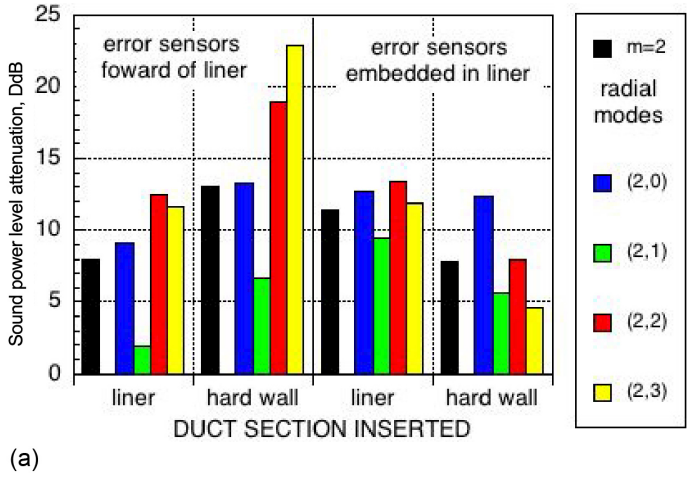

(a)

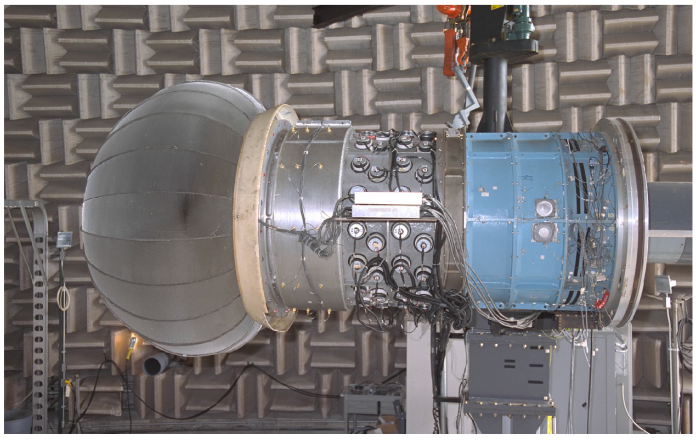

(b)

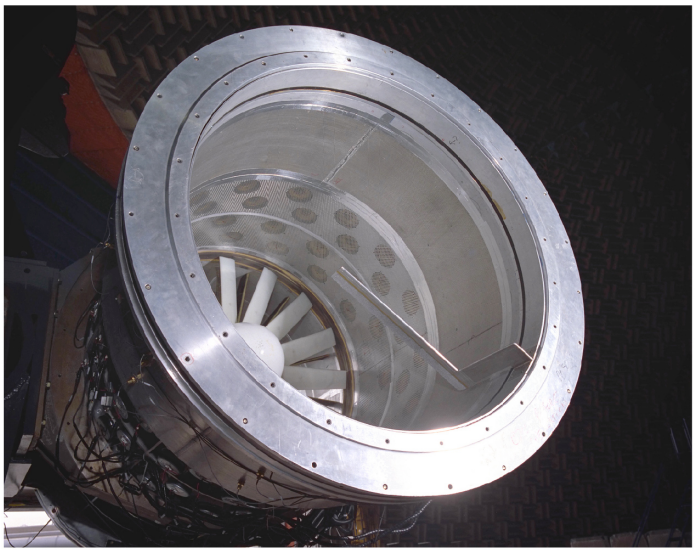

(c)

Figure 45.—Strategic Research Fund demonstration of error sensors embedded in liner. Concern about loss of treatment or increased duct length that would be required with hard wall (HW) placement of microphones. Integration of error sensors into treatment could possibly lead to development of new Active Noise Control (ANC) algorithm. Embedding microphones in liner results in similar performance compared to all microphones upstream or compared to HW ANC at same microphone locations. (a) Acoustic power level attenuation versus location of sensors in duct section. (b) Error sensor external mounting locations. (c) Rotating Rake over liner.

3.4.6 Reduced Component Count

The components required for successful ANC are specified by the physics of duct propagation. The full specification resulted in very high component counts (microphones and actuators) that are probably not feasible on an in-service turbofan. Therefore, attempts were made to reduce the component count.

In the first attempt at simplification,[45] an axially distributed array was used to detect $m = 2$ instead of the complete circumferential arrays. This assumes that the target mode, $m = 2$, is dominant in the acoustic signature since an axial array does not allow for circumferential modal decomposition (a situation known from the character of ANCF). The minimum number of microphones required is still equal to the number of radial modes present (in this case, four in the inlet and three in exhaust for a total of seven). In the inlet, a single microphone from each of the four-circumferential arrays was chosen to form a four-element axial line array, and in the exhaust, a single microphone from each of the three arrays on the inner wall was selected based on the error-array optimization results. A steering filter modeling the transfer function between the error sensors and radial was used to attempt control of individual radial modes. In summary, a linear subset, axially distributed, of error microphones was chosen. A matrix weights the microphones such that only an individual radial mode is sensed, and therefore controlled. The steering array was implemented in the inlet using three available microphones with four actuator sets and four microphones (three by four control) with seven actuator sets (four by seven control). The weighting matrix was implemented to control each of the three radial modes propagating at 1,900 RPMc. In both cases, all seven actuator arrays were activated. Figure 46 shows the reductions in the far-field directivity for the target mode for the linear control array. The results show that the reduction obtained is very modest, and there are even slight increases. It is important to recognize that the extraneous modes (nontarget modes) generated by imperfections in the actuators and/or input signals did not provide a fair test for the linear error array, though the modest reductions indicated the concept might be valid.

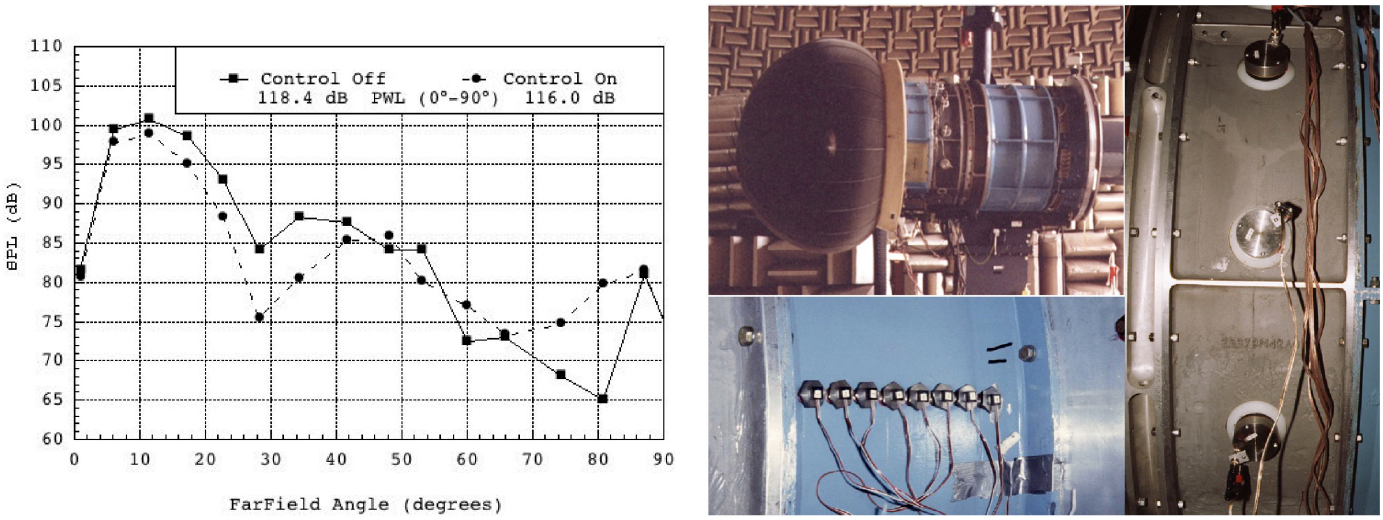

Figure 46.—Virginia Polytechnic Institute linear array. Concern over number of components in fully specified system. Combined linear error sensor array with sparse circumferential to couple to wave number. Selected single antisource plane to couple into three radials. Rare-earth magnets used in actuators. Substantially reduced component count limited reductions confined to narrow revolutions per minute range and angle. (a) Acoustic power level versus far-field angle. (b) Liner sensor array mounting locations.

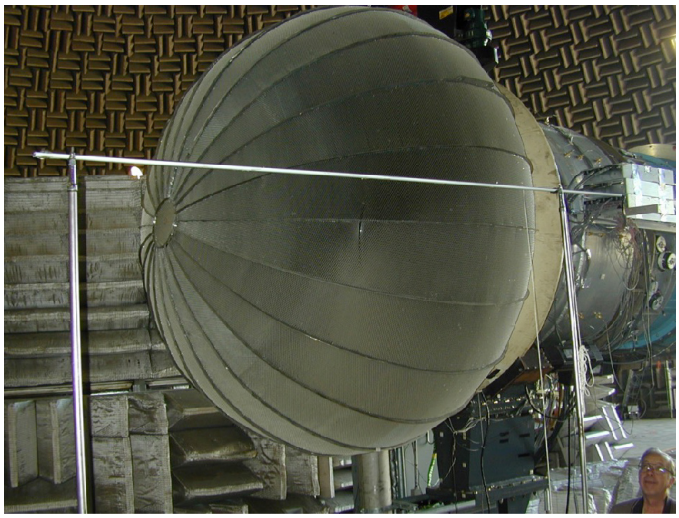

Figure 47.—Hersh Walker Acoustical Engineering, Inc., exterior linear microphone boom array alongside Advanced Noise Control Fan. Results were limited due to modal spillover of actuators (boom array less sensitive to this). Inlet duct length was not limiting. Four radials controlled with six microphones in linear array spaced to detect approximately equal subtended angles. Two cases attempted with best performance of 3.5 dB acoustic power level (PWL) for radial control and 6.2 dB PWL for sector control.

3.4.7 Novel Locations (Boom and Pylon Array)

The standard location for the ANC error sensors has typically been the duct walls. As seen earlier, this arrangement can have difficulty detecting radial modes. Alternative locations were investigated[46] on the ANCF.

A boom was located outside the fan duct in the horizontal plane, approximately 10 ft from the centerline as shown in Figure 47. The goal was to demonstrate the feasibility of reducing selected sectors of the far-field directivity that have the greatest impact on noise. This could be a more realistic application of the far-field error microphone technique, perhaps being mounted off an aircraft wing or fuselage. The boom array error-sensing input weighting used two methods: a radial-based filtering to attempt to control individual radials and an angle-based method to control sectors in the far field.

The best results with the radial-based filtering method were achieved by applying control weighting to the $m = 2$ mode. Control weighting of other individual radials was not successful in providing reductions in the $m = 2$ mode or for the corresponding individual radials. As was found with the steering array, the targeted mode was not necessarily the one reduced the most. This may indicate the propagation from the duct was not properly determined, possibly due to contamination from other noise sources.

An angle-based method was applied in an attempt to control two sectors (i.e., 45° and 30°) over a fan speed range of 2,000 to 2,300 RPMc. At 2,300 RPMc, the 30° sector control reduced the (2,0) mode dramatically and the higher radials modestly. The 45° control was more distributed over the radials, resulting in better control in the total mode. As the fan speed is reduced, the 30° control becomes less effective while the 45° control stays equally effective over the full range. This is due to the primary lobe radiating at a higher far-field angle as the cutoff ratio (i.e., RPMc) is reduced.

Turbofan engines typically have a pylon or bifurcation in the exhaust duct. The ANCF exhaust duct was modified by installing two radial surfaces 180° apart in the vertical plane to simulate a bifurcation, as illustrated in Figure 48. This surface can provide additional locations to mount error-sensing microphones. In addition, the radial extent of the pylon and bifurcation can provide radial information to the control system. Twenty microphones were distributed radially (five on each surface). The pylon control array was unsuccessful above the cut-on of the three radial modes in the exhaust. Several subsets of the pylon microphones, some configured with circumferential arrays, were used for error inputs. The

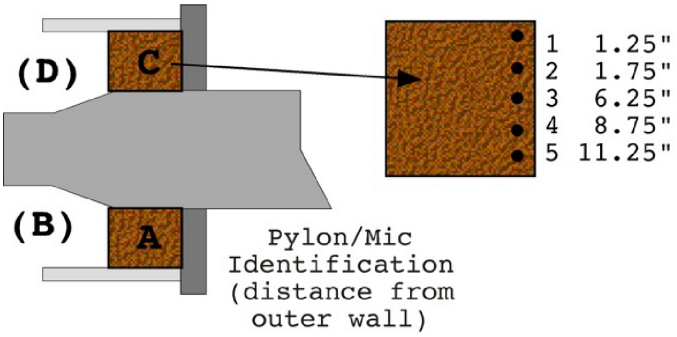

(a)

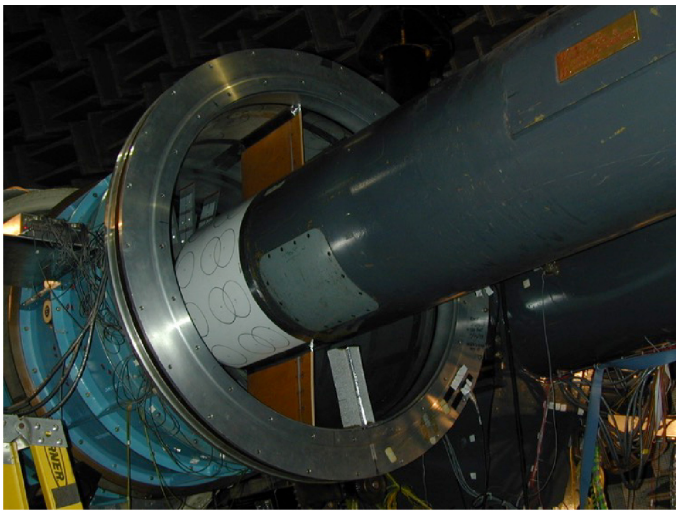

(b)

Figure 48.—Hersh Walker Acoustical Engineering, Inc., pylon error sensor array. Need to consider effects of m-order reflection due to pylon. Pylon array: radial distribution better radial mode resolution single axial plane. Best exhaust performance of 9.1 dB acoustic power level (PWL) of two radials and 6.7 dB PWL of three radials. (a) Pylon sensor array diagram and distances. (b) Plywood pylons and radially spaced microphones in Advanced Noise Control Fan exhaust duct. Where Mic is microphone.

controller converged to a reduction, but the radial array was apparently unable to distinguish between the radials at different *m*-orders due to profile similarity. The pylon array achieved reduction in $m = 2$ PWL. The best configuration used an inner and outer circumferential array with four pylon microphones (two each from two pylon sides). This is considered the baseline since the two circumferential arrays alone meet the criteria to control two radials. The configuration using six microphones (three each on two pylon faces) performed very well and met the goal of using only radially distributed microphones. It was suggested that more microphones are required in the radial distribution than the number of radials present.

3.4.8 NASA Active Noise Control (ANC)/Advanced Noise Control Fan (ANCF) Program Conclusions

The ANCF demonstrated that tonal-based ANC is possible, potentially significantly reducing multiple harmonics. It demonstrated that fully integrating the active system into a liner is necessary as well as close coupling the actuators. It was generally recognized that the benefits of tonal control did not justify the added complexity, and attempts at reducing the complexity did not improve that cost/benefit ratio. The ANCF effort also demonstrated that the most critical component of the ANC system is the control algorithm. That should be the basis of any research attempted in BB ANC, which could potentially enable the cost/benefit ratio to become viable.

3.5 Novel Fan Noise Reduction Concepts

3.5.1 Trailing-Edge Rotor Blowing (TERB)

The velocity deficit due to the viscous wakes of the rotor blades is the primary source of RS interaction noise. The periodic wake disturbance interacts with the stator, causing unsteady surface pressures on the stator vane that in turn couple to the duct acoustic modes. The strength of the deficit correlates to the acoustic levels. It has been demonstrated analytically that reducing the harmonic content of the wake will have a substantial effect on reducing the fan noise tone component. One method to reduce the velocity deficit is to fill the wakes by injecting air into the wakes from a slot in the trailing edge. Prior experiments using rotor trailing edge blowing in a blow-down facility[47] and inlet guide vane

trailing edge blowing[48] showed that filling the wake through trailing edge blowing reduces the harmonic content of the wake responsible for interaction tones.

An experimental proof-of-concept test was conducted[49] on the ANCF to demonstrate reduction of RS interaction noise through rotor trailing edge blowing. Composite hollow rotor blades with internal flow passages were designed based on analytical codes modeling the internal flow. This hollow blade features interior guide vanes that create flow channels through which externally supplied air flows from the root of the blade to the trailing edge. The velocity deficit from the viscous wake of the rotor blades was reduced by injecting air into the wake through a trailing-edge slot. The impact of the rotor wake-stator interaction on the aeroacoustics was also predicted analytically. Figure 49 depicts the TERB configuration.

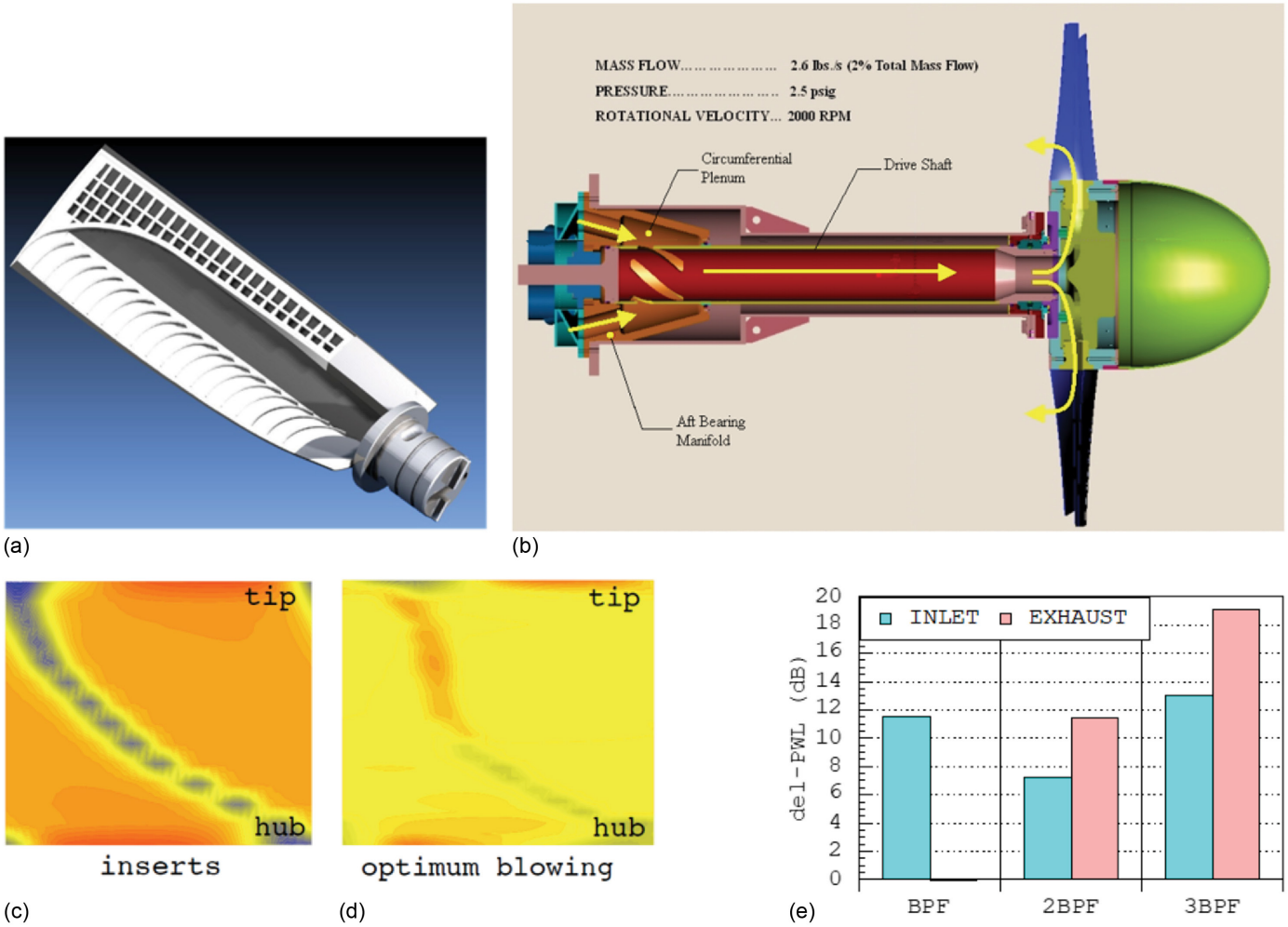

Figure 49.—Trailing-edge rotor blowing (TERB) configuration and illustrative results. (a) Internal flow channel shapes designed using three-dimensional (3D) viscous computational fluid dynamics code Rotor Viscous Code Quasi-3-D in an iterative process. (b) Cross section of TERB full system. (c) Measured wake velocity profile with trailing-edge inserts. (d) Measured wake velocity profile with optimum blowing. (e) Inlet and exhaust acoustic power level reductions for different blade passing frequencies (BPFs).

The ANCF/TERB rotor was designed using a modified version of the NASA-developed compressor design program in conjunction with a three-dimensional (3D) viscous computational fluid dynamics (CFD) code for turbomachinery, Rotor Viscous Code Quasi-3-D (RVC3D). Through an iterative design process, several key aerodynamic parameters needed by the design code were obtained and adjusted based on the CFD simulation results. In particular, the spanwise distributions of blade row total-pressure loss and exit flow deviation angle (turning) were determined from the CFD solutions. A two-dimensional (2D) viscous CFD code, Duct Viscous Code 2D (DVC2D),[50] was used to a limited extent to simulate the flow field in the axisymmetric inlet upstream of the rotor, providing inlet boundary condition data for the rotor computational domain.

The design codes used in this work were validated as reliable tools for predicting the behavior of trailing edge blowing for low-speed fans. Simulations of the TERB ANCF rotor using the RVC3D code, augmented with a one-dimensional (1D) flow model for the TERB flow characteristics, predicted the experimental values very well. Using these results as input, the V072 acoustic code predicted the measured noise reductions reasonably well.

The types of data acquired were (i) two-component hotwire behind the rotor, (ii) unsteady surface pressures on a stator vane, (iii) acoustic duct modes, and (iv) far-field directivity. These data were analyzed for tonal character.

Reduction in the fan tone levels by filling the rotor viscous wake through trailing edge blowing has been demonstrated to achieve substantial tone reduction at 1.6 to 1.8 percent of the fan mass flow rate. Indirect methods indicate potential reduction of RS interaction BB noise.

A fortuitous result of the TERB test was a rotor blade design that was more realistic than the original ventilation fan set. A set of blades based on the TERB plan form, but with a sharp trailing edge, were built, and the baseline aeroacoustic data set was updated.[10,13] In addition, trailing-edge inserts were made using rapid prototype methods and materials to study passive mixing of the viscous wake (e.g., serrated or wavy (Figure 50)).

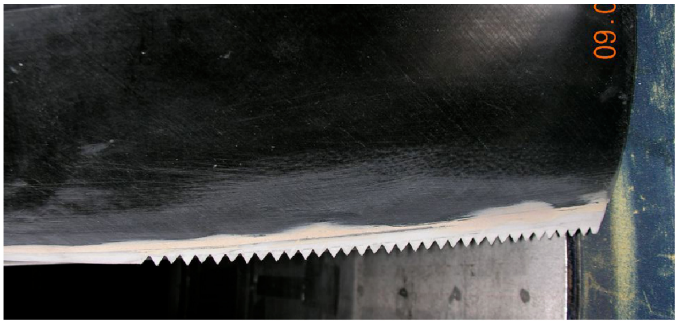

(a)

(b)

Figure 50.—Trailing-edge inserts adapted from trailing-edge rotor blowing blades. (a) Serrated trailing-edge insert developed by Glenn. (b) Marcelled trailing-edge insert developed by General Electric.

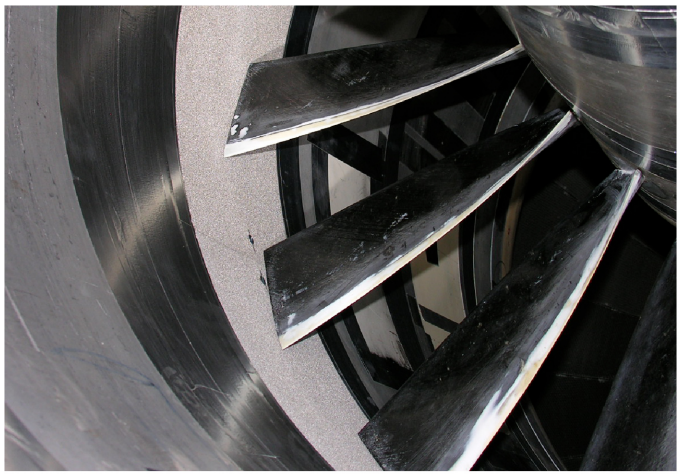

(a)

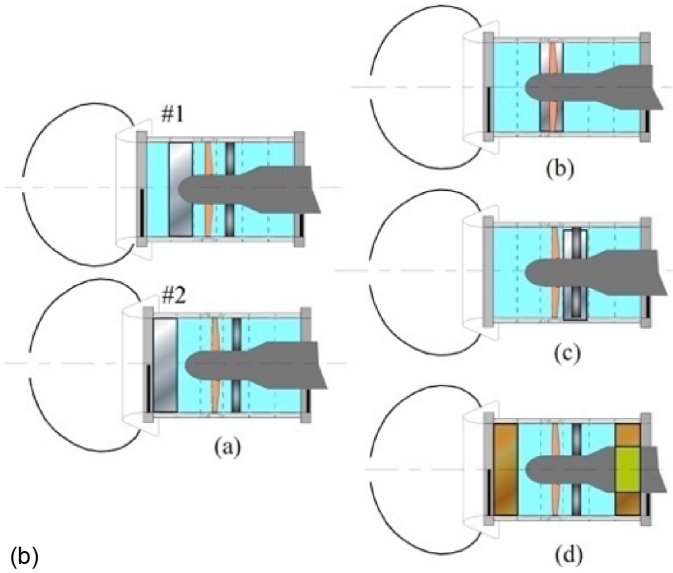

(b)

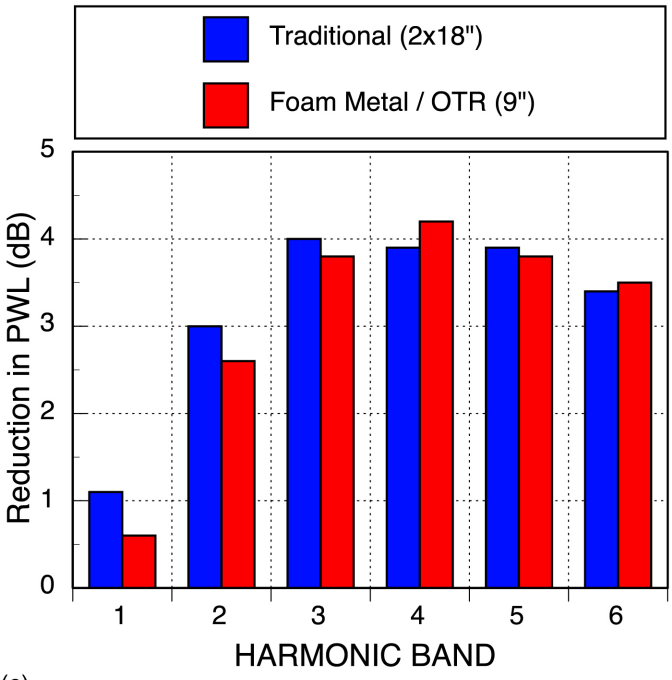

(c)

Figure 51.—Over-the-rotor (OTR) foam-metal liner (FML) configurations (where L = 9 in. D = 2 in., 80 ppi at 6 to 8 percent) and illustrative results. (a) Closeup of rotor blades with FML installed OTR. (b) FML configurations tested where (a) FML in two inlet locations, (b) FML OTR and 2 in. depth with 1/32- and 3/32-in. tip gap, (c) FML over the stator, and (d) single degree of freedom liner (18 in. each) in inlet and exhaust ducts. (c) Acoustic power level reduction versus harmonic band.

3.5.2 Foam-Metal Liner (FML) Over the Rotor (OTR)

A widely used method to attenuate the noise in the turbofan duct is to use acoustic liners.[5] Standard liners with single degree of freedom (SDOF) perforate-over-honeycomb design are typically tuned to maximize attenuation at the blade passage frequency. These liners have traditionally been installed in the inlet or exhaust segments of the nacelle, a relatively benign environment. It is desirable to install liners closer to the rotor or even OTR, which is a much harsher pressure and temperature environment. If designed correctly, liners placed in this region can provide a pressure release

surface, mitigating the acoustic near field, and thereby reduce the far-field noise emitted by the engine. This may result in more attenuation than can be achieved due to conventional liner installations. Foam metal has the potential to survive in this environment. OTR FMLs installed at or near the fan rotor provide acoustic absorption of rotor noise generated at the tips of the rotor blades. They also present a pressure release boundary condition, inhibiting the rotor noise generation source. This can result in higher attenuation levels than could be achieved using liners located in the nacelle inlet. In addition, FMLs could potentially replace the fan rub-strip and containment components, ultimately reducing engine components, and thus weight, which can result in system-level benefits in noise reduction and engine performance.

An FML for attenuation of fan noise was developed for and tested on the ANCF[51] (Figure 51). The acoustic characteristics of foam-metal samples were determined using a normal incidence-impedance tube (NIT). An FML was designed based on the absorption characteristics of the foam metal and the known acoustic characteristics of a low-speed fan. The attenuation characteristics of the FML installed in the inlet matched the predicted absorption spectra reasonably well. Additional attenuation bandwidth, beyond that predicted from the impedance tube tests, occurred with the FML-installed OTR.

The acoustic performance of the liner was significant, especially when placed OTR, achieving BB attenuation in both the inlet and aft far field. This compared favorably to the performance of SDOF liners installed in both the inlet and aft duct sections in terms of achieving similar global attenuation. This suggests FMLs installed OTR could provide the opportunity to eliminate the conventional liners, possibly shortening the ducts and reducing nacelle weight.

The FML effect on the flow affected the pressure near the wall in the region of the rotor and increased the size and strength of the rotor tip vortex. These measurements indicate the attenuation observed from the FML-installed OTR is due to a combination of acoustic attenuation and source modification. Due to the characteristic of the low-speed, low-pressure rise fan, the impact on thrust and efficiency cannot be effectively measured using the ANCF testbed, and therefore detailed information on these parameters was not determined. A follow-on test of an FML OTR on a production turbofan[21] was performed and the impact on fan performance quantified based on these ANCF tests.

3.5.3 Over-the-Rotor (OTR) Liner Technology Readiness Level (TRL) Range

In order to better understand the physical effects of OTR acoustic treatments, a series of tests[52,53] were performed at multiple TRLs with various treatment concepts shown in Figure 52 of which tests on the ANCF were in the middle. As was done previously, the first testing was completed with 2-in-square treatment samples in the NIT at NASA Langley Research Center. Four of the treatments and two baseline configurations were designed and fabricated for testing on the ANCF at NASA Glenn Research Center. Two positions were tested: (i) in a traditional inlet locationw and (ii) in an OTR location. The HW with grooves configuration was used as a reference to compare the effect of the other treatments. The goal was to measure the insertion loss of the four liners in the OTR configurations and compare it to the same liners in the inlet, thereby providing some insight into the relative impact of the two physical mechanisms mentioned earlier. Each liner was evaluated in the ANCF in terms of acoustic reduction efficacy. Finally, the same configurations were tested in the W–8 Single Stage Compressor Facility at Glenn using the Source Diagnostic Test (SDT)/R4 fan hardware.

Due to the minimal axial extent of the treatment, its effect when placed in the inlet position compared to the baseline configuration with no treatment is minimal. In the OTR position, several of the liner designs were shown to have a reduced fan noise (Figure 53). The comparison of the reduction achieved in rotor-alone versus noise indicated that the attenuating mechanism is a combination of source modification and a reduction in the propagating acoustic waves from the RS interaction, which is very noticeable in the forward arc. An important observation is that, for some treatments, the noise is increased, probably due to a modification in the rotor tip vortex impinging on the stator vanes.

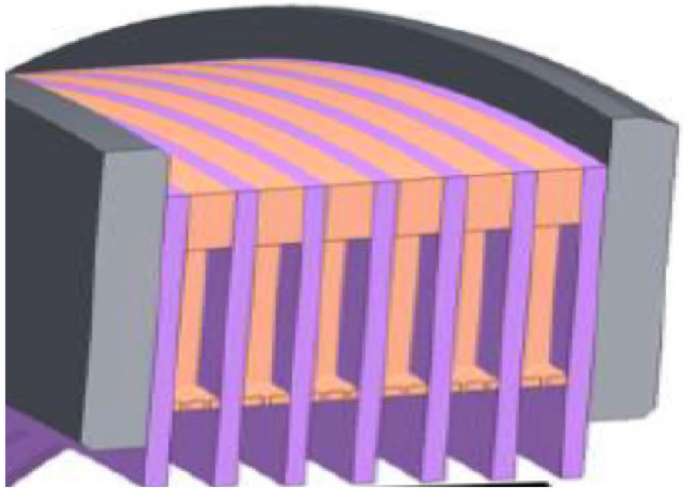

(a)

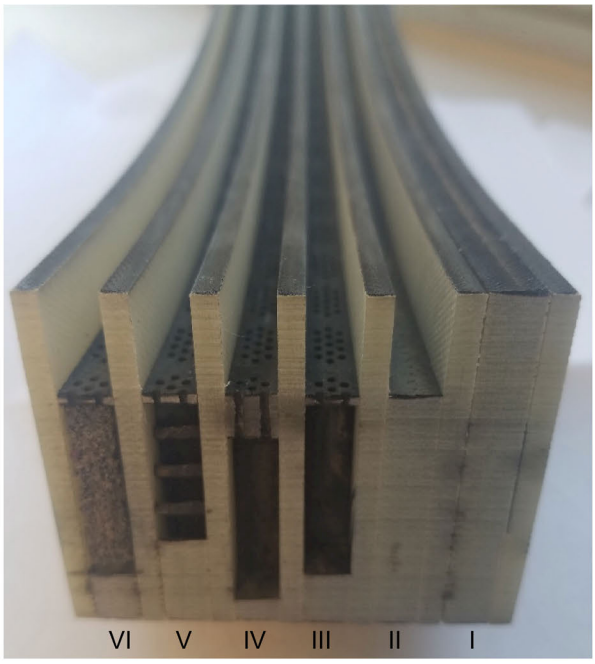

Configuration ID	Description
I	Hard wall
II	Hard wall with grooves
III	Empty chamber with thin face sheet
IV	Empty chamber with thick face sheet
V	Expansion chamber with thin face sheet
VI	Foam metal with thin face sheet

(b)

Figure 52.—Multiple over-the-rotor liner configurations. (a) Grooved casing treatment concept. (b) Fan acoustic casing treatments (shown individually).

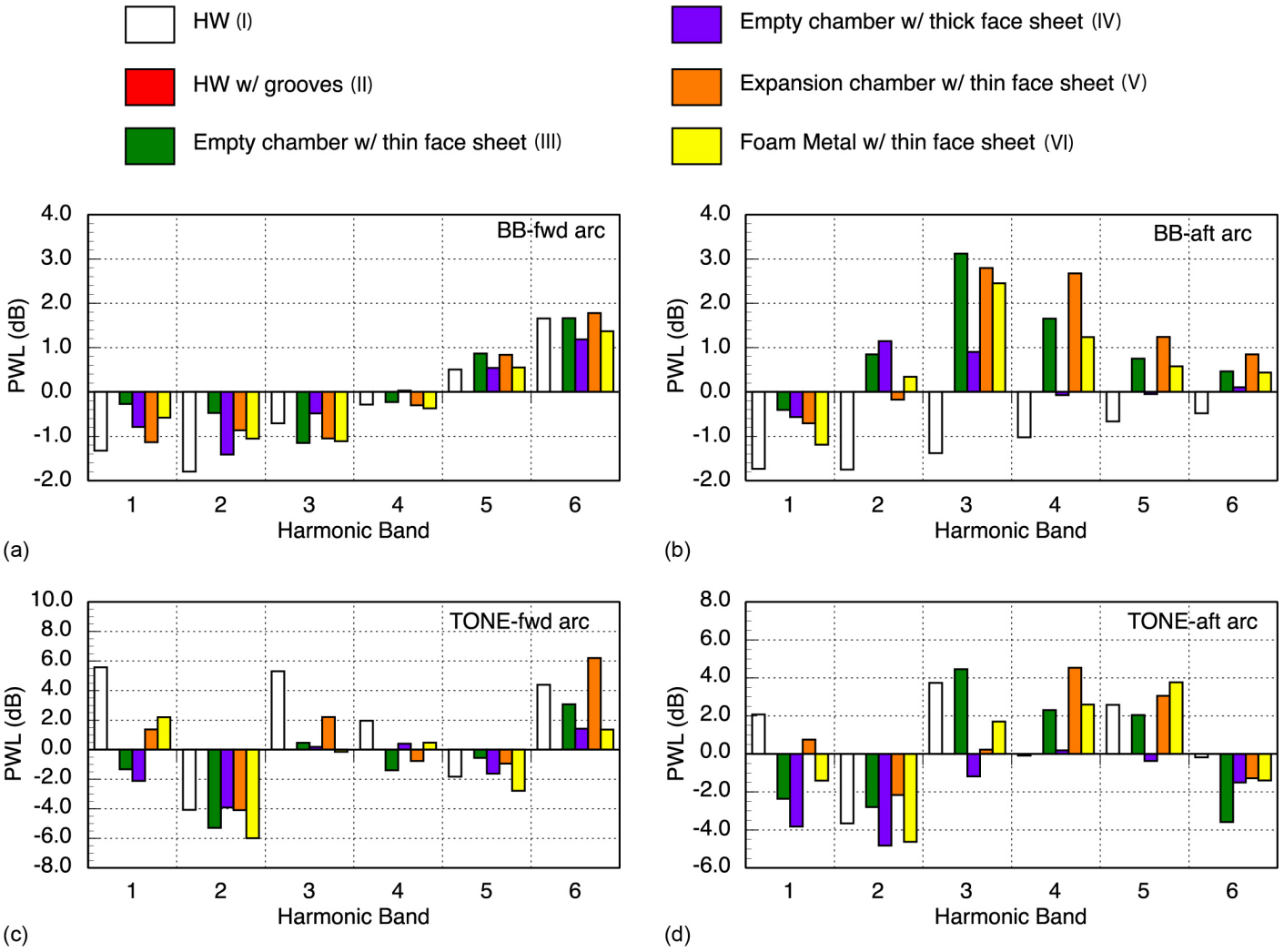

Figure 53.—Multiple over-the-rotor liners sample results. (a) Broadband (BB) attenuation in forward far-field microphone arc. (b) BB attenuation in aft far-field microphone arc. (c) Tonal attenuation in forward far-field microphone arc. (d) Tonal attenuation in aft far-field microphone arc. Where HW is hard wall.

3.5.4 Soft Stator Vanes

Extending the concept of passive treatment to locations other than the outer duct walls provides opportunities for additional attenuation. One potential location is the stator vane, where a portion of the stator vane surface is made porous to allow communication between pressure fluctuations at the vane surface and multiple, internal, resonant chambers. The internal chambers and porous surface are designed to an optimum impedance, such that maximum sound absorption is achieved. This impedance boundary condition also provides pressure release (relative to the rigid surface it replaces) at the surface of the stator vane. This concept has been termed "soft vane"[54] and is intended to reduce noise from RS interaction.

Several soft vane configurations were tested on the ANCF, all utilizing the basic vane design. An exploded view of this concept is shown in Figure 54. These are (i) two rows of the interior partition beads filled with ceramic beads, (ii) the same plus a 200 MKS rayls fibermetal cover sheet over the porous area, (iii) the fibermetal cover sheet with only the interior partition, (iv) the fibermetal cover sheet with no partition, completely filled with ceramic beads, and (v) the fibermetal cover sheet with an empty vane. Configuration (ii) was the primary design and in fact achieved the best BB attenuation relative levels from the original solid aluminum stator vanes.

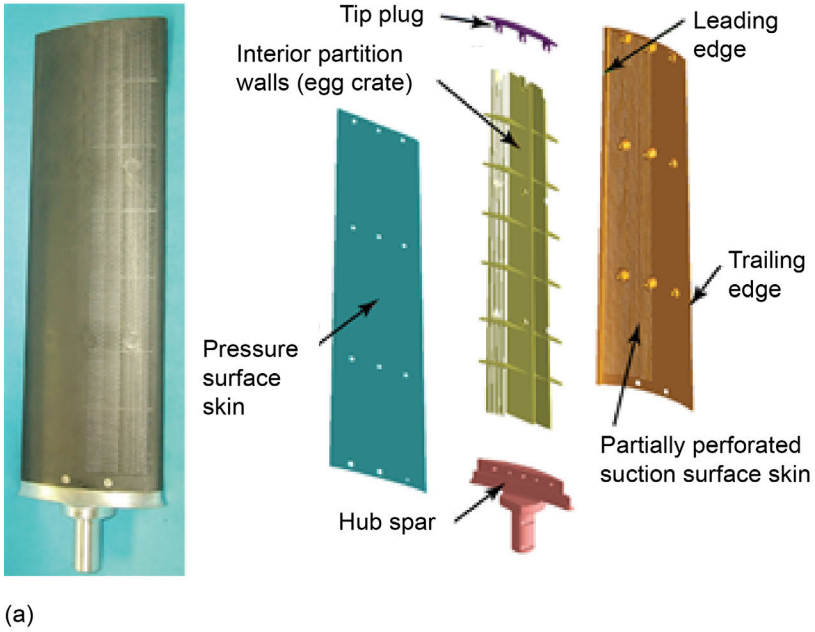

Figure 54.—Soft-vane configurations and illustrative results. (a) Exploded view of soft vane. (b) Acoustic power level attenuation versus harmonic band.

Approximately 1 to 2 dB far-field sound power level attenuation was measured over the entire frequency range of investigation in both the forward and aft arcs. This BB noise reduction was a very encouraging result, leading to a test on the high-speed ducted fan in the 9×15 Low-Speed Wind Tunnel.

3.6 Novel Liner Development

As discussed earlier, the ANCF was designed to approximate the frequency range impacting the EPNL calculation. Any successful noise reduction over that range would benefit the public. The current state of the art for attenuating that frequency range is the application of passive liners. The ANCF was used to evaluate several passive advanced liners.

3.6.1 Herschel-Quincke (HQ) Tubes

The main objective of this experimental effort was to investigate the performance of HQ tubes combined with high-resistance liners for the control of aft fan noise radiation. An HQ tube is a waveguide placed on the outer wall of the duct. An acoustic wave enters from the upstream opening of the tube and is reinjected into the duct at a downstream location. As that acoustic wave will be traveling a different path length, it may constructively or destructively interfere with the original wave propagating in the duct. To this end, a series of tests were performed in the ANCF rig (Figure 55) at Glenn. In addition, testing of the HQ tubes with the HW duct condition (liners in the duct walls replaced by HWs) was also performed. The HQ tubes were specifically designed to attenuate the x tone and the BB frequency range around it (designated 2BB). Alternately, the liner was designed for optimum BB performance between 2.5 to 5.5BPF, where the HQ contribution expected to be small. The HQ-liner system performed well attenuating both the 2BPF tone and BB component at the design fan speed of 1,800 RPMc. Despite the high resistance of the liner, the HQ tubes contributed to power reduction of the 2BPF tone and 2BB frequency range, respectively (determined by testing the liner alone and subtracting the results). Power reduction due to HQ tubes on HW was also promising, considering the high resistance of the liner wire mesh placed at the tubes' openings to limit cavity tones. In general, the HQ-tubes provided good results for all the fan speeds tested.

The HQ liner systems performed well with a measureable contribution from the HQ tubes, in particular at lower frequencies where the liner was not very effective. However, it is believed that the HQ tubes' performance can be significantly improved by lowering the liner's face screen resistance locally at the HQ tube liner interfaces. This approach should yield a highly resonant HQ device, which is the original intent of the technology.

The HQ liner test and results were used to justify the inclusion of HQ tubes on the Honeywell TFE731 technology maturation test program.[20]

3.6.2 Liner Insertion Loss Measurements

Figure 56 shows the schematic of the ANCF configuration for the evaluation of insertion loss due to a liner. The liner used was an SDOF liner.

The Rotating Rake was installed in one of two locations: upstream of the liner to measure the modal PWL at the entrance or downstream of the liner to measure the modal PWL at the liner exit. Comparing the two measurements provides the liner insertion loss (positive number indicates attenuation). Rake measurements at these locations were performed both with the liner exposed and taped over (to simulate a HW baseline).

Figure 56 shows the mode PWLs measured at the entrance and the exit for the HW and the liner. At BPF, the insertion loss is minor, not surprising as this frequency was not the design frequency of the liner. Note that in general the comparison of the mode strength at the entrance to the HW is comparable to the mode strength at the entrance of the liner. An exception is that mode $m = 4$ HW to soft wall (SW) entrance comparison shows a huge variation in PWL. This is thought to be due to that mode being close to cutoff, and therefore being more susceptible to reflections. The insertion loss at 960 Hz, near the target design of the liner (shown in Figure 56), is greater and increases as the mode number increases. This is expected as the higher mode numbers have lower cutoff ratios; it is generally accepted that liners are more effective at cutoff ratios near unity[55] since the mode angle is propagating into the liner.

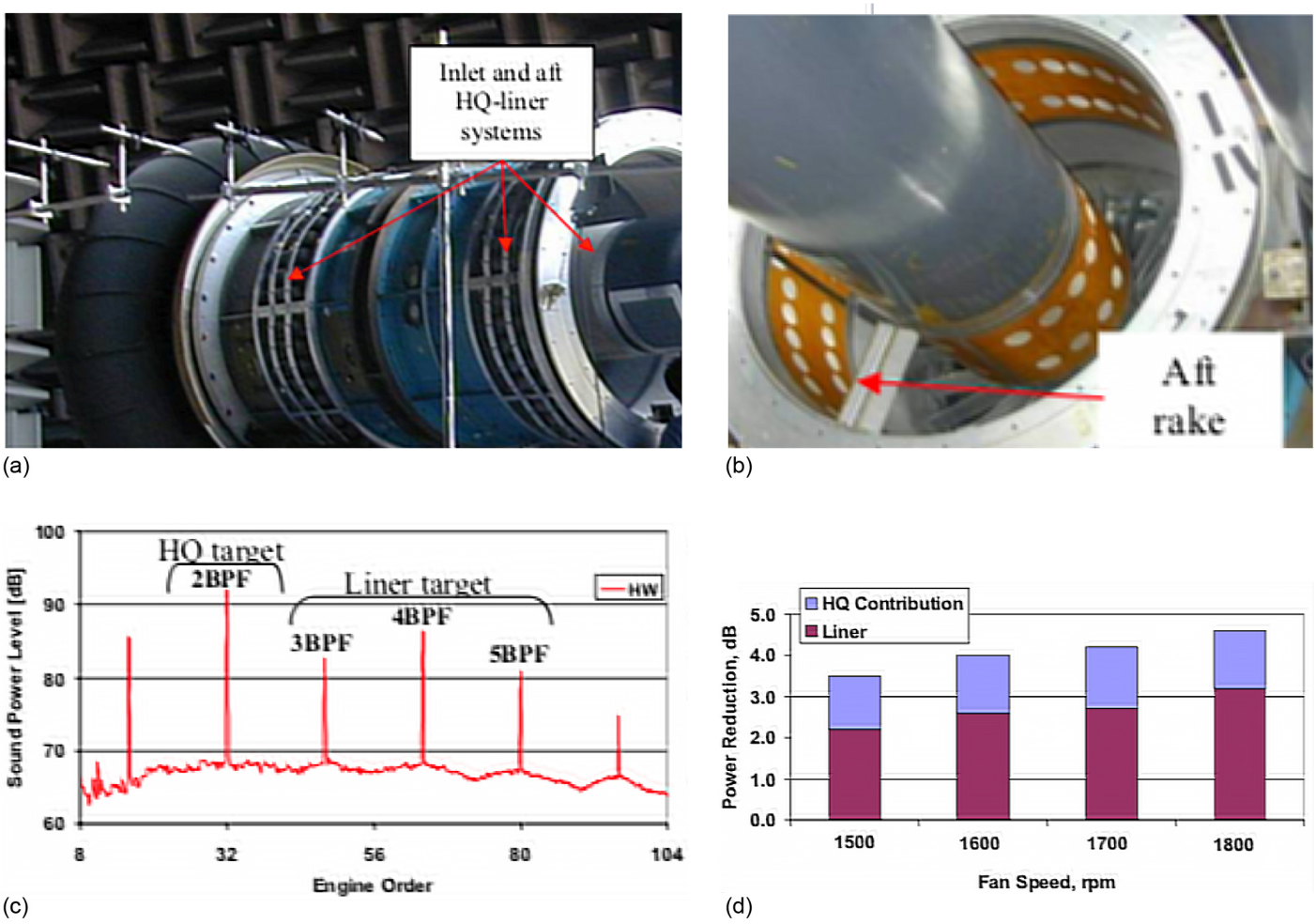

Figure 55.—Herschel-Quincke (HQ) tube installation and design. (a) Inlet and aft HQ liner installed on Advanced Noise Control Fan. (b) Aft rake location. (c) Sound power level versus engine order. (d) Power reduction versus fan speed. Where BPF is blade passing frequency.

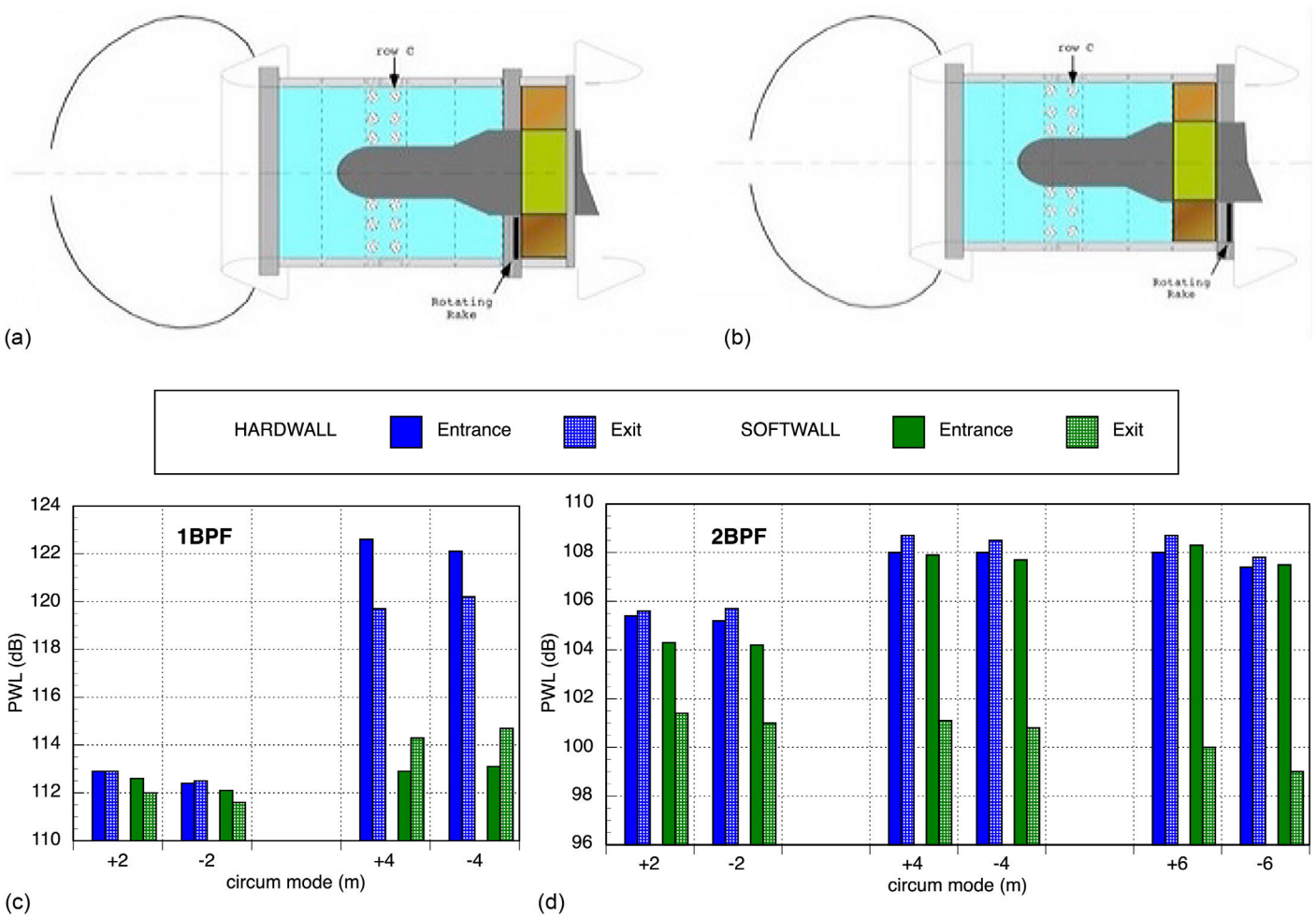

Figure 56.—Insertion loss measurement configuration and illustrative results comparing measured acoustic power levels (PWLs) with rake installed at liner entrance to that installed at liner exit. (a) Rotating Rake installed at entrance. (b) Rotating Rake installed at exit. (c) PWL versus circumferential mode for 1 blade passing frequency (1BPF). (d) PWL versus circumferential mode for 2BPF.

The effect of pylons on the liner efficacy was also investigated during this test. Two pylons were manufactured: (i) a large one that extended the full axial length of the liner and (ii) a smaller one approximately 25 percent of the liner length. Configurations tested were with both pylons mounted, or the large pylon only, for either the HW or liner. The results are summarized in Figure 57. This investigation built upon an earlier one that showed pylons reflect modes into the opposite rotation.

This type of measurement provides a more detailed evaluation of the physics of the liner efficacy compared to just measuring the insertion loss in the far field as it takes into account internal reflections and other acoustic effects.

3.6.3 Multidegree of Freedom (MDOF) Liner

Two BB liner designs[56] were produced that were predicted to provide increased attenuation over conventional tonal designs for the full range of frequencies and operating conditions considered. Both designs incorporated a septum to create two chambers. The first liner incorporated a septum with a constant depth (same depth in each chamber) to provide a constant impedance liner design. The second design incorporated a unique variable depth septum, creating a variable-impedance liner. The insertion loss for each liner was measured experimentally. The objective of the experimental portion of this effort was to validate the efficacy of the design process by comparing the experimentally measured insertion losses for each liner to those predicted. The experimental results are presented in Reference 57.

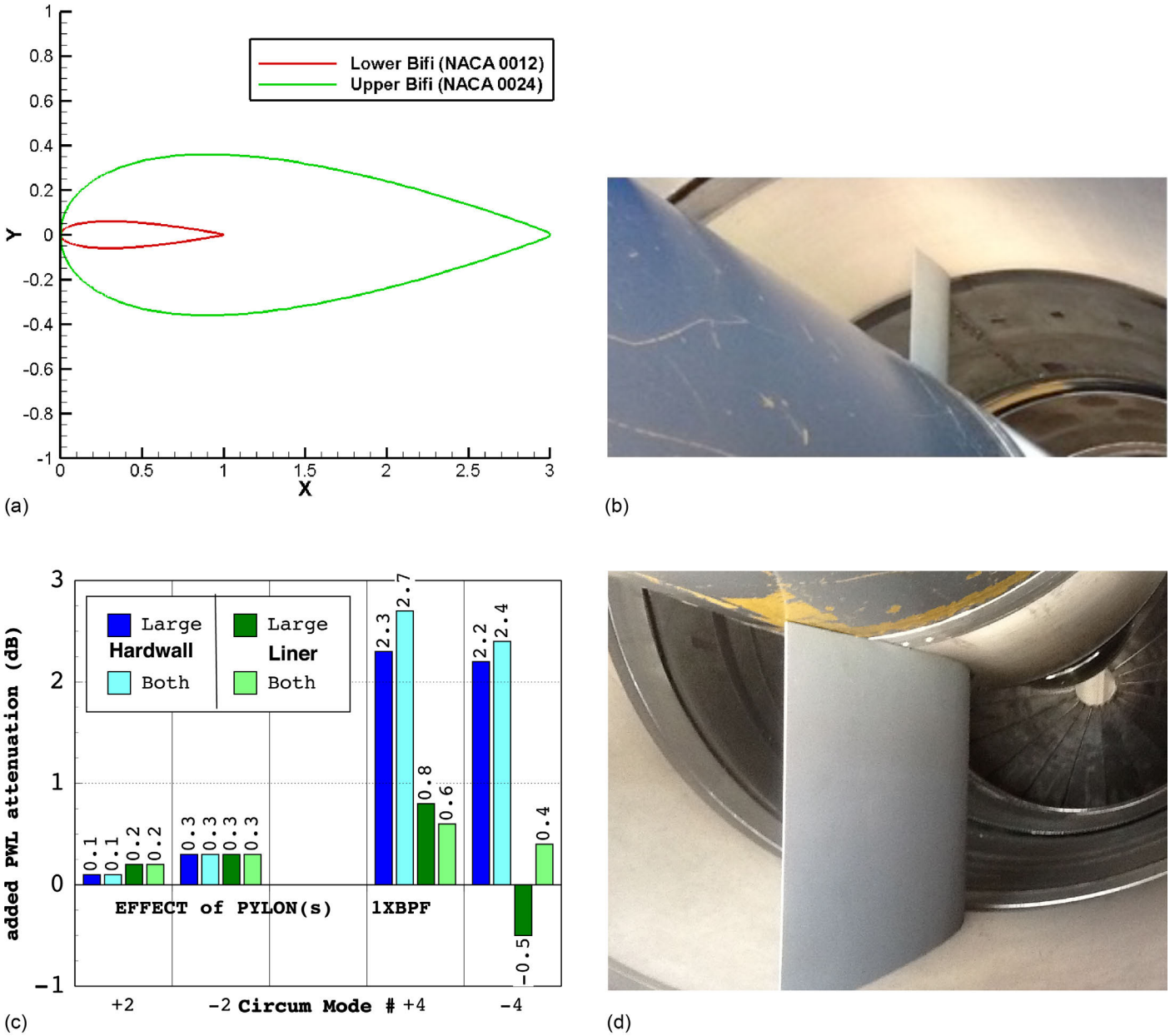

Figure 57.—Effect of pylon and liner interaction and typical results. (a) Planform of lower and upper pylons. (b) Photograph of upper pylon. (c) Photograph of lower pylon with Rotating Rake in foreground. (d) Changes in PWL due to pylons versus circumferential mode. Where BiFi is bifurcation and BPF is blade passing frequency.

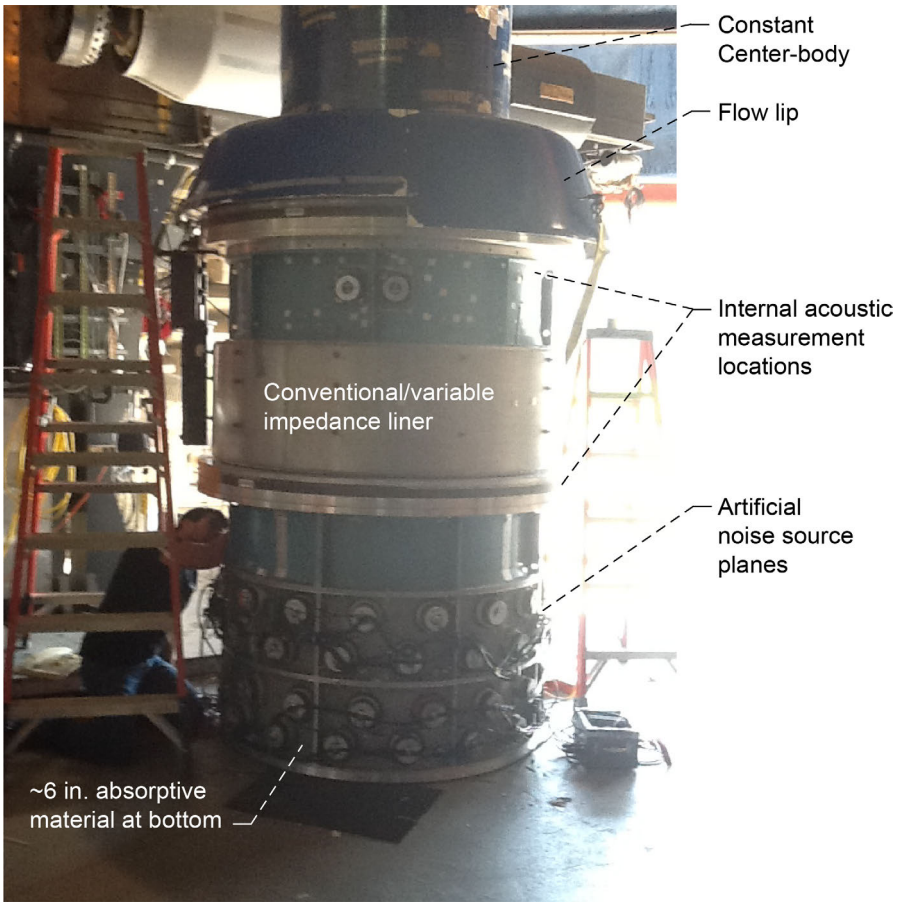

Figure 58.—Configuration of Advanced Noise Control Fan in vertical orientation to obtain liner insertion loss measurements. Significant portion of data acquired with rig built up in vertical orientation (off of stanchion, no rotor/stator, no flow, and very clean internal lines). Unique configuration allowed for very precise analytical solutions to evaluate efficacy of liner(s) and accuracy of CDUCT-LaRC.

In order to provide a clean, annular duct for this experiment, the ANCF was built up off of the stanchion-pylon assembly that normally supports the fan and duct sections that make up the nacelle (Figure 58). That is, the spool pieces were stacked up in a vertical orientation on the floor. This removed the ANCF centerbody and support pylon from the arrangement, providing a constant area annular duct. Two configurations were tested in this setup: (i) a constant 24-in.-diameter cylindrical tube centerbody and (ii) a constant 36-in.-diameter cylindrical tube centerbody. These provided an equivalent annular duct hub-to-tip ratio of 0.5 and 0.75, respectively (inner diameter of the outer wall is 48 in.). The entire stack rested on the floor, and approximately 6 in. of foam material was placed in the bottom of the stack to minimize reflections from the floor. Only in-duct Rotating Rake measurements using the CFANS as a noise source were acquired in this configuration. Obviously, in this orientation, there was no flow. Rotating Rake data were acquired at the entrance and exit of the liner. This was the primary setup for all liner configurations.

Selected liner configurations were also installed on the standard ANCF configuration (Figure 59). The fan was used as the primary source at the standard range of 1,400 to 2,000 RPM. Two stator counts were utilized, 0 (rotor alone) and 14 vanes at 0.5 chord spacing. The liner was installed in the aft converging section where the hub-to-tip ratio transitions from 0.375 to 0.5. Rotating Rake measurements upstream and downstream of the liner were acquired. Far-field directivity measurements were acquired as well. The CFANS was also used to generate BB noise as described above (no flow) and far-field measurements were acquired.

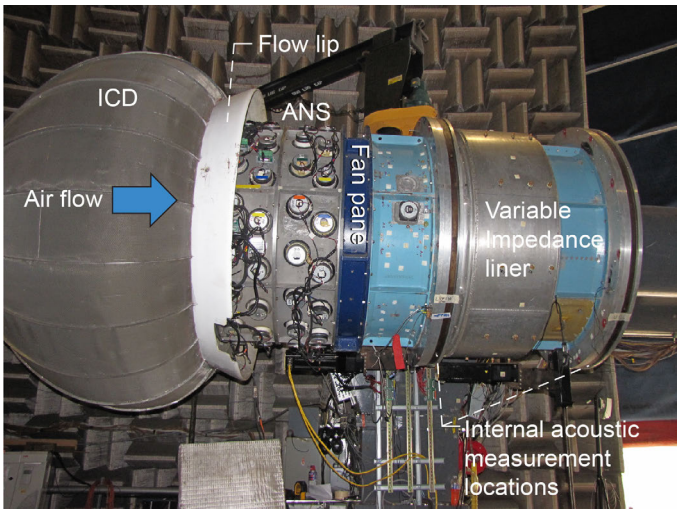

Figure 59.—Configuration of Advanced Noise Control Fan in horizontal orientation to obtain liner insertion loss measurements (standard mode of operation). Selected configurations were tested on stanchion with fan generating acoustic signature. This provided for inclusion of flow and nonuniform geometry effects. Also, measurements of far-field acoustic directivity were acquired for confirmation of community impact. Where CFANS is Configurable Artificial Noise Source and ICD is inflow control device.

These tests were used to assess NASA's ability to design acoustic liners using construction with embedded mesh-cap technique (developed by Hexcel Inc.). Data from the ANCF were compared with predictions from aeroacoustic propagation codes to demonstrate the prediction capabilities and to compare results from different types of liner configurations. Based on the success in the ANCF (as well as the NIT and grazing flow impedance tube (GFIT) at Langley), similar liners were designed for tests on the DGEN Aero-Propulsion Research Turbofan (DART).[58] This test clearly demonstrated that the MDOF configuration could be fabricated for a very difficult inlet configuration (14 in. diameter with strong curvature). This was used to convince program officials that this type of design could be built in a flightworthy product and flight tested on a Boeing 737 MAX Quiet Technology Demonstrator testbed.[22]

3.7 Measurement Technology Development

For reasons similar to those given for code validation (Section 3.3), the ANCF is well suited for development and improvement of aeroacoustic measurement techniques.

3.7.1 Rotating Rake Enhancements

3.7.1.1 Modal Measurement Over Liners

Expansion of the Rotating Rake measurement and analysis technique to include measurements over treated sections was validated using the ANCF. A rake with an extension was utilized to measure the pressure profile over a passive liner (Figure 60). The methodology obtained radial basis functions for the least-squares-fit matrix to determine modal decomposition[16] that are based on wall impedance boundary conditions. The assumption made in this technique that a smaller least-squares-fit error implies a more accurate impedance boundary condition.

Where the closed-form analytical solution exists (i.e., constant duct area and Mach number) it was used directly and analytical equations were developed to estimate mode power. Several modes and frequencies were generated by the CFANS and liners with differing impedances were evaluated. In addition to experimental validation on ANCF, the technique was verified by decomposing and analyzing radial pressure profiles generated numerically by using the Eversman code.[59]

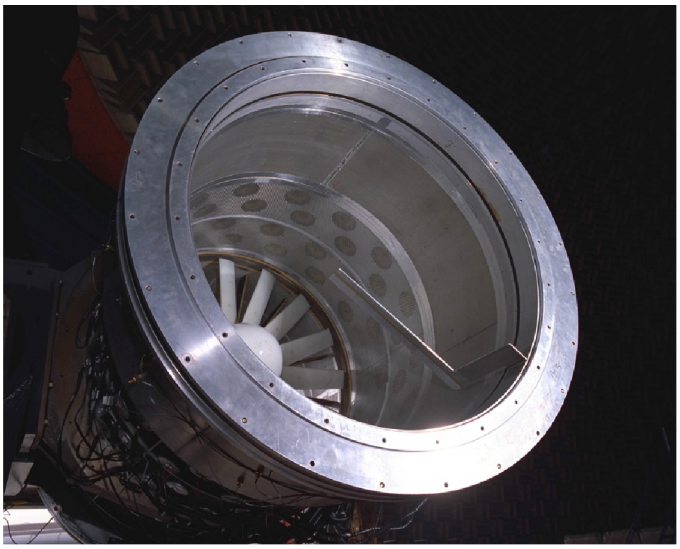

Figure 60.—Modal measurement over passive liner using extended Rotating Rake.

For ducts with SWs and mean flow, the radial basis functions were numerically computed. The linear companion matrix method is used to obtain both the eigenvalues of interest and the radial basis functions.[60] In addition, a nonlinear least squares method is used to adjust the wall impedance to best fit the data in an attempt to potentially use the rotating system as an in-duct wall impedance measurement tool.

Rotating Rake data from the ANCF with different liners were acquired: a liner with a design resistance of 1.0 and another with a design resistance of 1.7. The modal data were reduced to determine the best fit to the data shown in Figure 61 using either the closed-form analytical solution or the numerical solution with plug or shear flow. The best fit was determined from the lowest least-squares-fit error in the solution. Using the impedance boundary conditions resulted in better mode measurement solutions, which are presented in detail in References 59 and 60.

The methodology and analysis were directly inspired by the groundbreaking work of Dr. Edward J. Rice.[61]

3.7.1.2 Dual Rake (Mode Reflections)

Typically, a single rake, extending from the outer wall to the duct centerline, has been inserted to measure duct modes at a single axial location. It has been known[62] that measurement at a single axial location will not account for reflections in the duct, therefore, for this experiment,[63] an additional rake was mounted on the same rotating ring as the original. This second rake was adjustable in the axial direction over the range of 2.5 to 10.5 in., in 1-in. increments and was mounted 180° in the circumferential direction from the original rake, which remained fixed. Figure 62 shows this arrangement. Data were simultaneously acquired from both rakes to provide the two-point axial variation needed to compute the reflection.

Reflections were created using two methods. The first method relies on the natural reflections due to an open-ended exit termination. The ring containing the dual Rotating Rake system was mounted at the exit of the ANCF stackup (Figure 62). The single driver row (*C*) farthest from the exit termination was used to generate the modes in Table I. This configuration was run with the flow lip attached—this was assumed to minimize reflections and with the flow lip removed, creating a sharp 90° flanged exit—and this was assumed to create stronger reflections. A second configuration was used to generate artificial reflections as shown in Figure 63. This was accomplished by locating the dual-rake ring in the center of the stackup. Driver row C was used to generate the primary wave and driver row B was used to generate the reflected wave. Each driver row was actuated independently and the dual rakes measured the modes. Then, both sets were activated simultaneously and the resulting superposition was measured.

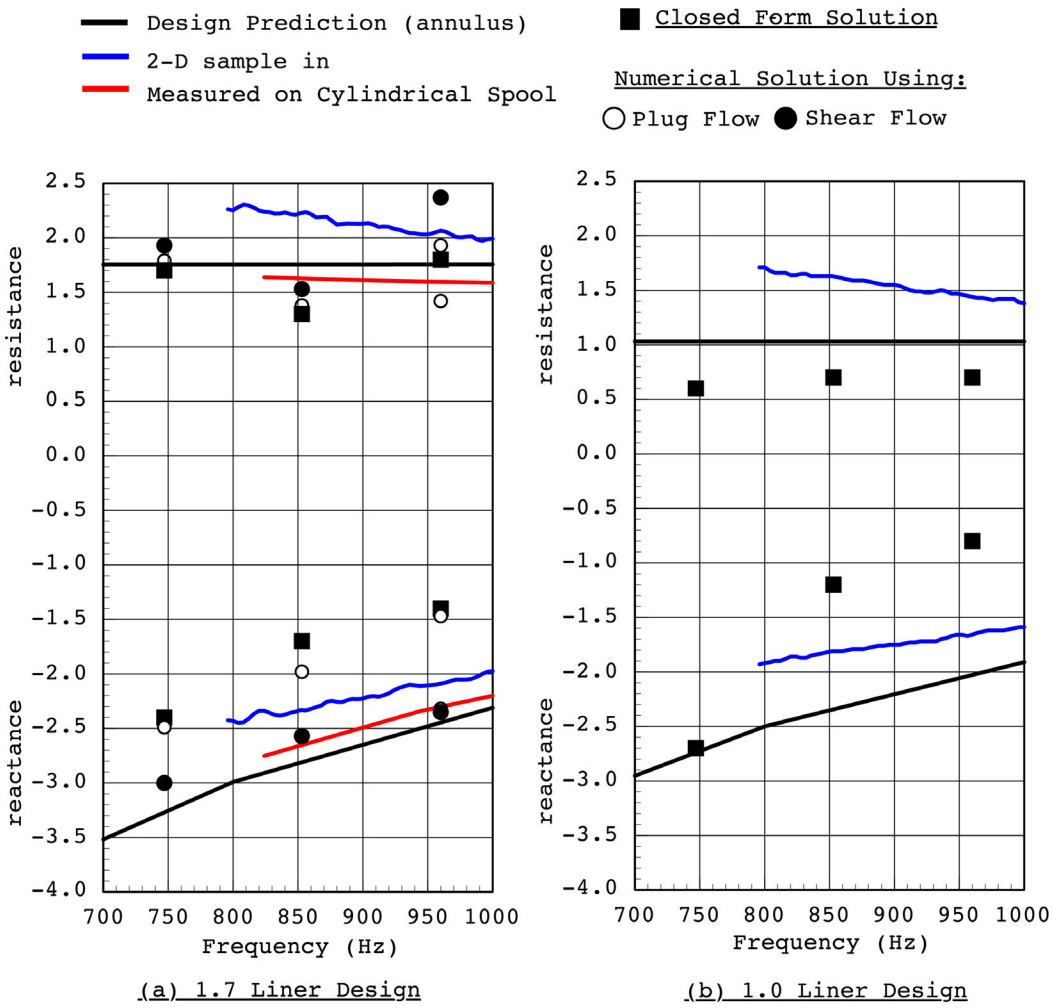

Figure 61.—Rotating Rake mode measurements over passive section illustrative results. (a) Liner design resistance of 1.7. (b) Liner design resistance of 1.0.

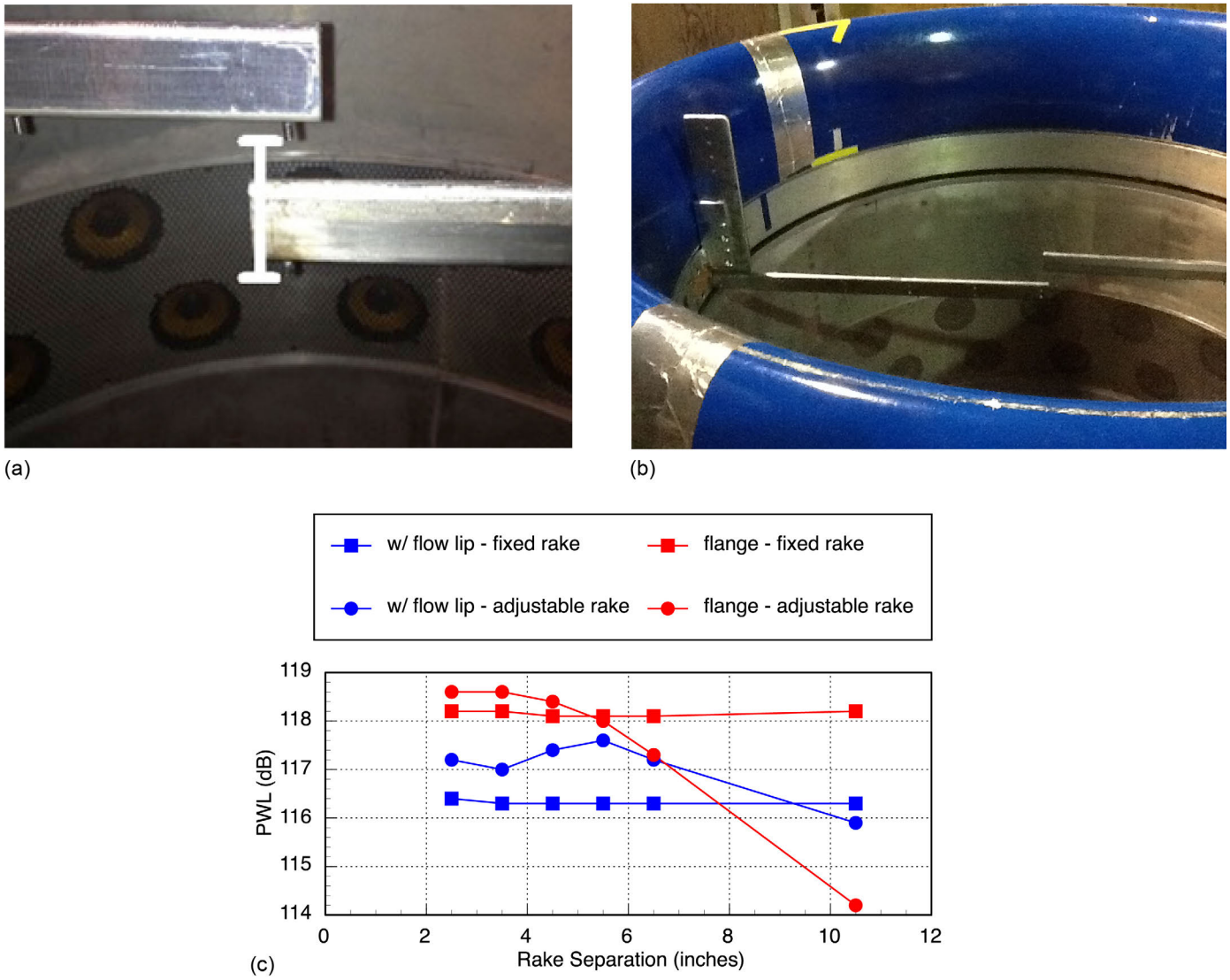

Figure 62.—Dual-rake modal measurement configuration and illustrative results. Rotating Rake measures at single axial location and measures superposition of forward propagating and reflective wave. Identified as concern in 1995 as follow-on report to original Advanced Ducted Propulser Rotating Rake 9×15/UHB (Ultra-High Bypass) entry (Ref. 62). A technique using dual rake to separate forward propagating and reflected wave was developed to address this issue (Ref. 63). (a) Closeup showing separation of dual rakes at duct centerline. (b) Second rake position offset relative to duct lip. (c) Acoustic power level versus rake separation. Where ADP is Advanced Ducted Propulser.

The concept is that the measured combination $\overline{B+C}$ is the resulting superimposed mode and is equal to B+C measured independently and mathematically combined. Thus, any technique to separate the primary from the reflected wave will result in amplitudes B and C that can be compared to the independent measurements for code validation. (B and C are arbitrary amplitudes generated by driver rows B and C.) This assumes that there are no other reflections, either from the duct exit, the anechoic termination, or the rakes themselves. It also assumes that the driver rows generate the same mode PWL (magnitude and phase) independently and when combined. It also assumes that the rake response is independent of the mode propagation direction. (The dual-rake measurements were evaluated to determine if the basic assumptions were correct. Data from each rake were acquired when installed separately, in each of the two circumferential locations, in a reverse orientation, and with both rakes installed so that the adjustable upstream rake blocked the fixed rake. Cursory analysis showed the assumptions were reasonable).

The fixed-rake mode PWLs were compared to the adjustable rake levels as a function of separation distance. At 480 Hz, a single radial mode is cut-on. The flow lip on and flow lip off cases are compared. The data show that the mode PWL variation in axial distance is greater with the flow lip removed, indicating a stronger reflection, due to constructive and destructive interference, as expected. Note also that the fixed-rake measurements are constant as the movable rake is adjusted (also as expected).

Figure 63 shows a sample of the data from the dual-row configuration. In this sample, $m = 2$ was generated and the rakes were separated axially by 6.5 in. The amplitude of driver row *C* was held constant. The amplitude of driver row *B* was varied to simulate variation of the strength of the reflection from 1.0 to 0.25. This is indicated on the plot by *G*, the ratio of the driver row *B* amplitude to driver row *C* amplitude. The mode PWL from each row actuated alone and together is presented. Variations in $\overline{B+C}$ are seen as the strength of the artificially generated reflection is modified. In this case, the interference is destructive, but it could be constructive in other circumstances.

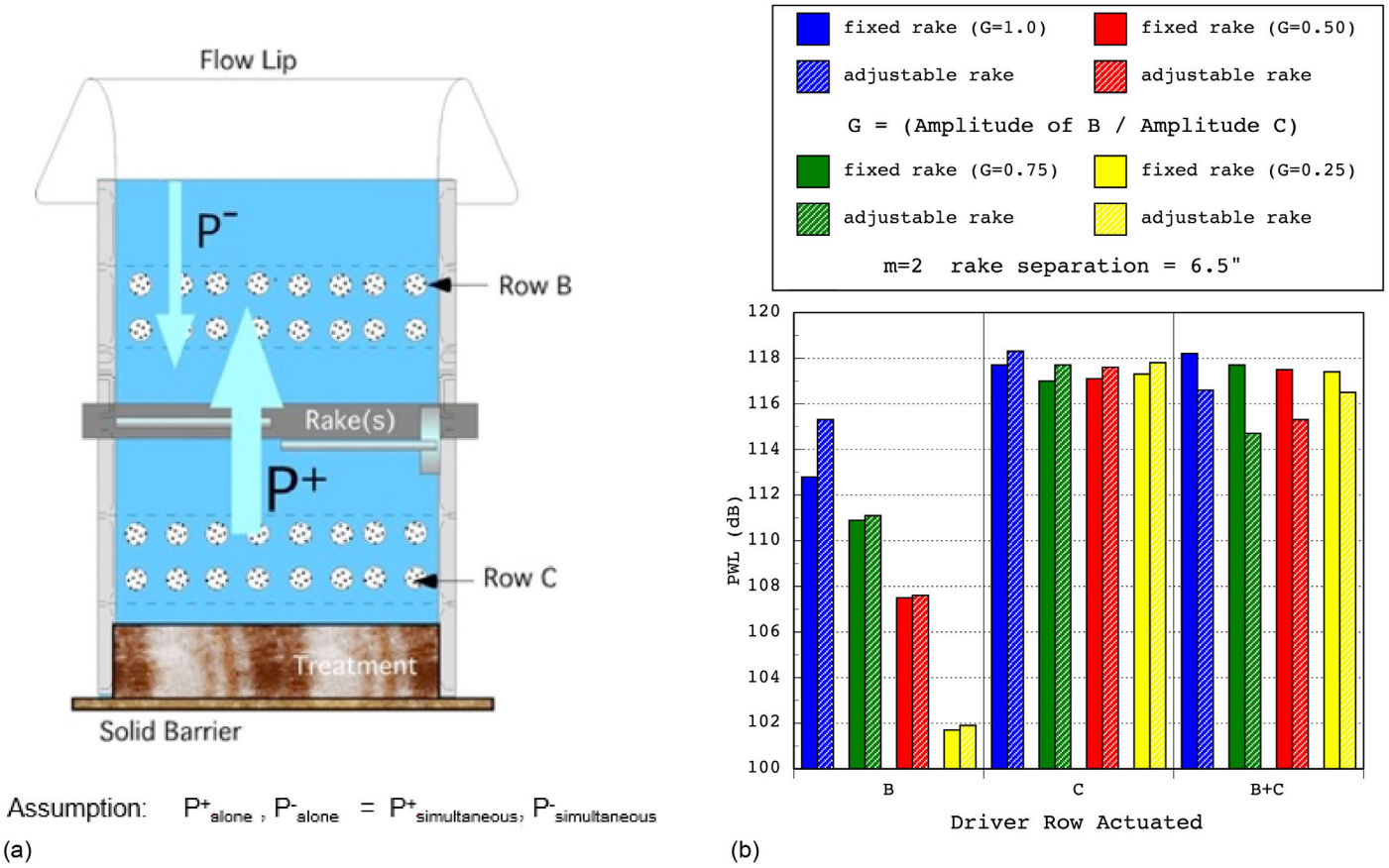

Figure 63.—Artificial mode reflection generation and illustrative results. Typical database set for artificially created forward propagating and reflected waves. Driver sets were run independently and then simultaneously. It is this that experimentally provides propagating and reflected waves. (a) Schematic of Advanced Noise Control Fan showing experimentally generated propagating and reflecting waves. (b) Acoustic power level versus driver row actuated at 1 blade passing frequency (1BPF), with m = (2,0). Where B is amplitude of driver row B (driver row closest to exit termination), C is amplitude of driver row C (driver row farthest from exit termination), and m is circumferential mode, P^+ is propagating wave, and P^- is reflected wave.

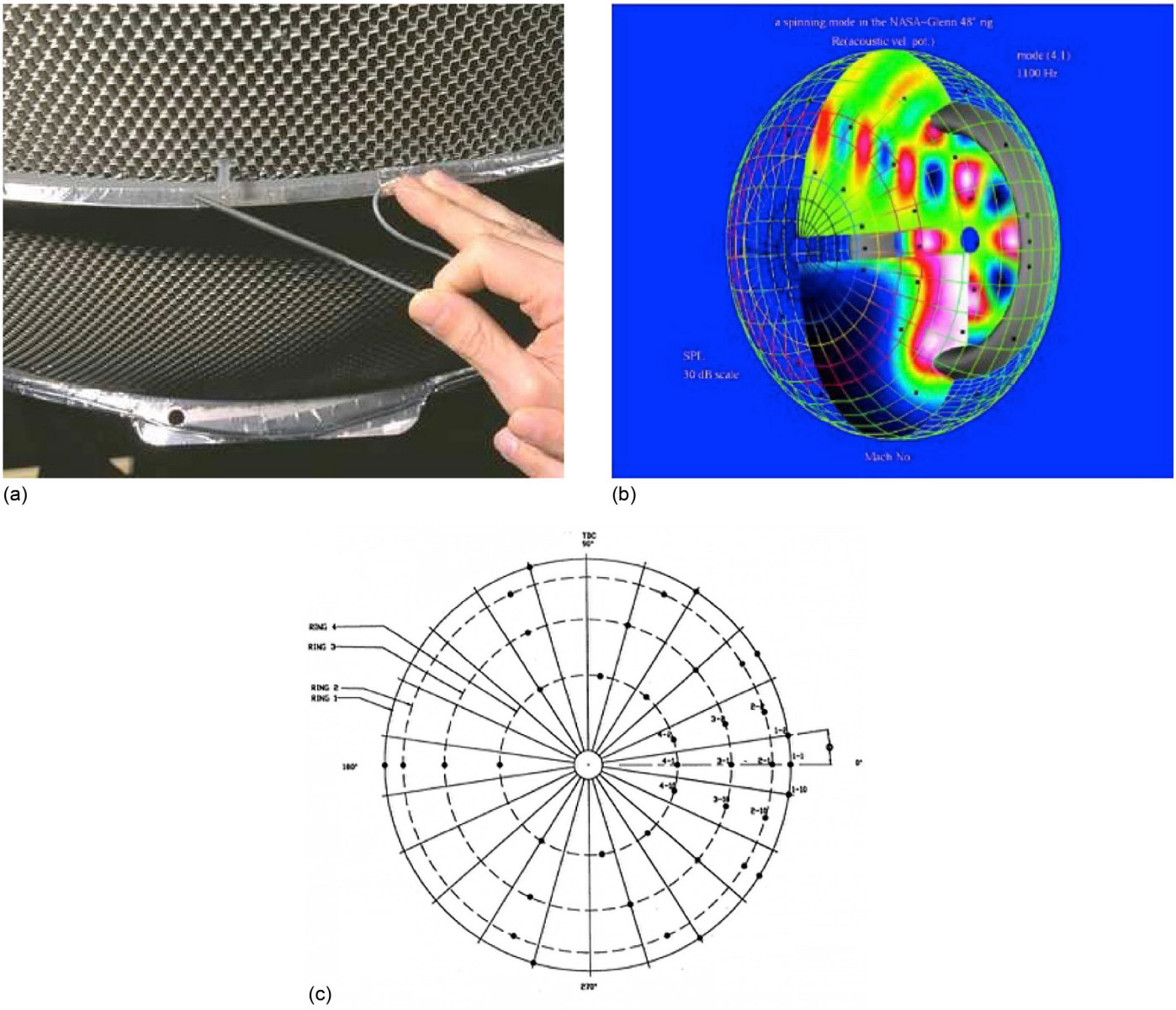

Figure 64.—Source imaging using an inflow control device (ICD) array. ICD surface used for acoustic measurement (especially useful in static engineering testing). Compare to gold standard: Rotating Rake/far field. (a) Closeup of a single microphone being inserted into ICD. (b) ICD array sound power level contour plot. (c) ICD array schematic with microphone locations.

3.7.2 Array Development

3.7.2.1 Mode Measurements Using the Inflow Control Device (ICD)

An available location for phased microphone arrays for determining engine inlet propagating mode distributions is the ICD (used on static engine tests). A proof-of-concept test[64] was performed on the ANCF since the modal distribution of the fan tone harmonics could be accurately measured by the Rotating Rake system. An array of 40 microphones was installed on the ANCF ICD (Figure 64). An acoustic duct propagation code, CDUCT, was used to generate the steering vector predictions, which are required for classical phased-array beamforming analysis. The steering vectors consist of the CDUCT-predicted complex acoustic pressure at the microphone locations for each propagating mode. The phase-accurate microphone data is then projected in the steering vector directions in order to determine the modal distribution. The dominant circumferential modes indicated by the ICD array match those from the Rotating Rake. The current ICD

array has more difficulty in accurately determining the radial mode distribution. The signal to noise also decreases in the presence of more than one dominant mode. The CDUCT-calculated steering vectors are accurate for well cut-on modes. However, errors are larger for modes closer to cutoff, which can adversely affect the signal-to-noise capabilities of the ICD array. This increase in errors is consistent with the small-angle parabolic approximation used in CDUCT. It is noted that examining microphone contour plots on the ICD can provide quick and useful information about the modal distribution of the inlet noise.

Another external technique that was investigated was a planar array in front of inlet, which may be more applicable for use in wind tunnels. The methodology utilized was to adapt the generalized inverse method and compute radiation patterns by approximating the Rayleigh integral (Tyler-Sofrin) as a coherent sum over beamform map points. A correction was applied by incorporating the Rayleigh integral with Kirchhoff factor. The HW and pressure release modes were included. Figure 65 shows the array and the in-duct results along with a comparison of the projected and measured far-field results.

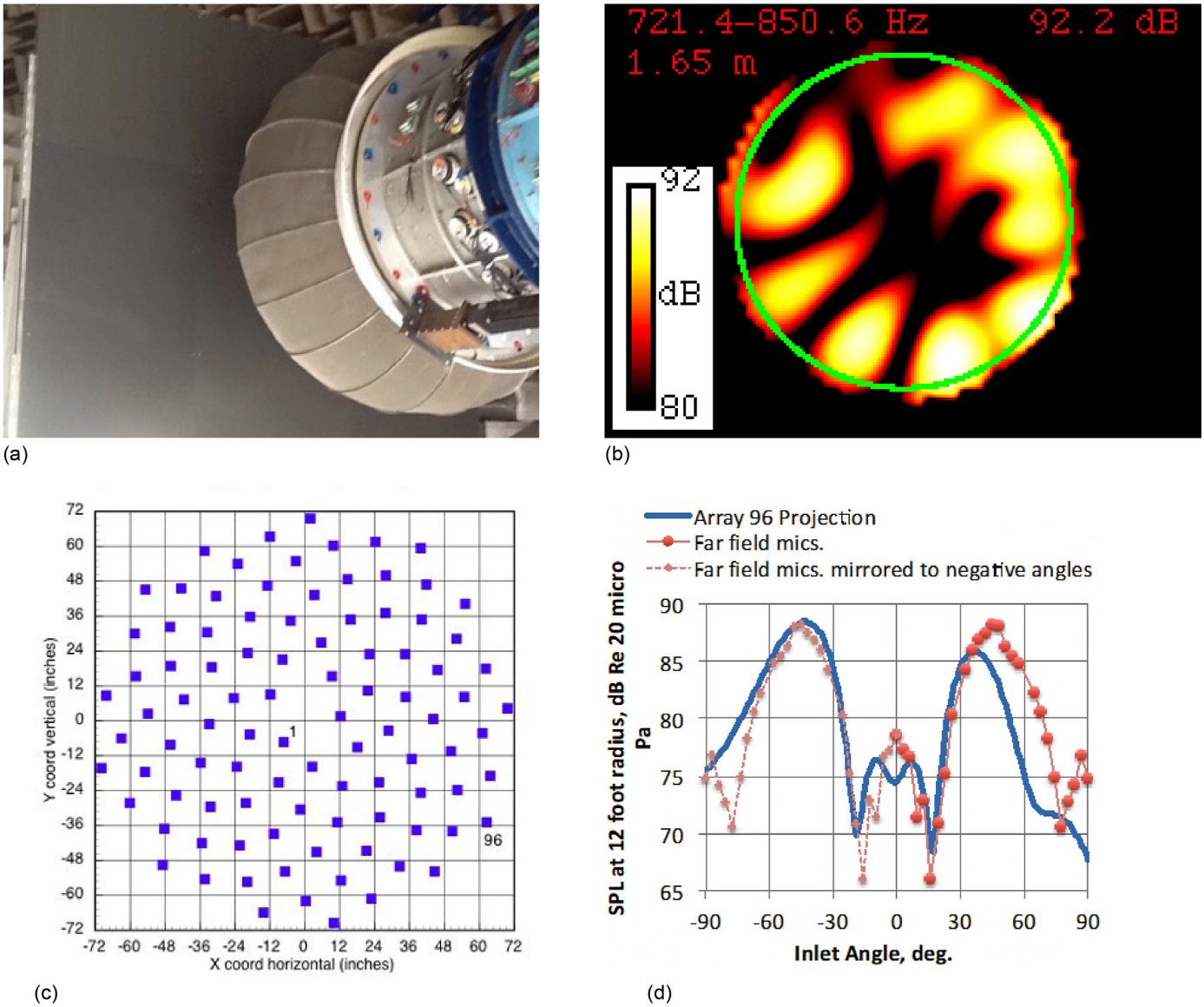

Figure 65.—In-duct imaging from Array-96 external flow-through array. (a) Array-96 mounted in front of Advanced Noise Control Fan inflow control device. (b) In-duct sound power level (SPL) contour plot. (c) Microphone locations on Array-96 (horizontal x coordinate versus vertical y coordinate). (d) SPL versus inlet angle at 12 ft radius. Where mics. is microphones.

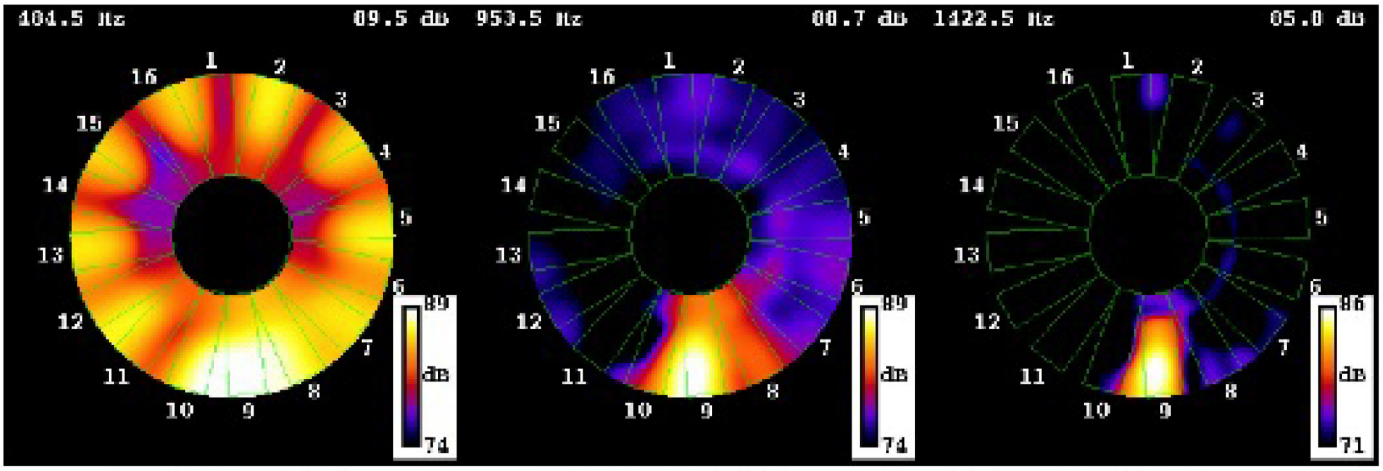

(a)

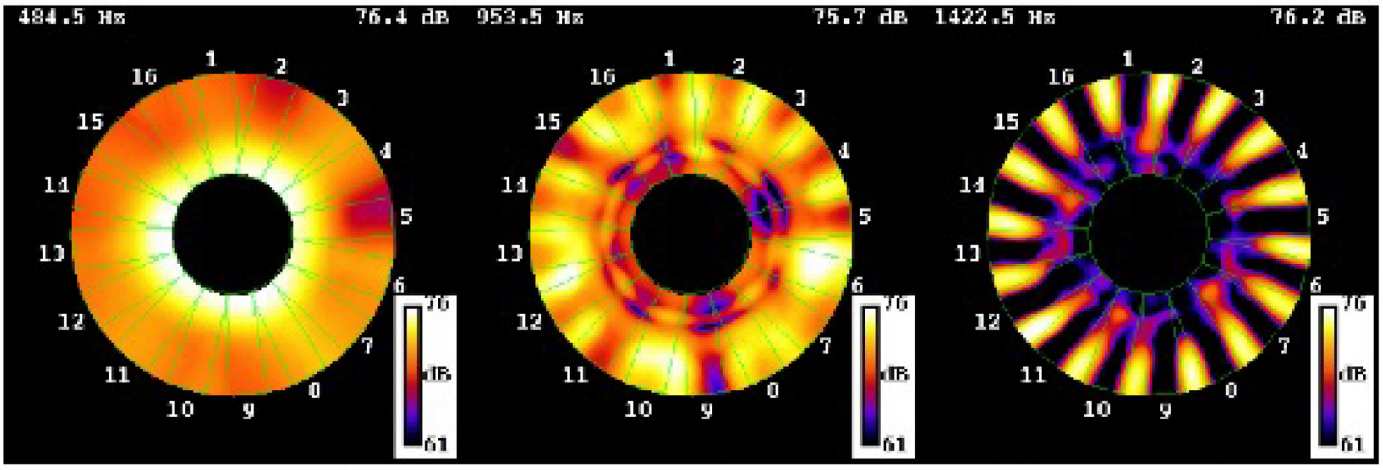

(b)

Figure 66.—Reference frame comparisons with rod installed at bottom dead center. (a) Sound power levels (SPLs) measured in stationary frame for 3 harmonics. (b) SPLs measured in virtual rotating frame for three harmonics.

3.7.2.2 Source Localization

An in-duct beamforming technique for imaging rotating BB fan sources was developed and evaluated.[65] A phased array consisting of one or more rings of microphones was employed. The data are mathematically resampled to a frame of reference rotating with the fan and subsequently used in a conventional beamforming technique in the rotating frame. The steering vectors for the beamforming are derived from annular duct modes, so that effects of reflections from the duct walls are reduced. In contrast with other work, the steering vectors represent the effect of the unsteady pressure at the fan, rather than Green's function. This improves the condition of the formulation and provides a connection to analytical studies. The test included a condition in which two of the fan blades were altered to create noise sources at known locations to provide a challenge. The CLEAN-SC[66] analysis method was applied in an attempt to remove array resolution effects from the results. Comparisons of images obtained with a stationary rod installed in the bottom dead center of the inlet using the virtual rotating microphone (VRM) technique are shown in Figure 66. The separation of the

stationary source generated by the rod from the rotating sources from the fan blades is evident. The technique was evaluated by applying it to data from the ANCF rig (Figure 67) with the FML-installed OTR. The evaluations suggested improvements to the technique could be made, which were subsequently implemented.

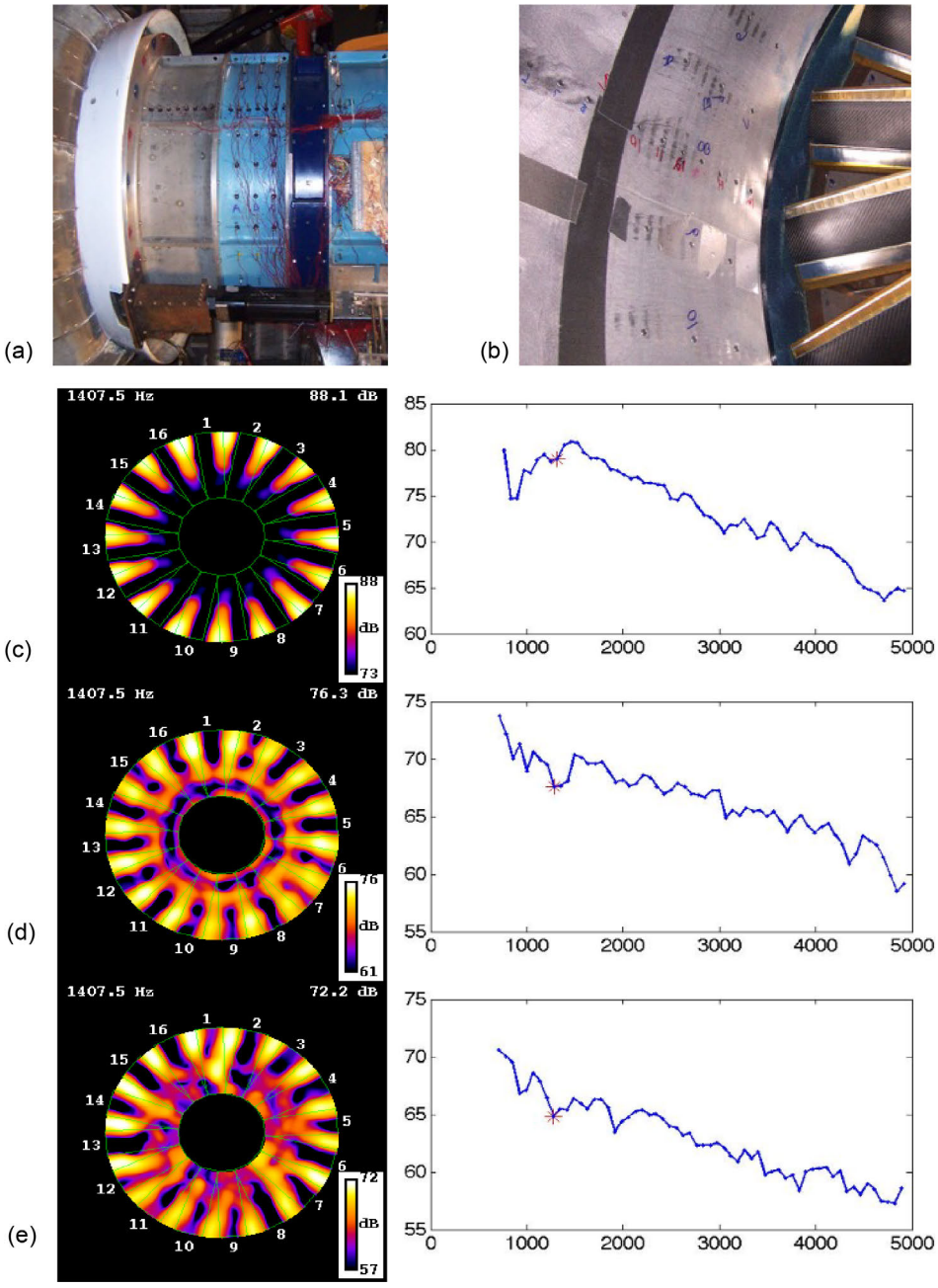

Figure 67.—Source localization using an in-duct array. Advanced in-duct imaging system with higher frequency and combined rotating and stationary sources using virtual rotating microphone method. (a) Advanced Noise Control Fan side view with microphones mounted. (b) Rotor internal view showing closeup of microphones flush-mounted to inner duct wall. (c) Measured sound power level (SPL) contours from hard wall (HW) with 1/64-in. tip gap. (d) Measured SPL contours from HW with 5/64-in. tip gap. (e) Measured SPL contours from HW with foam-metal liner with 5/64-in. tip gap.

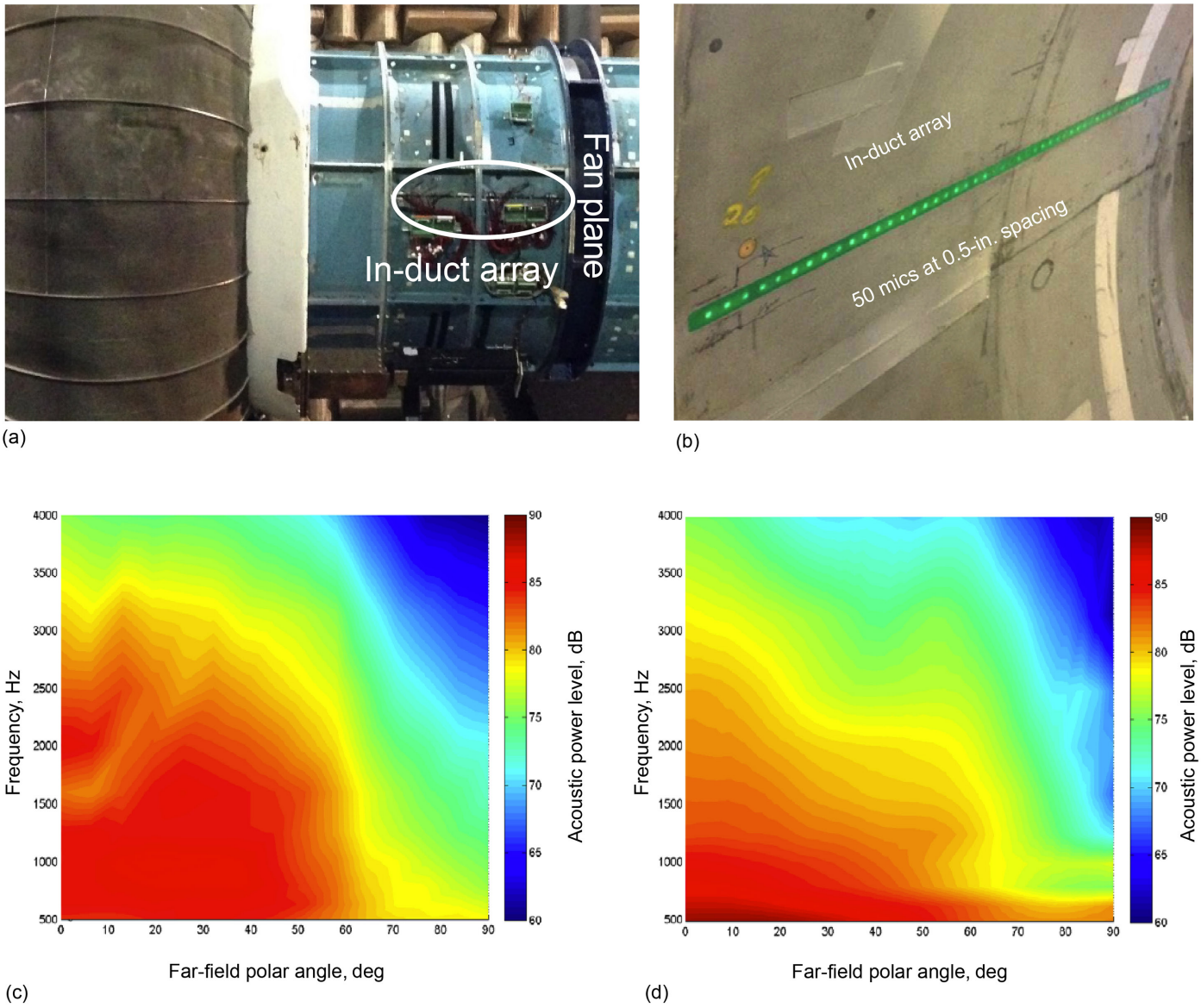

Figure 68.—Far-field projection from in-duct array. Overall objectives were to develop a validated, robust code that will determine bypass far-field absolute noise level and directivity from in-duct wall pressure measurements. Also, to separate out fan noise from other sources of noise in bypass duct in order to assess duct liner performance. Relevance to industry includes in-cell turbofan tests, that is, nonanechoic, with no far-field microphones. (a) In-duct array external mounting. (b) In-duct array internal microphone spacing. (c) Measured far-field contour plot. (c) Projected far-field contour plot.

3.7.2.3 Projection to Far Field

Far-field inlet fan noise can be measured under anechoic conditions in some model scale fan rig test facilities, but far-field aft fan noise measurements are often not possible because the bypass flow is typically ducted away through a throttle into an exhaust stack. A beamformer-based technique was developed[67] for processing measurements taken with an in-duct axial (phased) array in the bypass duct of the ANCF, which, with certain modeling assumptions, enables the fan BB noise level and directivity to be predicted in the far field. Validation with a realistic fan noise source was partially achieved by using experimental data from the ANCF low-speed fan rig (Figure 68). The modal transfer functions are

computed using a plug flow exhaust model based upon a well-established Wiener-Hopf technique (in this case the GXMunt code) but since the measured far-field data is located at three duct diameters from the exhaust, modal transfer functions are also computed at that distance with a spreading jet model using a linearized Euler code (called FLESTURN). Both models yield predictions that agree reasonably well with measured data, but the latter is more accurate at small angles to the jet axis.

3.7.3 Hot-Film Dual Overheat

Typically, voltage values obtained from a hotwire must be corrected if the experimental temperature is different from the calibration. The exact experimental temperature is often not known due to limitations in placement of a temperature measurement device. In addition, the temperature may vary in any of the dimensions hotwire data is acquired. Generally, this is not a major cause for concern since (1) the temperature variations during acquisition are small and (2) the mean values are of less concern than relative or fluctuating values. Therefore, a single bulk experimental temperature is often used to correct all voltage measurements in a given run.

Using a single temperature across the entire revolution was unacceptable for the TERB application[68] (Section 3.5.1) because of the significant temperature rise in the injected air. The compressor that supplied the injected air had a 30 to 40 °F temperature rise. In addition, the large temperature difference between the calibration (~70 °F) and the experiment (~30 to 40 °F) is probably greater than can be accurately adjusted by the standard temperature correction.

Therefore, the two-overheat method was used to determine the true velocity and temperature across a passage.[69] The hotwire probe was calibrated and data were acquired behind the rotor at two overheat ratios. Data were processed and a temperature profile due to the injection of the hotter air was assumed. The temperature profile across each blade wake at a given radial location due to injection was assumed to be identical (i.e., no blade-to-blade variation in the injected profile.) The assumed temperature correction was applied to each overheat data set independently. The passage-averaged velocity was calculated based on applying the correction from the temperature profile across the passage. The velocity at a given point in the passage from each overheat data set was compared. The temperature at that given point in the circumferential passage was adjusted by iteration until the velocities from each overheat data set agreed to within 0.5 ft/s. Thus, passage-averaged velocity and temperature profiles were obtained from the reduction process simultaneously.

Figure 69 shows the results with bulk temperature correction and iterated passage-averaged temperature correction for a typical radial location of self- and optimum-blowing cases. The significant temperature rise in the wake changes the reduced velocity profile substantially when compared to the uncorrected, presumably inaccurate, profile obtained using a constant temperature across the passage profile.

For the blowing case, it is expected that there is a temperature rise in the wake. The iterative method indicated that the peak rise is ~4.5 °F near the centerline. In addition, the variation in the wake results in an iteratively converged velocity that has a significantly different characteristic than the velocity profile from either overheat ratio. The presumed actual velocity profile is shown to be overblown, a characteristic not indicated from the unadjusted profiles. In addition, both cases have nearly identical (~11.5 °F) bulk temperature increases that are probably due to the systematic error in the temperature correction due to the large difference between the temperatures used for the calibration and the experiment.

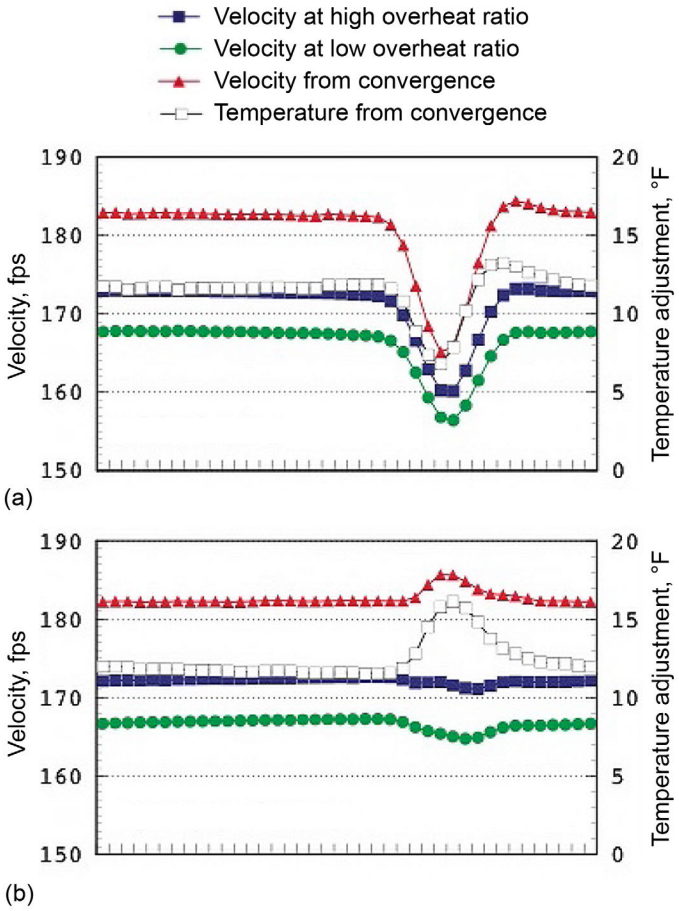

Figure 69.—Hot-film dual overheat sample results. Injected air naturally had a temperature rise due to compression. Temperature difference between wake and mean flows caused measurement error. Two-overheat method implemented to correct this, which is essentially two unknowns (V_i, T_i) and two equations. (a) Results from self blowing. (b) Results with optimum blowing. Where T_i is unknown temperature and V_i is unknown velocity.

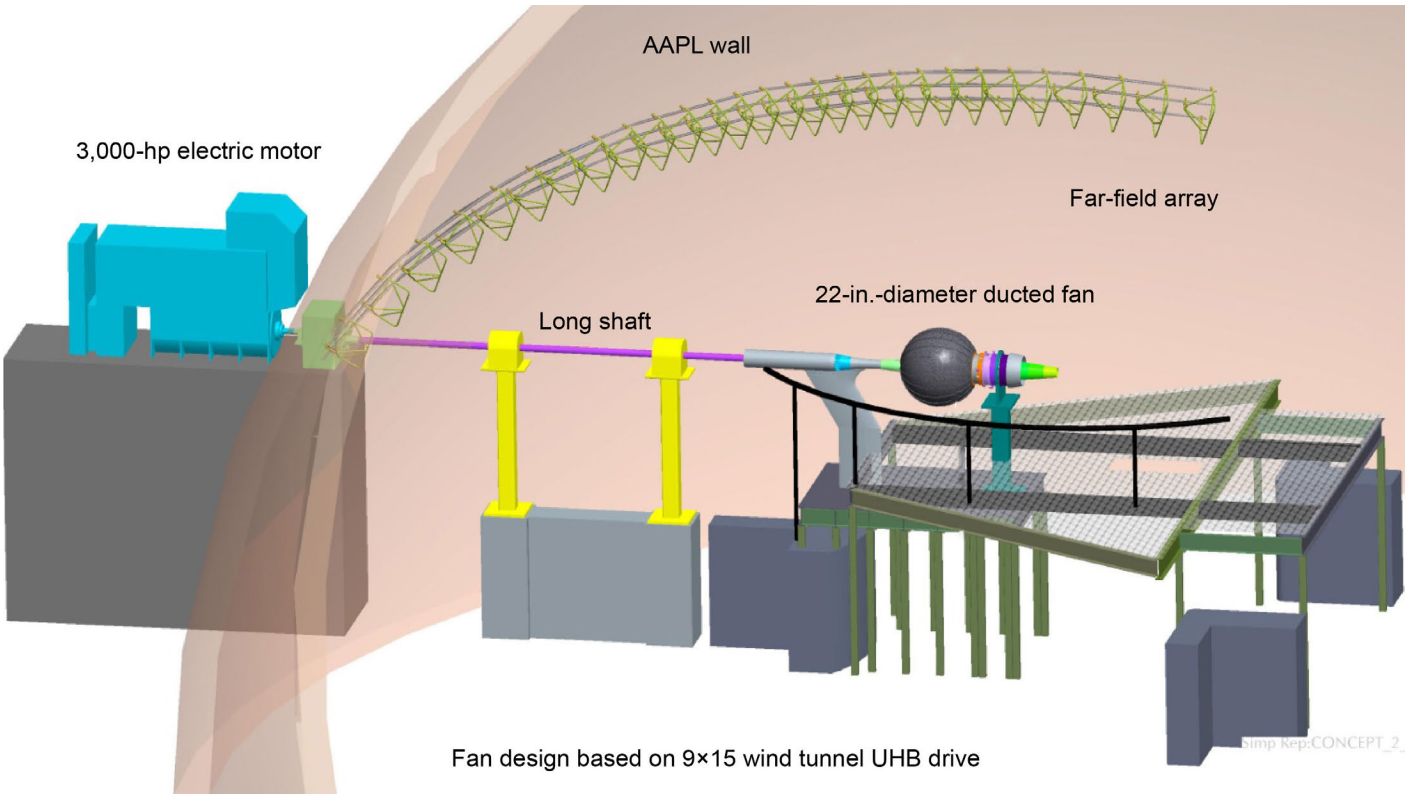

Figure 70.—Proposed Advanced Noise Control Fan II concept. Specifications: ±3,000 to 4,000 hp shaft driven, 10,000- to 15,000-RPM max. speed, externally sited motor and gearbox, able to flip orientation, and can drive fan from aft for acoustically clean inlet with exhaust collector required for aft-driven fan. Where AAPL is Aero-Acoustic Propulsion Laboratory and UHB is Ultra-High Bypass.

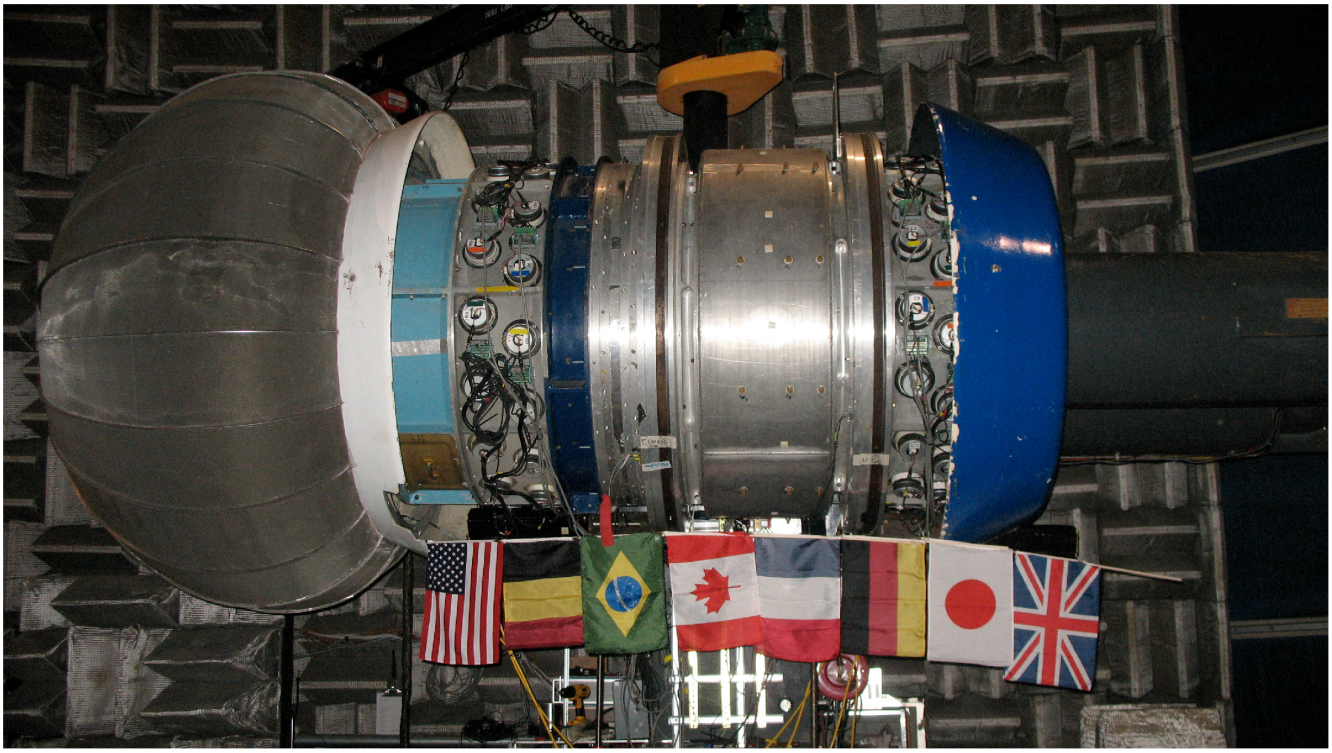

Figure 71.—Representative international collaboration shown by flags.

♦ 4 ♦

Epilogue

4.1 Proposed Replacement

Since 1995, the Advanced Noise Control Fan (ANCF) has substantially contributed to the advancement of understanding of the physics of fan tone noise generation and the development of multiple fan noise reduction technologies. However, as the low speed, loading, and pressure rise of characteristics of the ANCF are not fully representative of the physics of fan broadband noise generation, a replacement was considered necessary. In April 2010, a consultation with industry, academia, and Government stakeholders was held at the NASA semiannual Acoustic Technical Working Group meeting to solicit opinions and high-level future needs. This led to a request for resources to conduct a concept study for a potential replacement, the ANCF II.

The concept study team spent a year evaluating performance levels, infrastructure requirements, and multiple drive options. Industry comments were solicited, budgetary constraints noted, and results incorporated into a final recommendation. The ANCF II concept study results were presented to the project office on June 2011. The project office approved the further work on the concept and committed resources through the Preliminary Design Review, which was held in September of 2012.

The team recommended to the aeroacoustics community a design[70,71,72] for a 3,000-hp electric motor, shaft-driven fan in a 22-in.-diameter duct that could be driven from either the front or aft to enable clean far-field measurements in either arc. Unfortunately, the estimated costs were not within the budgetary scope and the effort was halted. Figure 70 presents a conceptual layout of the proposed ANCF II that would have been located on the mezzanine in the Aero-Acoustic Propulsion Laboratory (AAPL).

4.2 Collaboration

In addition to the highly prolific NASA studies accomplished, international collaboration using the ANCF on an explicit test, and/or its all-encompassing database of geometry and aeroacoustic data occurred.

Several students earned advanced degrees based on collaborations centered on the ANCF. A student from the University of Akron proposed and participated in custom modifications to the operating procedure to acquire transient data for his master's thesis.[73] Students from the Federal University of Brasilia (FUB) developed a Computational AeroAcoustics (CAA) code for their master's[74] and Ph.D. degrees[75] theses using the 2008 geometry and data set for validation. At the University of São Paulo (USP), a student based his master's degree topic[76] on in-duct array modal measurements from an internal array installed on the ANCF and comparisons to the Rotating Rake. A student from the University of Southampton based a part of her Ph.D. thesis on a collaborative test with interstage liners.[77]

The University of Sherbrook[78] and the Office National d'Etudes et de Recherches Aérospatiales (ONERA) utilized the available data and/or geometry package to validate their in-house CAA codes. Commercial codes, for example, FINE™/Aeroacoustics (NUMECA) and PowerFLOW® (Exa Corporation),[79] were partially validated using the data and/or geometry package. An interesting YouTube video[80] was created to demonstrate the results.

There have been multiple Space Act Agreements, including three international (specifically with FUB, USP, and the Institute for Sound and Vibration (ISVR)), focusing on collaborations using the ANCF. A simplified version of the ANCF was designed and manufactured, and is used for research at USP.[81]

Figure 71 shows the flags of nations participating in ANCF research programs.

4.3 Relocation

In order to make room for a small turbofan engine test article (called DART[82]), the ANCF was relocated to the University of Notre Dame Turbomachinery Laboratory (NDTL). As a result of this change of venue, the ANCF will be

an outdoor test rig using ground-plane microphones[83] (Figure 72) and will be transported over one-quarter mile from the storage to the test site along the path shown in Figure 73. In spite of these significant differences, the far-field data comparison in Figure 74 of the data acquired in the AAPL facility to the new University of Notre Dame (UND) outdoor location is remarkably similar.

Transferring the ANCF to a university to jointly operate the ANCF will maintain the critical research capability and provide relevant STEM educational opportunities in the area of fan aeroacoustics.

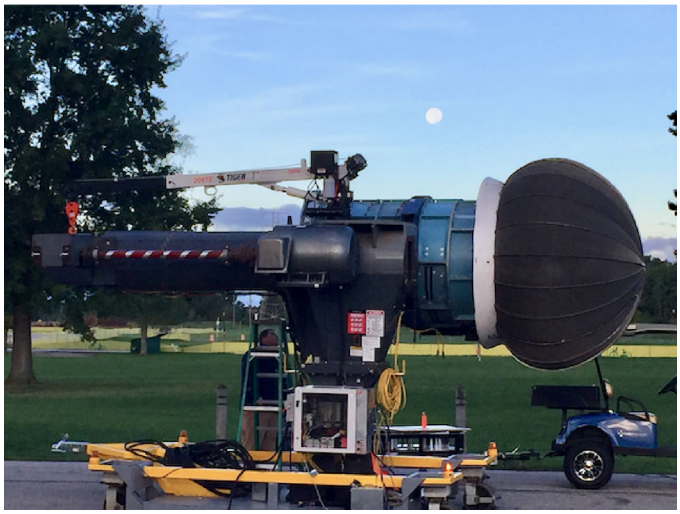

Figure 72.—Outdoor location of Advanced Noise Control Fan at University of Notre Dame.

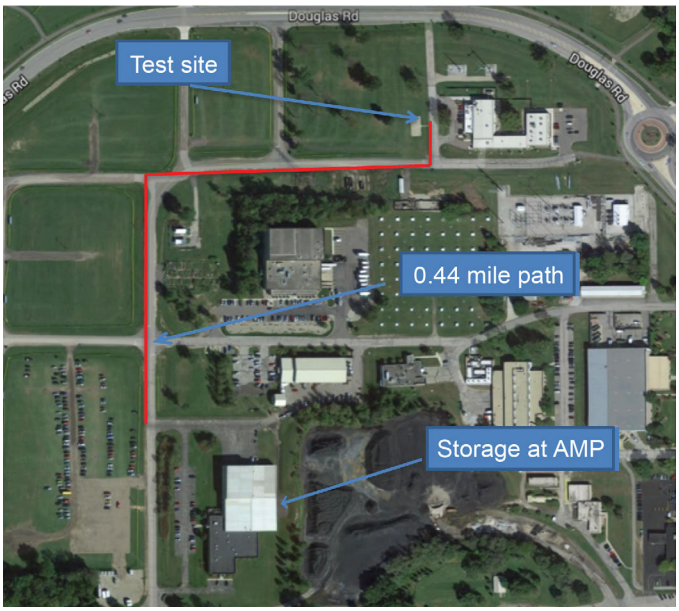

Figure 73.—Outdoor travel path of Advanced Noise Control Fan at University of Notre Dame.

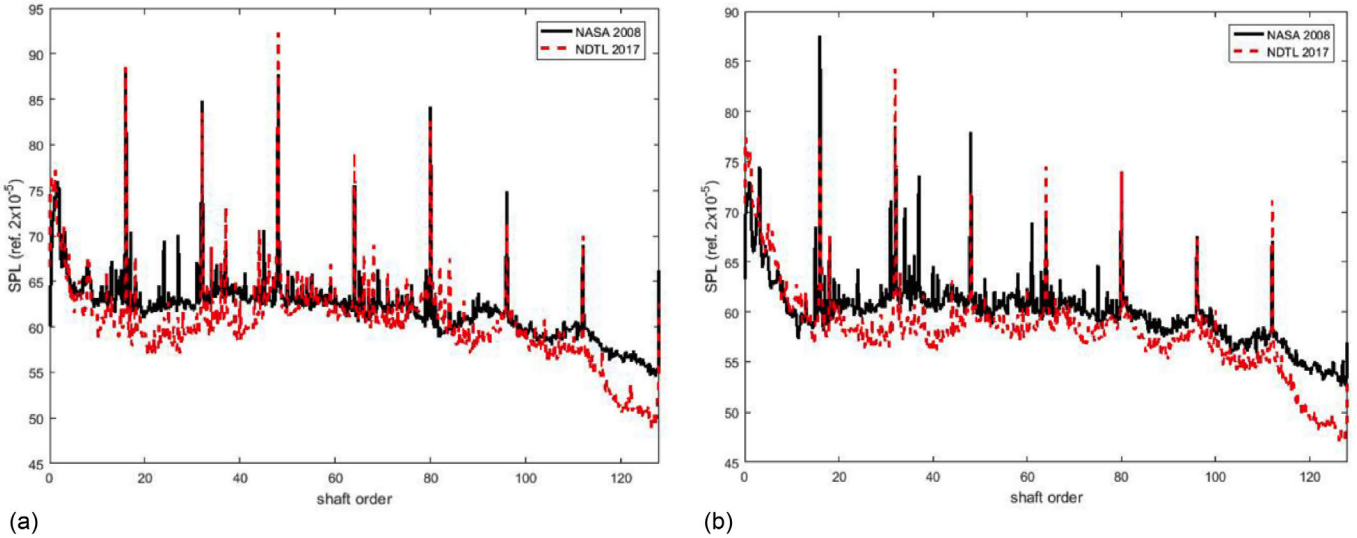

Figure 74.—Advanced Noise Control Fan commissioning test date comparison: Notre Dame Turbomachinery Laboratory (NDTL)—red, versus NASA Glenn Research Center—black. (a) Far-field spectra from microphone in forward arc. (b) Far-field spectra from microphone in aft arc.

♦ 5 ♦

Conclusions

The Advanced Noise Control Fan (ANCF) has contributed considerably to the various NASA Aeronautics Research Mission Directorate (ARMD) research programs focused on reducing aircraft noise and mitigating its impact on the public. It has a complete aeroacoustic data and/or geometry set publicly available. The ANCF served as a wide-ranging enabler of cross-center, academic, industry, and international collaborations. It is a flexible, adaptable, highly prolific test rig that evolved to make wide-ranging contributions to the field of aeroacoustics for over 20 years and beyond (Figure 75), including developing several technologies that were evaluated on production turbofans (static and flight test). Transferring the ANCF to the University of Notre Dame (UND) to jointly operate the test rig will maintain research its capability and provide relevant Science, Technology, Engineering and Mathematics (STEM) opportunities in the area of fan aeroacoustics.

Figure 75.—Evolution of Advanced Noise Control fan from 1994 to 2016. (a) Initial, very clean configuration. (b) Very cluttered configuration. (c) Beginning of disassembly for transport. (d) Arrival at University of Notre Dame.

♦ Appendix A ♦
Nomenclature

A–Q	adaptive-quadrature
AAPL	Aero-Acoustic Propulsion Laboratory
ADP	Advanced Ducted Propulser
AIAA	American Institute of Aeronautics and Astronautics
ANC	Active Noise Control
ANCF	Advanced Noise Control Fan
ARMD	Aeronautics Research Mission Directorate
AST	Advanced Subsonic Technology
BB	broadband
BPF	blade passing frequency
BiFi	bifurcation
CAA	Computational AeroAcoustics
CFANS	Configurable Fan Artificial Noise Source
CFD	computational fluid dynamics
D/A	digital to analog
DART	DGEN Aero-Propulsion Research Turbofan
DVC2D	Duct Viscous Code 2D
EPNL	effective perceived noise level
ERA	Environmentally Responsible Aviation
FIR	finite impulse response
FML	foam-metal liner
FUB	Federal University of Brasilia
GE	General Electric
GFIT	grazing flow impedance tube
GUI	graphical user interface
HAE	Hersh Acoustical Engineering, Inc.
HQ	Herschel-Quincke
HW	hard wall
HWAE	Hersh Walker Acoustical Engineering, Inc.
I/O	input/output
ICD	inflow control device
ID	identification
ISVR	Institute for Sound and Vibration
L/D	length to diameter ratio
LMS	least mean square
MASSCOMP	Massachusetts Computer Corporation
MDOF	multidegree of freedom
MIMO	multiple input, multiple output
Mic.	microphone
NATR	Nozzle Acoustic Test Rig
NDTL	Notre Dame Turbomachinery Laboratory
NESC	NASA Engineering and Safety Center
NIT	normal incidence-impedance tube

OA	overall
ONERA	Office National d'Etudes et de Recherches Aérospatiales
OTH	other
OTR	over the rotor
PWL	acoustic power level
PZT	lead zirconate titanate
QAT	Quiet Aircraft Technology
Rot	rotating
RS	rotor-stator
RPMc	revolutions per minute, corrected
RVCQ3D	Rotor Viscous Code Quasi-3-D
S/W	software
SDOF	single degree of freedom
SDT	Source Diagnostic Test
SISO	single-input single-output
SPL	sound power level
STEM	Science, Technology, Engineering and Mathematics
SW	soft wall
TERB	trailing-edge rotor blowing
THUNDER	Thin UNimorph DrivEr and sensor
TOT	total
TRL	technology readiness level
UCFANS	Ultrasonic Configurable Fan Artificial Noise Source
UHB	Ultra-High Bypass
UND	University of Notre Dame
USP	University of São Paulo
VPI	Virginia Polytechnic Institute
VRM	virtual rotating microphone
1D	one-dimensional
2D	two-dimensional
3D	three-dimensional

Symbols

B	amplitude of driver row B (driver row closest to exit termination)
C	amplitude of driver row C (driver row farthest from exit termination)
G	amplitude of B/C
m	circumferential mode
N	independent control channel
n	radial mode
P^+	propagating wave
P^-	reflected wave
T_i	temperature unknown
V	velocity
V_i	velocity unknown
V_{ang}	angular velocity
V_{avg}	average velocity

σ	hub-to-tip ratio
θ	flow angle
θ_{avg}	average flow angle

♦ Appendix B ♦
General Electric Global Research Correspondence

GE Global Research

Trevor H. Wood, Ph.D.
Principal Engineer
Aero Systems

1 Research Circle
Niskayuna, NY 12309
USA

T 518 387 6600
M 518 330 3193
F 518 387 4567
trevor.wood@research.ge.com

Daniel L. Sutliff, Ph.D.
NASA Glenn Research Center
Aeroacoustics Branch
Bld 54 Rm 207, MS 54-3
21000 Brookpark Road
Cleveland, OH 44135

May 29, 2014

Dear Dr. Sutliff:

I was disappointed to hear of the ANCF rig removal from the AAPL facility at NASA Glenn. The ANCF has proved to be an instrumental facility for fundamental research in fan noise and associated technologies that has benefited the aeroacoustics communities in academia, government and industry a great deal over the decades it has been in service.

GE specifically has benefited from the good work performed by you and your collaborators over the years. While the aerodynamic flow conditions are considerably less aggressive relative to aviation turbofans in operation, the ANCF is particularly well-suited to early TRL concept tests and downselection. You have helped me directly in your ability the make proof-of-concept testing affordable for limited research budgets typically available to uncertain concepts. That has made research tests at the ANCF particularly advantageous.

While I am certain it will be difficult for your organization to see this valuable research vehicle leave the NASA campus, the opportunity for students to have direct access to perform research on such a vehicle would provide an incredible experience for our upcoming engineers and scientists in aeroacoustics. I become almost envious when I imagine myself in that position as a student and think of how enriching an experience that would be. This will be such a great asset to the fortunate university that becomes the new home for the ANCF rig. I also hope this move may foster new opportunities for collaborative research involving academia, NASA and GE. In addition to the direct benefits of advancing a particular technology for fan noise, recruiting talent for industrial research is always made easier and more effective when drawn from fruitful collaborations early in one's experience as a student.

Please do not hesitate to contact me both during and after this transition to discuss ideas or opportunities for GE to cooperate in future programs where ANCF will continue to clarify key underlying questions in fan noise technologies.

Yours truly,

Trevor Wood

♦ Bibliography ♦

Papers Based on Advanced Noise Control Fan Geometry and/or Data

Theses

Brown, Clifford A., Analysis of Rotor-Stator Interaction Noise During a Speed Transient. University of Akron, Master's Thesis, 2001. http://library.uakron.edu/record=b2404148~S24

Caldas, L.C.: Beamforming e Análise Modal em Duto Utilizando Arranjo Circular de Microfones Para Caracterização de Ruído Banda-Larga em Motores Aeronáuticos Turbo-Fan. University of São Paulo, 2016.

Maldonado, Ana Luisa Pereira: N Predicão Numérica do Ruído Tonal Para o Advanced Noise Control Fan. Universidade de Brasília, 2002.

Maldonado, Ana Luisa Pereira: On the Prediction of the Effect of Interstage Liners in Turbofan Engines. Doctoral Thesis, Univ. of Southampton, England, 2016.

Pimenta, B.G.: Simulação Numérica de Ondas Não-lineares em Dinâmica dos Gases e Ruído de Interação Rotor-Estator em Turbofans Aeronáuticos. Ph.D. Thesis, Universidade de Brasília, 2016.

Journals

deLaborderie, Jerome; and Moreau, Stephane: Prediction of Tonal Ducted Fan Noise. J. Sound Vib., vol. 372, 2016.

Nallasamy, M.; Sutliff, D.L.; and Heidelberg, L.J.: Propagation of Spinning Acoustic Modes in Turbofan Exhaust Ducts. J. Propul. Power, vol. 16, no. 5, 2000.

Orselli, Reinaldo; Carmo, Bruno Souza; and Queiroz, Rudner Lauterjung: Noise Predictions of the Advanced Noise Control Fan Model Using Lattice Boltzmann Method and Ffowcs Williams—Hawkings Analogy. J. Braz. Soc. Mech. Sci. Eng., vol. 40, no. 1, 2018.

Sanjoséa, Marlene, et al.: Effect of Weak Outlet-Guide-Vane Heterogeneity on Rotor-Stator Tonal Noise. AIAA J., vol. 55, no. 4, 2017.

Sanjoséa, Marlene, et al.: Tonal Noise Prediction and Validation on the ANCF Rotor-Stator Configuration. Noise Control Eng. J., vol. 63, no. 6, 2015, pp. 552–562.

Smith, J.P., et al.: Active Noise Control on a Large-Scale Ducted Fan With Inlet Wave-Number Sensing. J. Acoust. Soc. Am., vol. 107, no. 5, 2000.

Sutliff, D.L., et al.: Low-Speed Fan Noise Reduction With Trailing Edge Blowing. Int. J. Aeroacoust., vol. 1, no. 3, 2002.

Sutliff, Daniel L.: Rotating Rake Turbofan Duct Mode Measurement System. Int. J. Aeroacoust., vol. 118, no. 3, 2005.

Sutliff, Daniel L.; and Dahl, Milo D.: Techniques for Analyzing Rotating Rake Mode Measurements Over Passive Treatment. Int. J. Aeroacoust., vol. 15, 2016, pp. 430–461.

Sutliff, Daniel L.; and Jones, Michael G.: Low-Speed Fan Noise Attenuation From a Foam-Metal Liner. J. Aircraft, vol. 46, no. 4, 2009.

NASA Technical Memorandums/AIAA Conference Papers

Bozack, Richard F., Jr.: Advanced Noise Control Fan Aerodynamic Performance. NASA/TM—2009-215807, 2009.

Brochine, Carlos C.; and Greco, Paulo: Implementation of a Semi-Analytical Method for Prediction of Fan Rotor-Stator Interaction Broadband Noise. AIAA 2013–2148, 2013.

Caldas, Luciano, et al.: In-Duct Beamforming Noise Source Estimation Mode Detection University of São Paulo Fan Rig. AIAA 2015–2233, 2015.

Caldas, Luciano, et al.: In-Duct Rotating Beamforming and Mode Detection of Fan Noise Sources. AIAA 2016–3034, 2016.

Casalino, Damiano, et al.: Towards Lattice-Boltzmann Prediction of Turbofan Engine Noise. AIAA 2014–3101, 2014.
Crunteanu, Daniel; and Rizea, Cezar: Advanced Trailing Edge Blowing Concepts for Fan Noise Control. INCAS Bulletin, vol. 4, no. 1/2012, 2012, pp. 15–22.
Dahl, Milo D.; and Hixon, Duane R.: Numerical Predictions of Mode Reflections in an Open Circular Duct: Comparison With Theory. AIAA 2015–2524, 2015.
Dahl, Milo D.; and Sutliff, Daniel L.: Analysis of Dual Rotating Rake Data From the NASA Glenn Advanced Noise Control Fan Duct With Artificial Sources. AIAA 2014–3316, 2014.
Dahl, Milo D.; and Sutliff, Daniel L.: Numerical Technique for Analyzing Rotating Rake Mode Measurements in a Duct With Passive Treatment and Shear Flow. AIAA 2007–3679 (NASA/TM—2007-214966), 2007. http://ntrs.nasa.gov
de la Riva, D.H.; Burdisso, R.; and Ng, W.: AFT Fan Noise Control Using Herschel/Quincke-Liner Systems. AIAA 2005–3071, 2005.
Dougherty, Robert P.; and Walker, Bruce E.: Virtual Rotating Microphone Imaging of Broadband Fan Noise. AIAA 2009–3121, 2009.
Dougherty, Robert P.; Walker, Bruce E.; and Sutliff, Daniel L.: Locating and Quantifying Broadband Fan Sources Using In-Duct Microphones. AIAA 2010–3736 (NASA/TM—2010-216931), 2010. http://ntrs.nasa.gov
Ferrante, Piergiorgio, et al.: Integrated "CFD-Acoustic" Computational Approach to the Simulation of Aircraft Fan Noise. ASME GT2014–26429, 2014.
Figueroa-Ibrahim, K., et al.: Evaluation of Radiated Sound From the Advanced Noise Control Fan Facility in an Outdoor Environment Using Ground Microphones. Submitted to 2019 AIAA Power and Energy Forum.
Gazella, Matthew R., et al.: Evaluating the Acoustic Benefits of Over-the-Rotor Acoustic Treatments Installed on the Advanced Noise Control Fan. AIAA 2017–3872, 2017.
Halasz, Christopher, et al.: Fan Flow Control for Noise Reduction Part 1: Advanced Trailing Edge Blowing Concepts. AIAA 2005–3025, 2005.
Heidelberg, Laurence J., et al.: A Unique Ducted Fan Test Bed for Active Noise Control and Aeroacoustics Research. NASA TM–107213 (AIAA–96–1740), 1996. http://ntrs.nasa.gov
Heidelberg, Laurence J.; Sutliff, Daniel L.; and Nallasmay, M.: Azimuthal Directivity of Fan Tones Containing Multiple Modes. NASA TM–107464 (AIAA 1997–1587), 1997. http://ntrs.nasa.gov
Hixon, Ray, et al.: Comparison of Computational Aeroacoustics Prediction of Acoustic Transmission Through a 3D Stator Geometry With Experiment. AIAA 2014–1405, 2014.
Jones, M.G., et al.: Assessment of Soft Vane and Metal Foam Engine Noise Reduction Concepts. AIAA 2009–3142, 2009.
Jones, Michael G.; and Howerton, Brian M.: Evaluation of Novel Liner Concepts for Fan and Airframe Noise Reduction. AIAA 2016–2787, 2016.
Ju, Hongbin, et al.: Investigation of Fan Wake-OGV Interaction Broadband Noise. AIAA 2013–2151, 2013.
Koch, L. Danielle: An Experimental Study of Fan Inflow Distortion Tone Noise. NASA/TM—2010-215844 (AIAA 2009–3290), 2009. http://ntrs.nasa.gov
Koch, L. Danielle: Predicted and Measured Modal Sound Power Levels for a Fan Ingesting Distorted Inflow. NASA/TM—2010-216782 (AIAA 2010–22312), 2010. http://ntrs.nasa.gov
Koch, L. Danielle: Predicting the Inflow Distortion Tone Noise of the NASA Glenn Advanced Noise Control Fan With a Combined Quadrupole-Dipole Model. NASA/TM—2012-217673 (AIAA 2012–2196), 2012. http://ntrs.nasa.gov
Koch, L. Danielle: Validation of the Predicted Circumferential and Radial Mode Sound Power Levels in the Inlet and Exhaust Ducts of a Fan Ingesting Distorted Inflow. NASA/TM—2012-217253, (AIAA 2011–2808), 2012. http://ntrs.nasa.gov

Lan, Justin H.; and Breard, Cyrille: Development and Validation of a 3D Linearized Euler Solver. AIAA 2006–2585, 2006.

Lan, Justin; Breard, Cyrille; and Guo, Yueping: Validation and Application of Two Frequency Domain Propagation Acoustic Codes. AIAA 2003–3244, 2003.

Lan, Justin H.; Premo, John W.; and Sutliff, Daniel L.: Inlet Mode Measurements With an Inflow Control Device Microphone Array. AIAA 2002–2563, 2002.

Langford, Matthew D., et al.: Fan Flow Control for Noise Reduction Part 3: Rig Testing of Optimal Design. AIAA 2005–3027, 2005.

Loew, Raymond A., et al.: Advanced Noise Control Fan. NASA/TM–2006-214368 (AIAA 2006–3150), 2006. http://ntrs.nasa.gov

Loew, Raymond A., et al.: The Advanced Noise Control Fan. AIAA 2006–3150, 2006.

Maldonado, A.L.P., et al.: Sound Propagation in Lined Annular Ducts With Mean Swirling Flow. AIAA 2015–2522, 2015.

Maldonado, Ana Luisa; Miserda, Roberto F. Bobenrieth; and Pimenta, Braulio G.: Computational Tonal Noise Prediction for the Advanced Noise Control Fan. AIAA 2012–2128, 2012.

Mann, Adrien, et al.: Advanced Noise Control Fan Direct Aeroacoustics Predictions Using a Lattice-Boltzmann Method. AIAA 2012–2287, 2012.

Mann, Adrien, et al.: Investigation of Inflow Condition Effects on the ANCF Aeroacoustics Radiation Using LBM. Proceedings of the 41st International Congress and Exposition on Noise Control Engineering 2012, Vol. 12, 2012.

McAllister, Joseph, et al.: The Advanced Noise Control Fan Baseline Measurements. NASA/TM—2009-215595 (AIAA 2009-0624), 2009. http://ntrs.nasa.gov

Miserda, Roberto F. Bobenrieth, et al.: Validation of a Moving-Body High-Order Immersed Boundary Method for Direct Tonal Noise Predictions of Rotor-Stator Interactions. AIAA 2013–2292, 2013.

Miserda, Roberto F. Bobenrieth; Maldonado, Ana L.; and Gutierrez, Braulio: A Moving-Body High-Order Immersed Boundary Method for Computational Aeroacoustics. AIAA 2011–2753, 2011.

Nallasamy, M.; Sutliff, D.L.; and Heidelberg, L.J.: Propagation of Spinning Acoustic Modes in Turbofan Exhaust Ducts. J. Propul. Power, vol. 16, no. 5, 2000.

Nark, Douglas M.; and Jones, Michael G.: Development of a Multifidelity Approach to Acoustic Liner Impedance Eduction. AIAA 2017–3181, 2017.

Nark, Douglas M.; Jones, Michael G.; and Sutliff, Daniel L.: Modeling of Broadband Liners Applied to the Advanced Noise Control Fan. AIAA 2015–2693, 2015.

Nark, Douglas M., et al.: Improved Broadband Liner Optimization Applied to the Advanced Noise Control Fan. AIAA 2014–3103, 2014.

Orselli, RM., et al.: Noise Predictions of the Advanced Noise Control Fan Model Using Lattice Boltzmann Method and Ffowcs Williams–Hawkings Analogy. Instability and Control of Massively Separated Flows, Proceedings of the International Conference on Instability and Control of Massively Separated Flows, Vassilis Theofilis and Julio Soria, eds., Prato, Italy, 2013, pp. 243–248.

Parente, C.A., et al.: Hybrid Active/Passive Jet Engine Noise Suppression System. NASA/CR—1999-208875 (NSL–RPT–98–002), 1999. http://ntrs.nasa.gov

Pasco, Y., et al.: Active Noise Control Simulation of Tonal Turbofan Noise in Aero Engines. AIAA 2014–3187, 2014.

Pimenta, Braulio G.; and Miserda, Roberto F. Bobenrieth: Direct Noise Computation of Linear and Nonlinear Rotor-Stator Interaction Modes in Transonic Cascades. AIAA 2014–2947, 2014.

Pimenta, Braulio G.; and Miserda, Roberto F. Bobenrieth: Validation of a Moving-Body High-Order Immersed Boundary Method for the Multiple Pure Tone Noise Generated by Supersonic Rotor Cascades. AIAA 2015–2518, 2015.

Rao, Nikhil M., et al.: Experimental Demonstration of Active Flow Control to Reduce Unsteady Stator–Rotor Interaction, AIAA J., vol 39, no. 3, 2001.

Sanjoséa, Marlene, et al.: Tonal Noise Prediction and Validation on the ANCF Rotor-Stator Configuration. Noise Control Eng. J., vol. 63, no. 6, 2015, pp. 552–562.

Sanjose, Marlene, et al.: Influence and Modeling of OGV Heterogeneity. AIAA 2016–2881, 2016.

Sugimoto, Rie; and Astley Jeremy: Validation and Application of a Hybrid Prediction Scheme for Bypass Duct Noise. AIAA 2006–2520, 2006.

Sutliff, D.L.: Fan Noise Reduction and Analysis. Technical Progress Report, Contract NAS3–00170, Task Order no. 17, Sest, Inc.

Sutliff, Daniel; Bridges, James; and Envia, Edmane: Comparison of Predicted Low Speed Fan Rotor/Stator Interaction Modes to Measured. NASA TM–107462 (AIAA 97–1609), 1996. http://ntrs.nasa.gov

Sutliff, Daniel L.: A Mode Propagation Database Suitable for Code Validation Utilizing the NASA Glenn Advanced Noise Control Fan and Artificial Sources. AIAA 2014–0719, 2014.

Sutliff, Daniel L.: Broadband Noise Reduction of Low-Speed Fan Noise Using Trailing Edge Blowing. AIAA 2005–3028 (NASA/TM—2005-213814), 2005. http://ntrs.nasa.gov

Sutliff, Daniel L.: Rotating Rake Mode Measurements Over Passive Treatment in a Ducted Fan. NASA/TM—2006-214493 (IN06–558), 2006. http://ntrs.nasa.gov

Sutliff, Daniel L.: Rotating Rake Turbofan Duct Mode Measurement System. NASA/TM—2005-213828, 2005. http://ntrs.nasa.gov

Sutliff, Daniel L.; and Dahl, Milo D.: Techniques for Analyzing Rotating Rake Mode Measurements Over Passive Treatment. Int. J. Aeroacoust., vol. 15, 2016, pp. 430–461.

Sutliff, Daniel L.; Dougherty, Robert P.; and Walker, Bruce E.: Evaluating the Acoustic Effect of Over-the-Rotor Foam-Metal Liner Installed on a Low Speed Fan Using Virtual Rotating Microphone Imaging. NASA/TM—2010-216800 (AIAA 2010–3800), 2010. http://ntrs.nasa.gov

Sutliff, Daniel L., et al.: Active Noise Control of Low Speed Fan Rotor-Stator Modes. NASA TM–107458 (AIAA 97–1641), 1996. http://ntrs.nasa.gov

Sutliff, Daniel L., et al.: Baseline Acoustic Levels of the NASA Active Noise Control Fan Rig. NASA TM–107214 (AIAA–96–1745), 1996. http://ntrs.nasa.gov

Sutliff, Daniel L., et al.: Low-Speed Fan Noise Reduction With Trailing Edge Blowing. AIAA 2002–2492, 2002.

Sutliff, Daniel L., et al.: Performance of an Active Noise Control System for Fan Tones Using Vane Actuators. NASA/TM—2000-210229 (AIAA 2000–1902), 2000. http://ntrs.nasa.gov

Sutliff, Daniel L.; Heidelberg, Laurence J.; and Envia, Edmane: Coupling of Low Speed Fan Stator Vane Unsteady Pressures to Duct Modes: Measured vs. Predicted. NASA/TM—1999-209050 (AIAA 99–1864), 1999. http://ntrs.nasa.gov

Sutliff, Daniel L.; and Jones, Michael G.: Foam-Metal Liner Attenuation of Low-Speed Fan Noise. AIAA 2008–2897, 2008.

Sutliff, Daniel L.; Jones, Michael G.; and Nark, Douglas M.: In-Duct and Far-Field Experimental Measurements From the ANCF for the Purpose of Improved Broadband Liner Optimization. AIAA 2014–3231, 2014.

Sutliff, Daniel L.; Remington, Paul J.; and Walker, Bruce E.: Active Control of Low-Speed Fan Tonal Noise Using Actuators Mounted in Stator Vanes: Part I Control System Design and Implementation. AIAA 2003–3190, 2003.

Sutliff, Daniel L.; Remington, Paul J.; and Walker, Bruce E.: Active Control of Low-Speed Fan Tonal Noise Using Actuators Mounted in Stator Vanes: Part III Results. AIAA 2003–3193, 2003.

Sutliff, Daniel L.; and Walker, Bruce E.: Artificial Noise Systems for Parametric Studies of Turbo-Machinery Aeroacoustics. Int. J. Aeroacoust., vol. 15, 2016, pp. 103–130.

Sutliff, Daniel L.; and Walker, Bruce E.: Multi-Mode Simultaneous Inlet/Exhaust Active Noise Control of Fan Tones. AIAA 2000–1907, 2000.

Tester, Brian J., et al.: Validation of an In-Duct to Far-Field Beamformer Method for Predicting Far-Field Fan Broadband Noise. AIAA 2016–2894, 2016.

Walker, B., et al.: Active Control of Low-Speed Fan Tonal Noise Using Actuators Mounted in Stator Vanes: Part 2: Novel Error Sensing Concepts. AIAA 2003–3191, 2003.

Walker, B.E., et al.: Active Resonators for Control of Multiple Spinning Modes in an Axial Flow Fan Inlet. AIAA 99–1853, 1999.

Walker, Bruce: Sensitivity Issues in Active Control of Circular Duct Modes Using Axially-Spaced Actuator Arrays. Noise Control Eng. J., vol. 49, no. 1, 2001.

Zhao, Yuan; and Morris, Philip J.: The Prediction of Fan Exhaust Noise Propagation. AIAA 2016–2420, 2016.

Contractor Reports

Burdisso, Ricardo A.; and Ng, Wing F.: Fan Noise Control Using Herschel-Quincke Resonators. NASA/CR—2003-212097, 2003. http://ntrs.nasa.gov

Cunningham, Cameron C.: Novel Engineering and Fabrication Techniques Tested in Low-Noise- Research Fan Blades. NASA/TM—2002-211333, 2002. http://ntrs.nasa.gov

Curtis, Alan R.D.: Active Control of Fan Noise by Vane Actuators. NASA/CR—1999-209156, 1999. http://ntrs.nasa.gov

Guillot, S.; Stitzel, S.; and Burdisso, R.: Fan Flow Control for Improved Efficiency and Noise Reduction. Phase I STTR Final Report NAS3–02042, Techsburg, VPI, November 1, 2002.

Kraft, R., et al.: Development and Demonstration of Active Noise Control Concepts. NASA/CR—2000-210037, 2000. http://ntrs.nasa.gov

Langford, M., et al.: Fan Flow Control for Improved Efficiency and Noise Reduction. Phase II STTR Final Report NAS3–03077, Techsburg, VPI, June 24, 2005.

Liberman, Robert A.; and Fite, Eric B.: Fan Flow Control for Improved Efficiency and Noise Reduction. Phase I STTR Final Report NAS3–02042, 2001. http://ntrs.nasa.gov

Parente, C.A., et al.: Hybrid Active/Passive Jet Engine Noise Suppression System. NASA/CR—1999-208875 (NSL–RPT–98–002), 1999. http://ntrs.nasa.gov

Pla, Frederic G.; Hu, Ziqiang; and Sutliff, Daniel L.: Active Control of Fan Noise: Feasibility Study. Volume 3: Active Fan Noise Cancellation in the NASA Lewis Active Noise Control Fan Facility. NASA CR–198511, 1996. http://ntrs.nasa.gov

Smith, J.P., et al.: Active Control of Inlet Noise at the NASA Lewis Ducted Fan Facility. VPI–ENGR 97–444, Nov 1997.

Sutliff, D.L.: Fan Noise Reduction and Analysis. Technical Progress Report, Contract NAS3–00170, Task Order no. 17, Sest, Inc.

Presentations

Jones, Michael G.: NASA Langley Activities on Broadband Fan Noise Reduction via Novel Liner Technologies. CEAS/X-Noise Workshop on Broadband Noise of Rotors and Airframe, La Rochelle, France, 2015.

Heidelberg, L.J.: An Overview of the Fan Active Noise Control Effort at NASA Glenn. Presented at a Joint Meeting of the ASA, EAA, DEGA, Berlin, Germany, 1999.

Sutliff, D.L.: The Advanced Noise Control Fan: A 20 Year Retrospective. Presented at the 20th Workshop of the Aeroacoustics Specialists Committee of the CEAS: Measurement Techniques and Analysis Methods for Aircraft Noise, University of Southampton, England, 2016.

Videos

CFD-Acoustic Integrated Simulation of the NASA Glenn Research Center's Advanced Noise Control Fan. 2013. https://www.youtube.com/watch?v=pkraAkYQwA Accessed March 20, 2019.

Demo of Active/Passive Resonators on the Active Noise Control Fan. 1998. https://images.nasa.gov/details-GRC-2018-CM-0135.html Accessed March 19, 2019.

NASA Glenn Research Center Engine Tone Noise Diagnostics Rotating Rake Technology. WO# 632869. https://images.nasa.gov/details-GRC-2019-CM-0101.html Accessed July 2, 2019.

♦ References ♦

[1]Huff, Dennis L.: NASA Glenn's Contributions to Aircraft Engine Noise Research. NASA/TP—2013-217818, 2013. http://ntrs.nasa.gov

[2]NASA Leader Explains Why Failure is Sometimes an Option. Smithsonian National Air and Space Museum, Washington, DC, 2017. https://airandspace.si.edu/stories/editorial/nasa-leader-explains-why-failure-sometimes-option Accessed March 11, 2019.

[3]Hubbard, H.H., ed.: Aeroacoustics of Flight Vehicles: Theory and Practice: Volume 1: Noise Sources, NASA Reference Publication 1258, Vol. 1, WRDC Technical Report 90–3052, 1991.

[4]Tyler, J.M.; and Sofrin T.G.: Axial Flow Compressor Noise Studies. SAE Transactions, vol. 70, 1962, pp. 309–332.

[5]Hubbard, H.H., ed.: Aeroacoustics of Flight Vehicles: Theory and Practice. Volume 2: Noise Control, NASA Reference Publication 1258, Vol. 2, WRDC Technical Report 90–3052, 1991.

[6]Huff, Dennis L.: Noise Reduction Technologies for Turbofan Engines. NASA/TM–2007-214495, 2007. http://ntrs.nasa.gov

[7]Woodward, Richard P., et al.: Benefits of Swept and Leaned Stators for Fan Noise Reduction. NASA/TM—1998-208661, 1998. http://ntrs.nasa.gov

[8]Heidelberg, Laurence J., et al.: A Unique Ducted Fan Test Bed for Active Noise Control and Aeroacoustics Research. NASA TM–107213 (AIAA–96–1740), 1996. http://ntrs.nasa.gov

[9]Sutliff, Daniel L., et al.: Baseline Acoustic Levels of the NASA Active Noise Control Fan Rig. NASA TM–107214 (AIAA–96–1745), 1996. http://ntrs.nasa.gov

[10]McAllister, Joseph, et al.: The Advanced Noise Control Fan Baseline Measurements. NASA/TM—2009-215595 (AIAA 2009-0624), 2009. http://ntrs.nasa.gov

[11]Cooper, Beth A.: A Large Hemi-Anechoic Chamber Enclosure for Community-Compatible Aeroacoustic Testing of Aircraft Propulsion Systems. Noise Control Eng. J., vol. 42, no. 1, 1994, pp. 1–7.

[12]Sutliff, D.L.: Acoustic Characteristics of the Active Noise Control Fan Located in the Compact Farfield Arena. Technical Progress Report, Contract NAS3–00170, Task Order no. 17, Sest Inc.

[13]Loew, Raymond A., et al.: Advanced Noise Control Fan. NASA/TM–2006-214368 (AIAA 2006–3150), 2006. http://ntrs.nasa.gov

[14]Bozack, Richard F., Jr.: Advanced Noise Control Fan Aerodynamic Performance. NASA/TM—2009-215807, 2009.

[15]Homyak, L.; Mcardle, J.G.; and Heidelberg, L.J.: A Compact Inflow Control Device for Simulating Flight Fan Noise. AIAA 83–0680 (NASA TM–83349), 1983. http://ntrs.nasa.gov

[16]Sutliff, Daniel L.: Rotating Rake Turbofan Duct Mode Measurement System. NASA/TM—2005-213828, 2005. http://ntrs.nasa.gov

[17]Sutliff, Daniel L.: Rotating Rake Turbofan Duct Mode Measurement System. Int. J. Aeroacoust., vol. 118, no. 3, 2005.

[18]Heidelberg, Laurence J.; and Hall, David G.: Inlet Acoustic Mode Measurements Using a Continuously Rotating Rake. J. Aircraft, vol. 32, no. 4, 1995.

[19]Sutliff, Daniel L.; and Walker, Bruce E.: Artificial Noise Systems for Parametric Studies of Turbo-Machinery Aero-Acoustics. Int. J. Aeroacoust., vol. 15, nos. 1–2, 2016, pp. 103–130.

[20]Weir, Don, ed.: Engine Validation of Noise and Emission Reduction Technology Phase I. NASA/CR—2008-215225 (Honeywell Report No. 21–13843A), 2008. http://ntrs.nasa.gov

[21]Sutliff, Daniel L.; Jones, Michael G.; and Hartley, Thomas C.: High-Speed Turbofan Noise Reduction Using Foam-Metal Liner Over-the-Rotor. J. Aircr., vol. 50, no. 5, 2013, pp. 1491–1503.

[22]Norris, Guy: Quiet Quest. Aviation Week, 2018, pp. 24–25.

[23]Walker, Bruce E.: Two-Dimensional Air-Flow Tests of the Effect of ITA Flowliner Slot Modification by Grinding/Polishing on Edge Tone Generation Potential. NASA/CR—2004-213405, 2004. http://ntrs.nasa.gov

[24]Sutliff, Daniel L.; Brown, Clifford A.; and Walker, Bruce E.: Hybrid Wing Body Shielding Studies Using an Ultrasonic Configurable Fan Artificial Noise Source Generating Typical Turbofan Modes. NASA/TM—2014-218119 (AIAA 2014–0256), 2014. http://ntrs.nasa.gov

[25]Wnuk, S.: ANCF Blade Failure Report. Working Report, Dec. 19, 1997.

[26]Envia, Edmane: Fan Noise Source Diagnostics Test—Vane Unsteady Pressure Results. NASA/TM—2002-211808 (AIAA 2002–2430), 2002. http://ntrs.nasa.gov

[27]Topol, David A.; and Mathews, Douglas C.: Rotor Wake/Stator Interaction Noise Prediction Code: Technical Documentation and User's Manual. NASA/CR—2010-216818, 2010. http://ntrs.nasa.gov

[28]Meyer, Harold D.; and Envia, Edmane: Aeroacoustic Analysis of Turbofan Noise Generation. NASA CR–4715, 1996. http://ntrs.nasa.gov

[29]Sutliff, Daniel; Bridges, James; and Envia, Edmane: Comparison of Predicted Low Speed Fan Rotor/Stator Interaction Modes to Measured. NASA TM–107462 (AIAA 97–1609), 1996. http://ntrs.nasa.gov

[30]Sutliff, Daniel L.; Heidelberg, Laurence J.; and Envia, Edmane: Coupling of Low Speed Fan Stator Vane Unsteady Pressures to Duct Modes: Measured vs. Predicted. NASA/TM—1999-209050 (AIAA 99–1864), 1999. http://ntrs.nasa.gov

[31]Eversman, Walter: Turbofan Acoustic Propagation and Radiation. Final Report NASA NAG3–2109, 2001. http://ntrs.nasa.gov

[32]Heidelberg, Laurence J.; Sutliff, Daniel L.; and Nallasmay, M.: Azimuthal Directivity of Fan Tones Containing Multiple Modes. NASA TM–107464 (AIAA 1997–1587), 1997. http://ntrs.nasa.gov

[33]Nallasamy, M.; Sutliff, D.L.; and Heidelberg, L.J.: Propagation of Spinning Acoustic Modes in Turbofan Exhaust Ducts. J. Propul. Power, vol. 16, no. 5, 2000.

[34]Koch, L. Danielle: An Experimental Study of Fan Inflow Distortion Tone Noise. NASA/TM—2010-215844 (AIAA 2009–3290), 2009. http://ntrs.nasa.gov

[35]Koch, L. Danielle: Predicted and Measured Modal Sound Power Levels for a Fan Ingesting Distorted Inflow. NASA/TM—2010-216782 (AIAA 2010–22312), 2010. http://ntrs.nasa.gov

[36]Koch, L. Danielle: Validation of the Predicted Circumferential and Radial Mode Sound Power Levels in the Inlet and Exhaust Ducts of a Fan Ingesting Distorted Inflow. NASA/TM—2012-217253 (AIAA 2011–2808), 2012. http://ntrs.nasa.gov

[37]Koch, L. Danielle: Predicting the Inflow Distortion Tone Noise of the NASA Glenn Advanced Noise Control Fan With a Combined Quadrupole-Dipole Model. NASA/TM—2012-217673 (AIAA 2012–2196), 2012. http://ntrs.nasa.gov

[38]Hixon, Ray, et al.: Comparison of Computational Aeroacoustics Prediction of Acoustic Transmission Through a 3D Stator Geometry With Experiment. AIAA 2014–1405, 2014

[39]Walker, Bruce: Sensitivity Issues in Active Control of Circular Duct Modes Using Axially-Spaced Actuator Arrays. Noise Control Eng. J., vol. 49, no. 1, 2001.

[40]Sutliff, Daniel L., et al.: Active Noise Control of Low Speed Fan Rotor-Stator Modes. NASA TM–107458 (AIAA 97–1641), 1996. http://ntrs.nasa.gov

[41]Walker, B.E., et al.: Active Resonators for Control of Multiple Spinning Modes in an Axial Flow Fan Inlet. AIAA 99–1853, 1999.

[42]Sutliff, Daniel L., et al.: Performance of an Active Noise Control System for Fan Tones Using Vane Actuators. NASA/TM—2000-210229 (AIAA 2000–1902), 2000. http://ntrs.nasa.gov

[43]Sutliff, Daniel L.; Remington, Paul J.; and Walker, Bruce E.: Active Control of Low-Speed Fan Tonal Noise Using Actuators Mounted in Stator Vanes: Part I Control System Design and Implementation. AIAA 2003–3190, 2003.

[44]Parente, C.A., et al.: Hybrid Active/Passive Jet Engine Noise Suppression System. NASA/CR—1999-208875 (NSL–RPT–98–002), 1999. http://ntrs.nasa.gov

[45]Smith, J.P., et al.: Active Control of Inlet Noise at the NASA Lewis Ducted Fan Facility. VPI–ENGR 97–444, Nov. 1997.

[46]Walker, B., et al.: Active Control of Low-Speed Fan Tonal Noise Using Actuators Mounted in Stator Vanes: Part 2: Novel Error Sensing Concepts. AIAA 2003–3191, 2003.

[47]Brookfield, John M.: Turbofan Rotor/Stator Interaction Noise Reduction Through Trailing Edge Blowing. Ph.D. Thesis, Massachusetts Institute of Technology, 1998.

[48]Rao, Nikhil M., et al.: Experimental Demonstration of Active Flow Control to Reduce Unsteady Stator–Rotor Interaction, AIAA J., vol 39, no. 3, 2001.

[49]Sutliff, D.L., et al.: Low-Speed Fan Noise Reduction With Trailing Edge Blowing. Int. J. Aeroacoust., vol. 1, no. 3, 2002.

[50]Tweedt, Daniel L.; and Chima, Rodrick V.: Rapid Numerical Simulation of Viscous Axisymmetric Flow Fields. AIAA 96–0449 (NASA TM–107103), 1996. http://ntrs.nasa.gov

[51]Sutliff, Daniel L.; and Jones, Michael G.: Low-Speed Fan Noise Attenuation From a Foam-Metal Liner. J. Aircraft, vol. 46, no. 4, 2009.

[52]Gazella, Matthew R., et al.: Evaluating the Acoustic Benefits of Over-the-Rotor Acoustic Treatments Installed on the Advanced Noise Control Fan. AIAA 2017–3872, 2017.

[53]Bozak, Richard F.; and Dougherty, Robert P.: Measurement of Noise Reduction From Acoustic Casing Treatments Installed Over a Subscale High Bypass Ratio Turbofan Rotor. AIAA 2018–4099, 2018.

[54]Jones, M.G., et al.: Assessment of Soft Vane and Metal Foam Engine Noise Reduction Concepts. AIAA–2009–3142, 2009.

[55]Rice, Edward J.: Spinning Mode Sound Propagation in Ducts With Acoustic Treatment. NASA TN D–7913, 1975. http://ntrs.nasa.gov

[56]Nark, Douglas M., et al.: Improved Broadband Liner Optimization Applied to the Advanced Noise Control Fan. AIAA 2014–3103, 2014.

[57]Sutliff, Daniel L.; Jones, Michael G.; and Nark, Douglas M.: In-Duct and Far-Field Experimental Measurements From the ANCF for the Purpose of Improved Broadband Liner Optimization. AIAA 2014–3231, 2014.

[58]Sutliff, Daniel L.; Jones, M.G.; and Nark, D.M.: Acoustic Directivity and Insertion Loss Measurements of Advanced Liners Installed the Inlet of the DGEN Aero-propulsion Research Turbofan. NASA/TM—2019-220161, 2018.

[59]Sutliff, Daniel L.: Rotating Rake Mode Measurements Over Passive Treatment in a Ducted Fan. NASA/TM—2006-214493 (IN06–558), 2006. http://ntrs.nasa.gov

[60]Sutliff, Daniel L.; and Dahl, Milo D.: Techniques for Analyzing Rotating Rake Mode Measurements Over Passive Treatment. Int. J. Aeroacoust., vol. 15, 2016, pp. 430–461.

[61]International Journal of Aeroacoustics Issue in Honor of Dr. Edward J. Rice. Int. J. Aeroacoust., vol. 15, nos 4–5, 2016.

[62]Cicon, D.E.; and Sofrin, T.G.: Method for Extracting Forward Acoustic Wave Components From Rotating Microphone Measurements in the Inlets of Turbofan Engines. NASA CR–195457, 1995. http://ntrs.nasa.gov

[63]Dahl, Milo D.; and Sutliff, Daniel L.: Analysis of Dual Rotating Rake Data From the NASA Glenn Advanced Noise Control Fan Duct With Artificial Sources. AIAA 2014–3316, 2014.

[64]Lan, Justin H.; Premo, John W.; and Sutliff, Daniel L.: Inlet Mode Measurements With an Inflow Control Device Microphone Array. AIAA 2002–2563, 2002.

[65]Dougherty, Robert P.; and Walker, Bruce E.: Virtual Rotating Microphone Imaging of Broadband Fan Noise. AIAA 2009–3121, 2009.

[66]Sijtsma, Pieter: CLEAN Based on Spatial Source Coherence. Int. J. Aeroacoust., vol. 6, no. 4, 2007, pp. 357–374.

[67]Tester, Brian J., et al.: Validation of an In-Duct to Far-Field Beamformer Method for Predicting Far-Field Fan Broadband Noise. AIAA 2016–2894, 2016.

[68]Sutliff, D.L. et al.: Low Speed Fan Noise Reduction with Trailing Edge Blowing. AIAA 2002–2492, 2002.

[69]Bruun, H.H.: Hot-Wire Anemometry: Principles and Signal Analysis. Section 7.4.2, Oxford University Press, Oxford, England, 1995.

[70]Lucero, John M.: Advanced Noise Control Fan Test Rig and Trade Study Summary. Presented at the Machinery Failure Prevention Technology 2012, Dayton, OH, 2012.

[71]Lucero, John: Advance Noise Control Fan II: Test Rig Fan Risk Management Study. Presented at the Machinery Failure Prevention Technology Conference, Cleveland, OH, 2013.

[72]Lucero, John: Advance Noise Control Fan II Test Rig Fan Support Bearings Trade Study. Presented at the 59th ISA International Instrumentation Symposium, Cleveland, OH, 2013.

[73]Brown, Clifford A.: Analysis of Rotor-Stator Interaction Noise During a Speed Transient. Master's Thesis, Univ. of Akron, 2001. http://library.uakron.edu/record=b2404148~S24

[74]Maldonado, Ana Luisa Pereira: N Predicão Numérica do Ruído Tonal Para o Advanced Noise Control Fan. Universidade de Brasília, 2002.

[75]Pimenta, B.G.: Simulação Numérica de Ondas Não-lineares em Dinâmica dos Gases e Ruído de Interação Rotor-Estator em Turbofans Aeronáuticos. Ph.D. Thesis, Universidade de Brasília, 2016

[76]Caldas, L.C.: Beamforming e Análise Modal em Duto Utilizando Arranjo Circular de Microfones Para Caracterização de Ruído Banda-Larga em Motores Aeronáuticos Turbo-Fan. University of São Paulo, 2016.

[77]Maldonado, Ana Luisa Pereira: On the Prediction of the Effect of Interstage Liners in Turbofan Engines. Doctoral Thesis, Univ. of Southampton, England, 2016.

[78]Sanjoséa, Marlene, et al.: Tonal Noise Prediction and Validation on the ANCF Rotor-Stator Configuration. Noise Control Eng. J., vol. 63, no. 6, 2015, pp. 552–562.

[79]Mann, Adrien, et al.: Investigation of Inflow Condition Effects on the ANCF Aeroacoustics Radiation Using LBM. Proceedings of the 41st International Congress and Exposition on Noise Control Engineering 2012, Vol. 12, 2012.

[80]CFD-Acoustic Integrated Simulation of the NASA Glenn Research Center's Advanced Noise Control Fan. 2013. https://www.youtube.com/watch?v=pkraAk1YQwA Accessed March 20, 2019.

[81]Martinez, Bernardo, et al.: Baseline Acoustic Levels of the EESC–USP Fan Rig. AIAA 2017–3384, 2017.

[82]Sutliff, Daniel L., et al.: Farfield Acoustic Characteristics of the DGEN380 Turbofan Engine as Measured in the NASA Glenn Aero-Acoustic Propulsion Laboratory. AIAA 2016–3006, 2016.

[83]Figueroa-Ibrahim, K., et al.: Evaluation of Radiated Sound From the Advanced Noise Control Fan Facility in an Outdoor Environment Using Ground Microphones. Submitted to 2019 AIAA Power and Energy Forum.

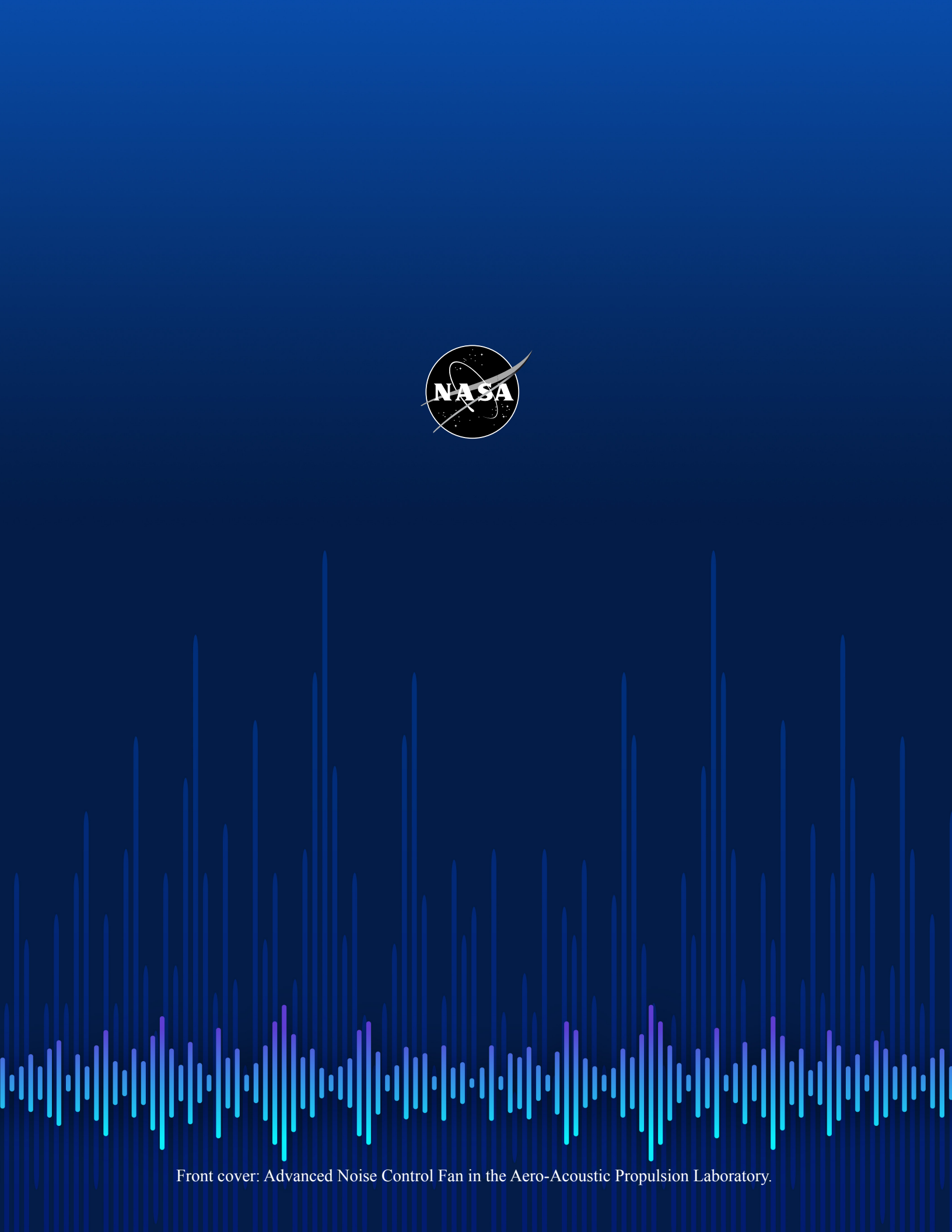

Front cover: Advanced Noise Control Fan in the Aero-Acoustic Propulsion Laboratory.